Summer 8-15-2019

Mechanism of Activation of UvrD Helicase by a Processivity Factor MutL

Yerdos Ordabayev
Washington University in St. Louis

WASHINGTON UNIVERSITY IN ST. LOUIS

Division of Biology and Biomedical Sciences
Computational and Molecular Biophysics

Dissertation Examination Committee:
Timothy M. Lohman, Chair
Peter M. J. Burgers
Eric Galburt
Roberto Galletto
Zhongsheng You

Mechanism of Activation of UvrD Helicase by a Processivity Factor MutL

by

Yerdos A. Ordabayev

A dissertation presented to
The Graduate School
of Washington University in
partial fulfillment of the
requirements for the degree
of Doctor of Philosophy

August 2019
St. Louis, Missouri

Table of Contents

List of Figures

Chapter I

Chapter II

Chapter III

Chapter IV

List of Tables

Chapter II

Chapter III

Chapter IV

List of Schemes

Chapter II

Acknowledgments

I thank my parents, my brother and his family for encouragement and support throughout my graduate studies. I thank my friends Timur for encouraging me to learn Python and Tlek for keeping me motivated. I thank the members of the Lohman Lab for the supportive lab environment. I thank Alex Kozlov and Binh Nguyen for teaching me how to use the lab instruments and analyze the data. I thank Eric Tomko for helpful discussions about UvrD, Nicole Fazio for political consultation, Min Kyung Shinn for being an "average" friend, and Linxuan Hao for sharing his lunchtime with me and discussions of philosophical ideas. I thank my committee members for sharing their experience and insight with me. Finally, I thank my mentor Tim Lohman for his persistent guidance and pushing me beyond my limits.

Yerdos Ordabayev

Washington University in St. Louis

August 2019

ABSTRACT OF THE DISSERTATION

Mechanism of Activation of UvrD Helicase by a Processivity Factor MutL

by

Yerdos A. Ordabayev

Doctor of Philosophy in Computational and Molecular Biophysics

Washington University in St. Louis, 2019

Professor Timothy M. Lohman, Chair

E. coli UvrD is a superfamily 1A helicase/translocase involved in DNA repair, recombination, and replication. I investigated the role of *E. coli* MutL, a regulatory protein involved in methyl-directed mismatch DNA repair, in the regulation of UvrD-catalyzed DNA unwinding. Using single molecule fluorescence resonance energy transfer (FRET) and single round stopped-flow DNA unwinding experiments I demonstrated that MutL can activate latent UvrD monomer helicase activity and also stimulate UvrD dimer helicase activity. Furthermore, using analytical ultracentrifugation experiments I determined that a single MutL dimer is sufficient to activate UvrD monomer helicase. DNA unwinding experiments with a series of DNA substrates of varying duplex length under single round unwinding conditions showed that MutL increases the amount of duplex DNA unwound by UvrD in a single binding event. Therefore, MutL acts as a processivity factor by binding to and presumably moving along with UvrD during unwinding. I also showed that MutL requires contacts with the 3' ssDNA tail for optimal activation of UvrD helicase activity.

The C-terminal tail of UvrD is highly variable among SF1A helicases and suggested to interact with MutL, however, the truncated UvrDΔ73 mutant lacking its C-terminal tail is

activated by MutL, indicating that the disordered C-terminal domain is not essential for stimulation. I also found that MutL is unable to activate the helicase activity of the structurally similar *E. coli* Rep helicase, indicating that MutL stimulation is specific to UvrD. Furthermore, MutL also fails to activate the helicase activity of chimeric UvrD containing the 2B sub-domain of Rep helicase. This result demonstrates that MutL activation of the monomeric UvrD helicase is regulated specifically by the 2B sub-domain of UvrD. Using single molecule and ensemble FRET experiments I showed that MutL binding to a UvrD monomer-DNA complex induces partial closing of the 2B sub-domain. Transient kinetic studies of MutL-induced activation of the UvrD helicase and MutL-induced changes in the UvrD 2B sub-domain showed that formation of the partially closed state is on the pathway to forming the active helicase. The kinetic analysis of these two sets of experiments revealed that under the experimentally used MutL concentrations the active MutL-UvrD species are formed predominantly through the conformational selection pathway (>90%) and to a lesser degree through the induced fit pathway (<10%).

Chapter I

Introduction

Introduction

Cells encode and store their heritable information as a sequence of nucleotides in deoxyribonucleic acid (DNA) molecules. The cellular genome consists of two complementary DNA strands forming a double-helical structure (Watson and Crick 1953). Before cell division can occur, the genetic information must be duplicated to create two copies of DNA for two new cells. To keep the genomic information consistent between generations, cells have to ensure high fidelity of the replication process and integrity of the genetic information between successive replications. Therefore, a great deal of cellular infrastructure is involved in ensuring proper maintenance of their DNA.

DNA molecules can be damaged as a result of exposure to chemical or physical sources of damage. Another source of mutations are errors that occur during DNA replication due to insertion of incorrect nucleotides or slippage of a DNA polymerase. Mismatched DNA sites, if unrepaired, will generate mutations in the subsequent round of replication. Accumulation of damages and mutations in genomic DNA can cause a cellular dysfunction or a disease within an organism. To prevent such deleterious effects and protect the integrity of the genome, cells have evolved multiple mechanisms to repair damaged DNA. One such mechanism is the DNA mismatch repair (MMR) system which is responsible for correcting replication errors and inhibiting recombination between divergent DNA sequences. Defects in human mismatch repair genes cause Lynch syndrome or hereditary non-polyposis colorectal cancer and 10–40% of related sporadic tumors (Kolodner 1995; Lynch and de la Chapelle 1999).

Most DNA metabolic processes, including DNA repair, replication, and recombination, require the separation of DNA strands to access the ssDNA. However, the double-helical DNA structure is thermodynamically stable, and the production of ssDNA necessitates the use of

helicases. Helicases are a class of enzymes that use energy derived from ATP binding/hydrolysis to move unidirectionally along the DNA chain and catalyze strand separation of the duplex DNA (Tuteja and Tuteja 2004; Singleton, Dillingham, and Wigley 2007; Timothy M. Lohman, Tomko, and Wu 2008; T. M. Lohman 1992; T. M. Lohman and Bjornson 1996; S. W. Matson and Morton 1991; Geider and Hoffmann-Berling 1981). A detailed understanding of how these motor proteins function and are regulated is important for a full understanding of cellular processes involved in DNA metabolism.

Much early work on SF1A helicase proteins has employed a reductionist approach in which individual helicase proteins are overexpressed, purified and studied in isolation. Single-stranded DNA translocation and DNA unwinding activities of isolated helicases were characterized using a combination of structural (Korolev et al. 1997; Velankar et al. 1999; J. Y. Lee and Yang 2006; Jia et al. 2011; Singleton, Dillingham, and Wigley 2007), thermodynamic (Maluf and Lohman 2003), kinetic (Lucius et al. 2003; Tomko, Fischer, and Lohman 2010; Ali and Lohman 1997; M. S. Dillingham, Wigley, and Webb 2000; Mark S. Dillingham, Wigley, and Webb 2002; Fischer and Lohman 2004; Fischer, Maluf, and Lohman 2004; Maluf and Lohman 2003; Maluf, Fischer, and Lohman 2003; Cheng et al. 2001), and single-molecule approaches (Ha et al. 2002; Myong et al. 2005; K. S. Lee et al. 2013; Comstock et al. 2015; Dessinges et al. 2004) . These studies facilitated a detailed mechanistic understanding of how these enzymes function, yielding information such as rates, step-sizes, processivities, conformational states, and stoichiometries of active helicase species. However, these mechanistic studies have generally focused on the activities of isolated enzymes, and only a few have specifically investigated interactions with accessory proteins (Mechanic, Frankel, and Matson 2000; Atkinson et al. 2009; Chisty et al. 2013; Sokoloski et al. 2016). However, it is now

apparent that helicases often function as part of larger multi-subunit complexes rather than in isolation and that protein partners impact motor activity and/or specificity (Timothy M. Lohman, Tomko, and Wu 2008; Mark S. Dillingham 2011). Therefore, by studying the interactions between helicases and their accessory proteins we will get one step closer to understanding how they function and are regulated *in vivo*.

This dissertation focuses on the mechanism of activation of UvrD helicase by MutL, a regulatory protein involved in methyl-directed mismatch DNA repair. UvrD, first referred to as Helicase II (Abdel-Monem, Chanal, and Hoffmann-Berling 1977; Abdel-Monem, Dürwald, and Hoffmann-Berling 1977), is a prototypic superfamily 1A helicase/translocase involved in DNA repair (Iyer et al. 2006; Sancar 1996), replication (Atkinson and McGlynn 2009; Heller and Marians 2007; Bruand and Ehrlich 2000), and recombination (Arthur and Lloyd 1980; Veaute et al. 2005; Petrova et al. 2015). UvrD protein can self-associate into dimers and tetramers (Maluf and Lohman 2003), and its assembly state can regulate its activities. Using a combination of kinetic, thermodynamic, and single-molecule approaches it was established that a UvrD monomer can processively and rapidly translocate in a 3′ to 5′ direction along single-stranded (ss) DNA but has little to no helicase activity *in vitro* (Fischer, Maluf, and Lohman 2004; Maluf, Fischer, and Lohman 2003; K. S. Lee et al. 2013), although DNA unwinding can be observed with the application of force (Comstock et al. 2015). In the absence of accessory proteins, formation of a least a UvrD dimer is required to processively unwind duplex DNA *in vitro* (Maluf, Fischer, and Lohman 2003; Maluf, Ali, and Lohman 2003; Ali, Maluf, and Lohman 1999; K. S. Lee et al. 2013; Comstock et al. 2015; Nguyen et al. 2017). Using single-turnover and multiple-turnover DNA unwinding experiments it was shown that MutL alone is sufficient to

stimulate UvrD-catalyzed DNA unwinding (Yamaguchi, Dao, and Modrich 1998; Mechanic, Frankel, and Matson 2000), however, the mechanism is not well understood.

Role of *E. coli* UvrD in DNA repair

Nucleotide Excision Repair

Nucleotide excision repair (NER) pathway is responsible for removing a wide range of DNA lesions, including cyclobutane–pyrimidine dimers and 6–4 photoproducts induced by UV radiation (Grossman et al. 1988; Sancar 1994). The NER pathway in E. coli involves UvrA, UvrB, UvrC, and UvrD proteins (Sancar 1994). NER is initiated when UvrA binds to a damaged DNA site. The lesion recognition is verified by UvrB which triggers the release of UvrA from the DNA. UvrB remains bound tightly to the lesion and activates downstream repair. This includes recruitment of a UvrC endonuclease which nicks the ssDNA strand containing the lesion on both the 3' (~4-5 nts away) and 5' (~8 nts away) side. Following the incision, UvrD is recruited to the nick and thought to displace the ~12 nt ssDNA containing the lesion. Missing bases are re-synthesized by DNA polymerase I using the undamaged complementary strand as a template. The DNA repair is completed by sealing two nicks in the phosphodiester backbone of DNA by the DNA ligase.

Methyl-Directed Mismatch DNA Repair

Mismatch repair is a highly conserved pathway responsible for identifying and correcting errors produced by DNA polymerase during replication, which substantially improves the overall fidelity of genome replication (Modrich and Lahue 1996; Iyer et al. 2006). The mismatch repair system is also responsible for preventing strand exchange between divergent DNA sequences. A series of biochemical and genetic studies have uncovered the primary

components of the *E. coli* methyl-directed mismatch repair (MMR) pathway, and include the mutator proteins (MutL, MutS, MutH and UvrD (previously referred as MutU or Helicase II)), several exonucleases, including ExoI, ExoVII, RecJ and ExoX, DNA polymerase III, ssDNA binding protein (SSB), DNA ligase and the Dam methylase (Burdett et al. 2001; Cooper, Lahue, and Modrich 1993; Grilley, Griffith, and Modrich 1993; Au, Welsh, and Modrich 1992; Welsh et al. 1987; Lahue, Su, and Modrich 1987; Viswanathan et al. 2001; Su and Modrich 1986). Furthermore, the complete *E. coli* methyl-directed mismatch repair reaction has been successfully reconstituted using purified proteins *in vitro* (Lahue, Au, and Modrich 1989). The overall mismatch repair reaction can be divided into several steps as depicted in Figure 1: mismatch recognition; strand discrimination and incision of the unmethylated strand at a hemi-methylated GATC site; excision of the damaged DNA strand spanning the single-strand break and the mismatch; filling the ssDNA gap by DNA polymerase and DNA ligase.

E. coli methyl-directed mismatch repair is initiated upon the recognition of a mismatch by the MutS protein. *E. coli* MutS, a 95 kDa polypeptide, and its homologs are dimeric proteins possessing a conserved ATPase activity (Haber and Walker 1991; Chi and Kolodner 1994). MutS recognizes and specifically binds to DNA sites containing mismatched bases and small insertion/deletion loops (Su and Modrich 1986; Jiricny et al. 1988; Su et al. 1988; Parker and Marinus 1992; Lamers et al. 2000; Obmolova et al. 2000). The search for mismatched base pairs in a vast excess of homoduplex DNA appears to occur by one-dimensional diffusion of the MutS-ADP sliding clamp on DNA (Gorman et al. 2007; Jeong et al. 2011; Gorman et al. 2012; Liu et al. 2016). Mismatch recognition triggers ADP→ATP exchange which results in release of the MutS-ATP sliding clamp from the mismatch (Allen et al. 1997; S. Gradia, Acharya, and Fishel 1997, 2000; Junop et al. 2001; Jeong et al. 2011; Cho et al. 2012; Liu et al. 2016). The

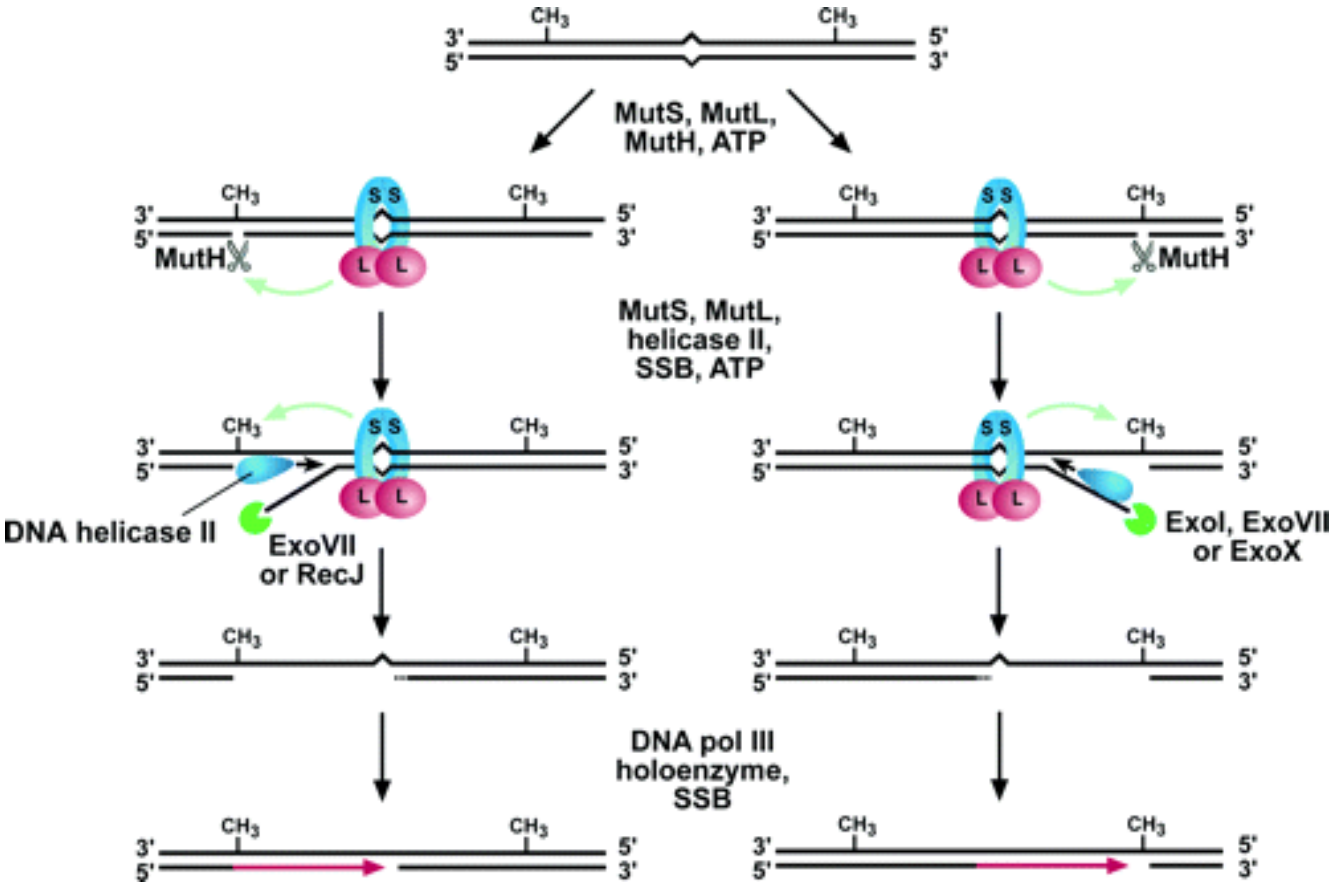

Figure 1. Schematic model of *E. coli* methyl-directed mismatch DNA repair (Iyer et al. 2006). UvrD is labeled as DNA helicase II. DNA unwinding is initiated from the nearest hemi-methylated GATC-site which can reside on either side of the mismatch.

MutS-ATP sliding clamp is very stable on DNA and diffuses along the DNA in an ATP-hydrolysis independent manner (Scott Gradia et al. 1999; Acharya et al. 2003; Jeong et al. 2011; Qiu et al. 2012). These and other findings support a "molecular switch" model for ATP binding; after identifying mismatch, ADP→ATP exchange induces a conformational change in MutS enabling it to passively slide along the DNA and transmit mismatch recognition to downstream events in MMR (Scott Gradia et al. 1999; S. Gradia, Acharya, and Fishel 1997).

E. coli MutL, a 68 kDa polypeptide, plays a critical role in the coupling of mismatch recognition by MutS to the activation of MutH and UvrD. *E. coli* MutL and its homologs are dimeric proteins possessing a weak ATPase activity (Grilley et al. 1989; Niedziela-Majka et al. 2011; Ban and Yang 1998; Ban, Junop, and Yang 1999). MutL is recruited to the heteroduplex in a MutS- and ATP-dependent manner (Drotschmann et al. 1998; Grilley et al. 1989; Galio, Bouquet, and Brooks 1999; Spampinato and Modrich 2000; Schofield et al. 2001; Acharya et al. 2003; Selmane et al. 2003; Liu et al. 2016). The assembled MutS-MutL complex activates MutH, a 25 kDa latent endonuclease, which cleaves the nearest unmodified strand of a hemi-methylated GATC site (Welsh et al. 1987; Au, Welsh, and Modrich 1992; Hall and Matson 1999a). The newly synthesized daughter strand is transiently unmethylated which acts as a strand discrimination signal. Strand cleavage can occur on either side of the mismatch depending on the location of the nearest hemi-methylated GATC site (Grilley, Griffith, and Modrich 1993). Interestingly, the requirements for both MutH and a hemi-methylated GATC site in *E. coli* mismatch repair can be bypassed by the presence of a preexisting nick suggesting that a single-strand break serves as the actual signal that directs the downstream excision reaction to the damaged strand (Längle-Rouault, Maenhaut-Michel, and Radman 1987; Lahue, Au, and Modrich 1989).

Following strand incision, UvrD initiates DNA unwinding from the nick and proceeds toward and past the mismatch in a MutS-, MutL-, ATP-, and mismatch-dependent manner (Yamaguchi, Dao, and Modrich 1998; Dao and Modrich 1998). Even though DNA unwinding can proceed in either direction from the nick, strand displacement by UvrD has a bias toward the mismatch (Dao and Modrich 1998). This suggests that MutS and MutL are responsible for loading UvrD on the proper strand and orienting the unwinding reaction toward the mismatch. Eventually the displaced strand is degraded by an exonuclease with the appropriate polarity (RecJ cleaves ssDNA with 5' to 3' polarity; EcoI and ExoX hydrolyze ssDNA with 3' to 5' polarity; ExoVII supports both 5' to 3' and 3' to 5' directionality) (Burdett et al. 2001; Viswanathan et al. 2001). The single-stranded gap produced after the excision reaction is filled in by DNA polymerase III and then sealed by DNA ligase in the final step of MMR (Lahue, Au, and Modrich 1989).

Structural properties of UvrD and MutL

Primary structure of UvrD

E. coli UvrD (Mr = 81,989 Da, 720 amino acids) is a member of the superfamily 1A (SF1A) DNA helicases/translocases which translocates 3' to 5' along ssDNA and are defined by eight conserved sequence motifs (Q, I, Ia, II-VI; see figure 2A) (Gorbalenya and Koonin 1993; Tanner et al. 2003). UvrD consists of four sub-domains 1A (1-89, 215-280 aa), 2A (281-377, 551-720 aa), 1B (90-214 aa), and 2B (378-550 aa). The two core sub-domains (1A and 2A) contain all of the conserved motifs involved in ATP binding/hydrolysis including the Walker A/B motifs (Tuteja and Tuteja 2004; Hall and Matson 1999b). The two auxiliary sub-domains (1B and 2B) have consistent length but low sequence conservation among UvrD homologs. The N-terminal and C-terminal regions of SF1 helicases are characterized by a low sequence

conservation and a high length variability. It has been suggested that the less conserved regions are responsible for specific protein-protein interactions (Brendza et al. 2005; Singleton, Dillingham, and Wigley 2007; Gwynn et al. 2013; Sanders et al. 2017), whereas the highly conserved 1A and 2A sub-domains are involved in catalytic activities. The closely related SF1 helicases, *E. coli* Rep and *B. stearothermophilus* PcrA, share ~40% sequence homology with UvrD with over 90% sequence similarity within conserved motifs.

Tertiary structure of UvrD

E. coli UvrD, *E. coli* Rep, and *B. stearothermophilus* PcrA all have the same topological structure of their four sub-domains (Korolev et al. 1997; Velankar et al. 1999; J. Y. Lee and Yang 2006; Jia et al. 2011; Subramanya et al. 1996). Crystal structures of an apo UvrD monomer (Jia et al. 2011) and a UvrD monomer in complex with a 3'-ss/dsDNA substrate (J. Y. Lee and Yang 2006) are shown in figures 2B,C. The conformations of the apo and DNA-bound UvrD monomers differ from each other by a rotation (~160°) of the 2B sub-domain about a hinge region connected to the 2A sub-domain. These two conformations are referred to as “open” and “closed”, respectively. Single-molecule and ensemble FRET experiments have shown that the UvrD 2B sub-domain is flexible and can assume a wide range of conformational states depending on solution conditions, DNA binding and dimerization (Jia et al. 2011; Comstock et al. 2015; Nguyen et al. 2017).

The ATP analog, AMPPNP, binds at the cleft separating the 1A and 2A sub-domains and interacts with all of the eight conserved motifs. The duplex and single-stranded regions of a 3’-ssDNA/duplex show a ~90° bend in a UvrD monomer-DNA complex (J. Y. Lee and Yang 2006). The 3’-ssDNA tail binds across the 1A and 2A sub-domains with a 3’ to 5’ orientation

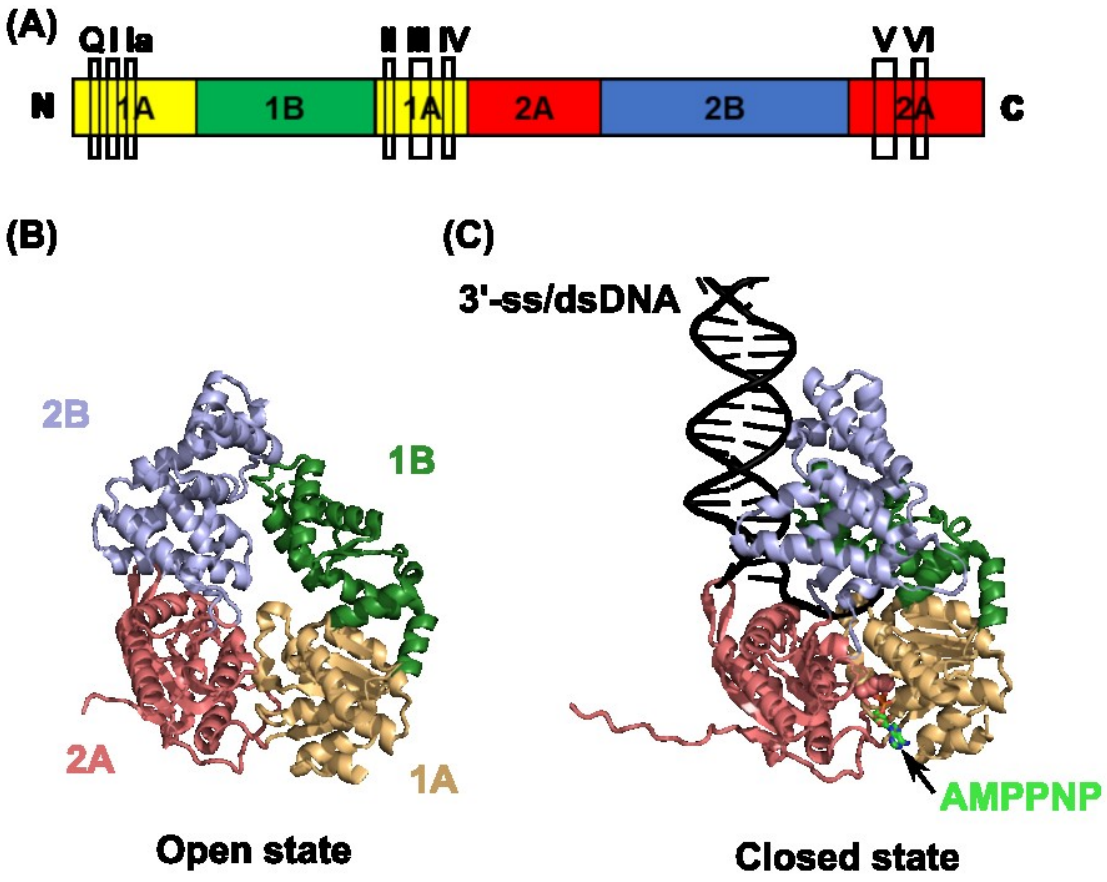

Figure 2. Structure of the *E. coli* UvrD monomer. (**A**) Linear diagram representing organization of the four sub-domains 1A, 2A, 1B, and 2B. The eight conserved SF1A helicase motifs are depicted as rectangles. (**B**) Crystal structure of the apo UvrD with the 2B sub-domain in the open conformation (Jia et al. 2011). (**C**) Crystal structure of the UvrD-DNA-AMPPNP complex with the 2B sub-domain in the closed conformation (J. Y. Lee and Yang 2006). The non-hydrolysable ATP analog, AMPPNP, is bound at the ATP binding site. UvrD monomer is bound at the 3'-ssDNA/dsDNA junction of a partial duplex DNA.

along the 1A and 2A sub-domains, respectively. The ssDNA interacts with the motifs Ia, III, and V. The 2B sub-domain in a closed conformation contacts the duplex region of DNA through a GIG motif which was proposed to facilitate DNA unwinding (J. Y. Lee and Yang 2006). However, whether this UvrD-DNA structure reflects a functional complex has been questioned since a UvrD monomer alone cannot unwind the 3'-dN_7-duplex DNA with which it was crystallized (Maluf, Fischer, and Lohman 2003). Furthermore, deletion of the 2B sub-domain of the *E. coli* Rep monomer activates its latent helicase activity indicating that the 2B sub-domain rather plays a regulatory role (Timothy M. Lohman, Tomko, and Wu 2008; Brendza et al. 2005; Makurath et al. 2019; Cheng et al. 2002).

Primary structure of MutL

E. coli MutL (Mr = 67,908 Da, 615 amino acids) contains an N-terminal ATPase region (1–335 aa) and a C-terminal dimerization region (439–615 aa) which are connected by an extended linker (336–438 aa). The N-terminal domain is highly conserved among all MutL homologs and contains an ATP binding domain which belongs to the GHKL superfamily of ATPases/kinases (Dutta and Inouye 2000). The C-terminal domain of MutL is essential for dimerization of MutL, however, the C-terminal region shares very limited sequence homology among MutL homologs (Guarné et al. 2004). The linker region shares no sequence similarity among MutL homologues and can tolerate sequence substitutions and large deletions without affecting its activity *in vivo* or *in vitro* (Guarné et al. 2004).

Tertiary structure of MutL

Crystal structures are available for both the N- and C-terminal regions of the *E. coli* MutL protein. The C-terminal 20 kDa region of MutL crystallizes as a dimer as shown in figure 3

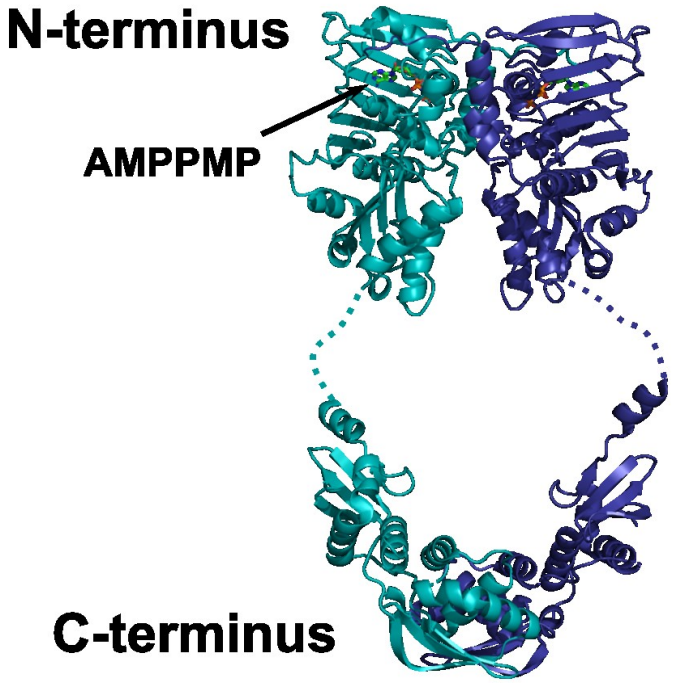

Figure 3. A model of intact *E. coli* MutL dimer composed from the crystal structure of the dimerized N-terminal ATPase in complex with AMPPNP (Ban, Junop, and Yang 1999), and the dimerized C-terminal dimerization domain (Guarné et al. 2004). The N- and C-termini are connected by the disordered linker region depicted as a dotted line.

(Guarné et al. 2004). In the absence of nucleotide, the N-terminal 40 kDa domain of MutL crystallizes as a monomer with partially disordered ATPase domain (Ban and Yang 1998). In the presence of the non-hydrolyzable ATP analog, AMPPNP, the N-terminal domain is dimeric with a fully folded ATP binding pocket (see figure 3) (Ban, Junop, and Yang 1999). Upon dimerization of the N-terminal domain in the presence of AMPPNP a positively charged groove is formed between the two protein subunits, a likely DNA binding site. The size of the groove is large enough to accommodate a single strand of DNA while an R266E mutation in the middle of the groove greatly reduces the DNA-binding affinity of the full-length MutL (Ban, Junop, and Yang 1999). Connecting the N- and C-terminal domains with the unstructured linker region generates a large central cavity in MutL dimers. The diameter of the central cavity is estimated to be ~100 Å for the extended form of the linker, large enough to encircle DNA duplex and small proteins (Guarné et al. 2004).

Biochemical properties of UvrD and MutL

Assembly state of UvrD

The assembly state of UvrD has been studied under a variety of solution conditions. UvrD is known to behave well in buffer T (10 mM Tris-HCl, pH 8.3, 20 mM NaCl, 20% (v/v) glycerol) which makes it the buffer of choice to study the DNA unwinding and ssDNA translocation activities of UvrD. The solubility of UvrD is sensitive to solution conditions and increases at higher pH, NaCl concentration, and glycerol concentration (Runyon, Wong, and Lohman 1993). Analytical ultracentrifugation studies showed that UvrD monomer can self-associate into dimers and tetramers in buffer T (Maluf and Lohman 2003). Increasing NaCl and glycerol concentrations shifts the equilibrium toward the monomeric UvrD species (Maluf and

Lohman 2003) explaining the higher solubility of UvrD under these conditions. Inclusion of nucleotide cofactors, ADP or ATPγS, does not have a significant effect on the assembly state of free UvrD in solution (Maluf and Lohman 2003). The assembly state of UvrD in the presence of DNA depends on the molar ratio of UvrD to DNA. In the presence of at least a two-fold molar excess of partial duplex DNA with a 3'-$(dT)_{20}$ tail UvrD binds DNA predominantly as a monomer. As the total DNA concentration exceeds the total UvrD concentration, the population of UvrD dimers bound to DNA increases, while the UvrD monomer–DNA population decreases (Maluf, Fischer, and Lohman 2003). UvrD binds tightly to ssDNA and ssDNA/dsDNA junctions, with higher affinity for the ssDNA/dsDNA junctions (Maluf, Fischer, and Lohman 2003; Tomko et al. 2010).

Assembly state of MutL

Sedimentation studies showed that MutL exists primarily as a stable dimer in buffer M (40.5 mM K_2HPO_4, 9.5 mM KH_2PO_4, pH 7.4, 50 mM KCl, 0.1 mM EDTA, 1 mM 2-mercaptoethanol) (Grilley et al. 1989; Niedziela-Majka et al. 2011), consistent with dimeric structures observed in crystallography studies (Ban, Junop, and Yang 1999; Guarné et al. 2004). In the presence of AMPPNP the MutL dimer becomes more compact, probably reflecting dimerization and conformational changes of the N-terminal ATPase domains. A single MutL dimer binds to an 18-bp duplex with a 3'-$(dT)_{20}$ ssDNA tail, with apparent affinity in the micromolar range (Niedziela-Majka et al. 2011).

Studying MutL and UvrD together requires determining solution conditions where both MutL and UvrD are well-behaved. Unfortunately, MutL forms large-molecular weight aggregates in buffer T, while UvrD forms larger complexes in buffer M (Niedziela-Majka et al.

2011). By varying buffer composition it was determined that PO_4^{3-} stabilizes MutL dimers in buffer M. Based on these findings, buffer M20/20 (40.5 mM K_2HPO_4, 9.5 mM KH_2PO_4, pH 7.4, 20 mM NaCl, 20% (v/v) glycerol, 1 mM 2-mercaptoethanol) was determined to support the helicase activity of UvrD and also allows studies of the assembly states of both UvrD and MutL (Niedziela-Majka et al. 2011).

Single-stranded DNA translocase activity of UvrD

UvrD monomer binds ssDNA with an apparent occluded site-size of ~10 nts on poly(dT) (Runyon, Wong, and Lohman 1993). In the presence of ssDNA UvrD can hydrolyze ATP and dATP (Abdel-Monem, Chanal, and Hoffmann-Berling 1977; S. W. Matson and George 1987) which is now known to be coupled to its ssDNA translocase activity (Abdel-Monem, Chanal, and Hoffmann-Berling 1977; S. W. Matson and George 1987; Fischer, Maluf, and Lohman 2004; Tomko et al. 2007, 2010; Tomko, Fischer, and Lohman 2012; Tomko and Lohman 2017). Single-round stopped-flow experiments showed that a UvrD monomer is capable of translocating along ssDNA with 3' to 5' directionality (Fischer, Maluf, and Lohman 2004) which has been confirmed by single-fluorophore tracking experiments (K. S. Lee et al. 2013). Quantitative analysis of stopped-flow ssDNA translocation time courses yielded a macroscopic translocation rate of ~190 nts/sec with a kinetic step-size of ~4-5 nts/step (Fischer, Maluf, and Lohman 2004; Tomko et al. 2007; Tomko, Fischer, and Lohman 2012). UvrD monomer is a highly processive ssDNA translocase and can translocate on average ~2500 nts before dissociating from ssDNA (Fischer, Maluf, and Lohman 2004; K. S. Lee et al. 2013). Analysis of stopped-flow experiments monitoring UvrD translocation and ATP hydrolysis demonstrated that UvrD translocation on ssDNA is tightly coupled to ATP hydrolysis (~1 ATP hydrolyzed per DNA base translocated)

without futile ATP hydrolysis during translocation (Tomko et al. 2007; Tomko, Fischer, and Lohman 2012).

UvrD monomer can initiate translocation from internal ssDNA sites (Fischer, Maluf, and Lohman 2004) or from a 5'-ssDNA/dsDNA junction (Tomko et al. 2010), whereas a 3'-ssDNA/dsDNA junction inhibits both the translocase and helicase activities of the UvrD monomer (Fischer, Maluf, and Lohman 2004). This indicates that the translocase and helicase activities of UvrD can be separated. Even though ssDNA translocation activity is necessary for helicase activity, it is not sufficient to enable DNA unwinding by a UvrD monomer. Some UvrD functions require ssDNA translocase activity alone as in its role to displace RecA filaments from ssDNA (Petrova et al. 2015). Therefore, it the oligomeric state of UvrD clearly can regulate the helicase/translocase activities of UvrD.

DNA helicase activity of UvrD

E. coli UvrD preferentially unwinds duplex DNA substrates with a flanking 3' ssDNA tail indicating that UvrD unwinds dsDNA with 3' to 5' polarity (Steven W. Matson 1986). A 3' ssDNA tail of at least 15 nucleotides is required to observe optimal unwinding of DNA (Maluf, Fischer, and Lohman 2003). The UvrD helicase is also able to initiate unwinding of duplex DNA from a blunt end or a nick, although unwinding of blunt ended or nicked DNA *in vitro* requires a large excess of UvrD protein (Runyon S and Lohman SBfl 1989; Runyon, Bear, and Lohman 1990). Nicked DNA substrates generated in cells during methyl-directed mismatch DNA repair and nucleotide excision repair pathways most likely require regulatory proteins to initiate DNA unwinding at a nick.

A crystal structure of UvrD in complex with 3'-$(dN)_7$ tailed partial duplex DNA contains one UvrD monomer at the ssDNA/dsDNA junction which was interpreted as representing the active form of the helicase (J. Y. Lee and Yang 2006). Another study has suggested that the monomeric UvrD is an active helicase, however, the experiments that compared the assembly state of UvrD and its helicase activity were performed under different solution conditions that affect the assembly state of UvrD (Mechanic, Hall, and Matson 1999). Furthermore, unwinding of short ~12 bp duplex DNA by UvrD monomers was observed when a pulling force is applied to the DNA (Comstock et al. 2015). However, a combination of analytical ultracentrifugation and single round DNA unwinding kinetic studies of the functional form of the UvrD helicase indicate that a UvrD dimer is the minimal form of the active helicase *in vitro* (Maluf, Fischer, and Lohman 2003; Maluf and Lohman 2003). First, UvrD monomers can tightly bind to DNA substrates with a 3'-ssDNA tail length as short as 4-6 nt, however, no unwinding is observed on DNA substrates with 3' tail length less than 12 nt in single round DNA unwinding experiments (Maluf, Fischer, and Lohman 2003). Second, the specific activity of UvrD-catalyzed DNA unwinding *in vitro* shows DNA substrate inhibition when the population of UvrD monomers bound to DNA increases as the total DNA concentration exceeds the total UvrD concentration (Maluf, Fischer, and Lohman 2003). Lastly, a series of single round DNA unwinding experiments were performed under stoichiometric binding conditions over a range of UvrD to DNA substrate ratios. The correlation between the total amount of unwound DNA substrate and the fraction of DNA bound by UvrD indicated that maximum activity is obtained when two UvrD monomers are bound to DNA substrate and that one monomer shows no helicase activity (Maluf, Fischer, and Lohman 2003). These results indicate that a UvrD dimer is required to

processively unwind DNA *in vitro* in the absence of force, which has been further confirmed by single-molecule studies (K. S. Lee et al. 2013; Nguyen et al. 2017).

Pre-steady state kinetic studies of the mechanism of formation of the active, dimeric UvrD-DNA complex indicate that the active dimeric complex can form by two different pathways, a pre-assembled dimer path and a path involving sequential binding of two UvrD monomers. In the faster pre-assembled dimer path, an active UvrD dimer directly binds a DNA substrate and immediately starts to unwind DNA (Maluf, Ali, and Lohman 2003). The slower monomer path proceeds via sequential binding to the DNA substrate of two UvrD monomers, which then assemble into an active dimer after a rate-limiting isomerization step (Maluf, Ali, and Lohman 2003). Both kinetic pathways were also directly visualized in single-molecule experiments where movement of individual fluorescently labeled UvrD molecules along DNA were tracked (K. S. Lee et al. 2013).

Quantitative methods developed to analyze single round DNA unwinding time courses using an n-step sequential mechanism allows a determination of the kinetic parameters of DNA unwinding (Ali and Lohman 1997; Lucius et al. 2003). For UvrD, the macroscopic rate of unwinding of 82±6 bps/sec, the average kinetic step size of 4.4 bp/step, and average processivity of 44 bps per binding event were determined by globally analyzing DNA unwinding time courses obtained from a series of 3'-$(dT)_{40}$ tailed DNA substrates with duplex regions ranging from 10 to 40 bp in buffer U (25 mM Tris-HCl, pH 7.5, 6 mM NaCl, 2.5 mM $MgCl_2$, 5 mM 2-mercaptoethanol, 10% (v/v) glycerol, 0.1 mg/ml BSA) (Ali and Lohman 1997). Under the solution conditions used to determine the stoichiometry of the UvrD-DNA complex (buffer T) a macroscopic rate of DNA unwinding of 81.5±1.8 bps/sec was determined from DNA unwinding time courses on a 3'-$(dT)_{20}$-ds18 DNA substrate (Maluf, Fischer, and Lohman 2003).

In a functional UvrD dimer both monomers must be active ATPases since the formation of a heterodimer using UvrD(K35I), that lacks ATPase activity, resulting in no DNA unwinding (Maluf, Fischer, and Lohman 2003). The role of the second UvrD monomer was elucidated in a study showing that upon formation of a UvrD dimer the 2B sub-domain of the lead UvrD subunit is shifted to a more closed state (Nguyen et al. 2017). In control experiments where Rep protein or UvrD(K35I) were used to bind to the UvrD monomer at the DNA junction, no significant change in the population of the closed state of UvrD was observed. This finding is consistent with other studies of UvrD homologs, *E. coli* Rep and *B. stearothermophilus* PcrA, showing that the closed conformational state of the 2B sub-domain correlates with DNA unwinding activity (Arslan et al. 2015; Comstock et al. 2015).

Stimulation of UvrD helicase by MutL

Interestingly, it was demonstrated that MutL alone is sufficient to stimulate unwinding of homoduplex DNA substrates by UvrD (Yamaguchi, Dao, and Modrich 1998; Mechanic, Frankel, and Matson 2000; Hall, Jordan, and Matson 1998; Steven W. Matson and Robertson 2006). Furthermore, the yeast two-hybrid system revealed a direct interaction between UvrD and MutL, and deletion analysis mapped interaction sites between UvrD and MutL onto the C-terminus of MutL and the N- and C-termini of UvrD which are the least conserved regions of each protein (Hall, Jordan, and Matson 1998). Based on *in vitro* biochemical studies it was proposed that MutL functions by continually loading multiple UvrD molecules onto a DNA substrate without affecting its unwinding processivity (Mechanic, Frankel, and Matson 2000).

Proposed mechanism for activation of UvrD helicase by MutL

DNA unwinding processivity

UvrD by itself has a limited DNA unwinding processivity in the absence of force (Ali and Lohman 1997). However, when force is applied to the DNA, unwinding processivity increases substantially (Dessinges et al. 2004; Comstock et al. 2015). However, in mismatch repair the distance from a nick, where UvrD initiates unwinding, to the mismatch site can be as long as 1–2 kb (Dao and Modrich 1998). It has been shown that MutL facilitates unwinding of long duplex DNA substrates by UvrD under multiple-turnover conditions (Mechanic, Frankel, and Matson 2000). Based on these observations two alternative mechanism were proposed: (i) MutL facilitates unwinding of long stretches of DNA by continually loading multiple UvrD molecules onto the DNA substrate (ii) MutL functions as a processivity factor by keeping UvrD tethered to the DNA (Mechanic, Frankel, and Matson 2000; Steven W. Matson and Robertson 2006). These two models make predictions that can be tested experimentally. The first model predicts that (i) MutL increases the rate of association of UvrD with the DNA, (ii) MutL dissociates from UvrD after the initiation of DNA unwinding, (iii) MutL does not affect UvrD unwinding processivity. On the other hand, the second model predicts that (i) MutL increases DNA unwinding processivity of UvrD under single round unwinding conditions, (ii) MutL decreases the rate of dissociation of UvrD from the DNA during unwinding, (iii) MutL forms a stable complex with UvrD throughout DNA unwinding. Matson's group has concluded from their DNA unwinding experiments that MutL only loads UvrD molecules onto DNA and does not increase processivity of UvrD (Mechanic, Frankel, and Matson 2000).

Stoichiometry of the active MutL-UvrD complex

Helicase activity of isolated UvrD is greatly influenced by its assembly state. Therefore, the possibility exists that interaction with MutL could affect the assembly state and helicase activity of UvrD. One possible mechanism for explaining the stimulation of the helicase activity of UvrD by MutL could be that MutL increases the stability of the UvrD dimer (or a higher oligomer) on the DNA (Maluf, Fischer, and Lohman 2003). Alternatively, MutL might activate the helicase activity of the UvrD monomer (Maluf, Fischer, and Lohman 2003). *E. coli* Rep monomer helicase can be activated through deletion of its 2B sub-domain (Brendza et al. 2005; Cheng et al. 2002) or covalent crosslinking of the 2B sub-domain in a closed conformation (Arslan et al. 2015) which demonstrates that a Rep monomer possesses all that is needed for helicase activity. Moreover, it has been demonstrated that monomeric PcrA helicase can be activated by accessory RepD protein (Chisty et al. 2013). The stoichiometry of the functional state of the MutL-UvrD complex can be determined by parallel investigation of the assembly state and single round DNA unwinding activity of the MutL-UvrD complex under identical solution conditions. Additionally, the helicase activity of the monomeric UvrD can be directly tested using single-molecule FRET experiments.

Regulation of UvrD activity by the 2B sub-domain

Formation of the active UvrD dimer on the DNA substrate shifts the 2B sub-domain of the lead UvrD to a more closed state (Nguyen et al. 2017). Furthermore, activation of the helicase activity of other UvrD-like helicases has also been correlated with a more closed conformation of the 2B sub-domain. RepD binding to the PcrA monomer-DNA complex is accompanied by closure of the PcrA 2B sub-domain (Arslan et al. 2015), and Rep monomer

turns into a highly processive helicase when the 2B sub-domain is covalently cross-linked in the closed form (Arslan et al. 2015). Based on these studies it was proposed that MutL might activate helicase activity of UvrD by modulating the rotational conformational state of the 2B sub-domain (Timothy M. Lohman, Tomko, and Wu 2008; Brendza et al. 2005; J. Y. Lee and Yang 2006). The rotational conformational state of the 2B sub-domain can be studied using genetically engineered double-cysteine UvrD mutant, UvrDΔCys(A100C,A473C), referred to as UvrD-DM-1B/2B, with cysteine residues in the 1B and 2B sub-domains (Jia et al. 2011). Cy3/Cy5 labeled UvrD-DM-1B/2B yields a high FRET signal in the closed state and low FRET signal in the open conformation which allows to monitor changes in the 2B sub-domain conformation using single-molecule or ensemble fluorescence methods (Jia et al. 2011; Comstock et al. 2015; Nguyen et al. 2017).

Chapter II

Activation of UvrD Helicase by a Processivity Factor MutL

Preface to the Chapter

In this chapter I describe the effect of MutL on UvrD helicase activity. Using a combination of single molecule FRET, single round stopped-flow DNA unwinding, and analytical ultracentrifugation experiments I showed definitively that MutL can activate the latent UvrD monomer helicase activity. Furthermore, single round DNA unwinding experiments with a series of DNA substrates with a varying 3' tail length showed that MutL also enhances UvrD dimer helicase activity beyond that is observed for a UvrD dimer alone. By measuring the extent of unwinding of DNA substrates with varying length of the duplex region I was able to demonstrate that the DNA unwinding processivity of MutL-UvrD monomer and MutL-UvrD dimer complexes are higher compared to UvrD dimer alone by 2- and 3-fold, respectively. This result indicates that MutL stimulates UvrD helicase activity by functioning as a processivity factor. Furthermore, I show that a single MutL dimer is sufficient to activate the UvrD monomer helicase activity and that optimal activation of UvrD by MutL requires contacts between MutL and the 3' ssDNA tail. I also demonstrated that MutL fails to stimulate the *E. coli* Rep monomer helicase activity, indicating that simulation by MutL is specific to UvrD. This work has been published in the Journal of Molecular Biology.

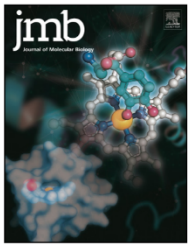

Regulation of UvrD Helicase Activity by MutL

Yerdos A. Ordabayev, Binh Nguyen, Anita Niedziela-Majka and Timothy M. Lohman

Department of Biochemistry and Molecular Biophysics, *Washington University School of Medicine, 660 S. Euclid Ave., Box 8231, St. Louis, MO 63110, United States*

Correspondence to Timothy M. Lohman: *lohman@biochem.wustl.edu*
https://doi.org/10.1016/j.jmb.2018.08.022
Edited by M Gottesman

Abstract

Escherichia coli UvrD is a superfamily 1 helicase/translocase involved in multiple DNA metabolic processes including methyl-directed mismatch DNA repair. Although a UvrD monomer can translocate along single-stranded DNA, a UvrD dimer is needed for processive helicase activity *in vitro*. *E. coli* MutL, a regulatory protein involved in methyl-directed mismatch repair, stimulates UvrD helicase activity; however, the mechanism is not well understood. Using single-molecule fluorescence and ensemble approaches, we find that a single MutL dimer can activate latent UvrD monomer helicase activity. However, we also find that MutL stimulates UvrD dimer helicase activity. We further find that MutL enhances the DNA-unwinding processivity of UvrD. Hence, MutL acts as a processivity factor by binding to and presumably moving along with UvrD to facilitate DNA unwinding.

Introduction

The DNA-unwinding and translocase activities of superfamily 1 (SF1) and SF2 helicases can be regulated by the assembly state of the enzyme as well as through interactions with accessory proteins [1]. As isolated enzymes, they display helicase and translocase activities *in vitro*; however, these enzymes rarely function in isolation *in vivo* but often function as components of larger molecular complexes that catalyze a wide range of processes in DNA metabolism. Therefore, investigation of the interactions between helicases and their accessory proteins is needed to fully understand how they operate and are regulated *in vivo*.

Escherichia coli UvrD is a prototypical SF1A DNA helicase/translocase involved in DNA repair [2,3], replication [4–7], and recombination [8–10]. UvrD protein can self-associate into dimers and tetramers [11], and its assembly state regulates its properties. A UvrD monomer can processively and rapidly translocate in a 3′ to 5′ direction along single-stranded (ss) DNA but has little to no helicase activity *in vitro* [12–15] unless a force is applied to the DNA [16]. In the absence of accessory proteins, formation of at least a UvrD dimer is required to processively unwind duplex DNA *in vitro* [12–19]. The monomeric forms of the structurally homologous SF1 helicases, *E. coli* Rep and *Bacillus stearothermophilus* PcrA, are also processive single-stranded DNA (ssDNA) translocases [20–23] and also display little helicase activity *in vitro* [22–24]. Activation of Rep and PcrA helicase activities also requires either self-assembly [22,24,25] or interaction with accessory proteins [26].

E. coli MutL protein plays a key role in methyl-directed mismatch repair of DNA [27–30]. MutL interacts with UvrD [31] and stimulates its helicase activity in multiple-turnover [29,32] DNA-unwinding reactions. Although MutL was shown to stimulate UvrD-catalyzed unwinding of both 20-base-pair (bp) and 92-bp partial duplex DNA under single-round conditions such that additional UvrD could not re-initiate on the DNA, it was proposed that MutL functions by continually loading multiple UvrD molecules onto a DNA substrate without affecting its unwinding processivity [32]. Furthermore, the potential effects of UvrD assembly state were not considered in previous studies [32].

Using single-molecule fluorescence and ensemble experiments, we show here that a single MutL

dimer can activate the latent helicase activity of a UvrD monomer as well as stimulate the activity of a UvrD dimer. We further show that MutL does increase the DNA-unwinding processivity of UvrD monomers and dimers indicating, that MutL remains in complex with UvrD as it moves along the DNA.

Results

MutL activates the helicase activity of a UvrD monomer

To determine whether MutL can activate DNA unwinding by a UvrD monomer, we performed single-molecule fluorescence resonance energy transfer (smFRET) DNA-unwinding experiments [33] using total internal reflection fluorescence (TIRF) microscopy. A UvrD variant containing a biotin–avidity tag on its N-terminus was used to attach it to a polyethylene glycol surface *via* a biotin–neutravidin linkage (Fig. 1a). The attachment of UvrD to the surface was performed at low UvrD concentrations (250 pM) to ensure that only UvrD monomers were immobilized on the surface. At this concentration, the fraction of UvrD dimers in solution is less than 0.1% [11]. As a further check, when immobilization was performed with Cy3-labeled UvrD, only single photobleaching events were observed indicating the absence of dimers. To examine DNA unwinding, we used a DNA substrate (DNA I) with an 18-bp duplex and a 3′-$(dT)_{20}$ tail labeled with a fluorescent donor (Cy3) and acceptor (Cy5) at opposite ends of the duplex (Fig. 1a). Binding of a single DNA molecule to a UvrD monomer on the surface can be observed as the sudden appearance of a fluorescence signal. DNA unwinding is expected to be accompanied by an increase in Cy5 fluorescence and an anti-correlated decrease in Cy3 fluorescence [34], followed by acceptor strand release (Cy5 fluorescence disappearance and Cy3 fluorescence

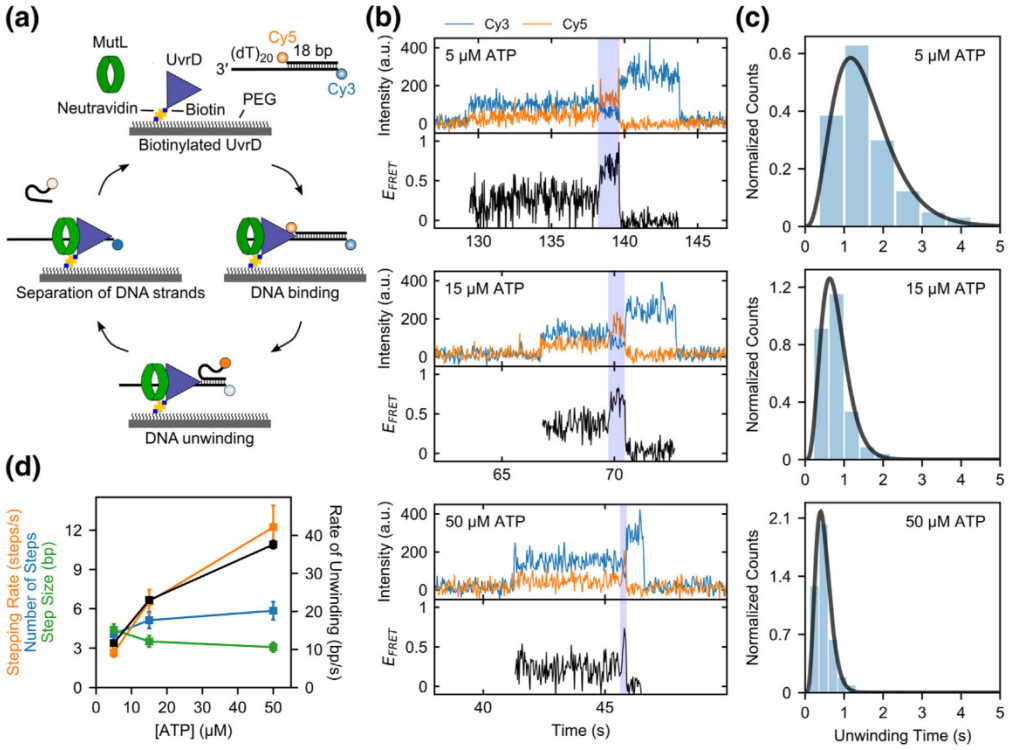

Fig. 1. Activation of UvrD monomer helicase by MutL. (a) Cartoon showing the steps in a single-molecule DNA-unwinding event. (b) Examples of single-molecule time traces for UvrD monomer unwinding of 1 nM DNA in the presence of 50 nM MutL dimer at varying ATP concentrations (5, 15, and 50 μM) in imaging buffer at 25 °C. (c) Histograms of the DNA-unwinding time durations and the best fits (black lines) to a gamma distribution (see Eq. (1)) at three ATP concentrations (5, 15, and 50 μM). (d) Best-fit values of the DNA-unwinding parameters with standard errors shown as error bars.

increase) and then donor strand release (loss of Cy3 fluorescence) upon complete unwinding (Fig. 1a).

Upon the addition of DNA (1 nM) and ATP (5 μM) to the surface immobilized UvrD monomers in imaging buffer at 25 °C, we observe DNA binding but little DNA unwinding (<2%) (2/112) (Supplementary Fig. 1a). This is consistent with previous studies indicating that UvrD monomers are unable to processively unwind even an 18-bp duplex DNA [12–15,18,19]. A rate constant for dissociation of DNA from a UvrD monomer of $k_d = 0.054 \pm 0.002\ s^{-1}$ was determined from analysis of the dwell times of DNA bound to UvrD (Supplementary Fig. 1b), which is consistent with a previous upper limit estimate of 0.12 s^{-1} determined from ensemble kinetic studies [12].

However, when an excess of MutL (50-nM dimer) was added along with DNA (1 nM) and ATP in imaging buffer, a significant number of DNA-unwinding events were observed (Fig. 1b). The percentage of DNA molecules unwound was 33% (251/767) at 5 μM ATP, 42% (333/789) at 15 μM ATP, and 36% (310/854) at 50 μM ATP. The time duration of each DNA-unwinding event (highlighted in blue in Fig. 1b) was measured as the time interval from the start of the increase in E_{FRET} to the loss of Cy5 signal (acceptor strand release). The mean unwinding duration time, $\bar{t}$, decreases with increasing ATP concentration (Fig. 1c and Table 1), as expected for DNA unwinding. We analyzed the DNA-unwinding time durations using the *n*-step sequential unwinding model in Supplementary Scheme 1 (Eq. (1)) to determine the stepping rate, *k*, and the number of steps, *n*, from which the unwinding rate, *r* (bp/s) and step size, *m*, can be calculated. The best-fit kinetic parameters were determined as described by Neuman *et al.* [35] using a maximum likelihood estimation analysis (Table 1 and Fig. 1d). As expected, the stepping rates, *k*, and unwinding rates, *r*, increase with increasing ATP concentration, while the number of steps, *n*, and step sizes, *m*, are relatively constant. The unwinding rates measured for UvrD monomer in the presence of MutL are similar to the unwinding rates determined for UvrD dimer previously [13,15,19,36]. These results demonstrate that the latent helicase activity of a UvrD monomer can be activated through interaction with the MutL protein.

MutL relieves DNA substrate inhibition of UvrD-catalyzed DNA unwinding

The specific activity of UvrD-catalyzed DNA unwinding *in vitro* shows inhibition when the [DNA] exceeds the [UvrD] [13]. This results from the fact that as the total [DNA] exceeds the total [UvrD], the population of UvrD monomers bound to DNA increases, while the UvrD dimer–DNA population decreases. Since UvrD monomers show no helicase activity *in vitro*, the specific helicase activity decreases with increasing [DNA] [11,13]. Based on the observation that MutL can activate UvrD monomer helicase activity, we examined whether MutL can eliminate this DNA substrate inhibition. DNA unwinding was monitored under single-round conditions using an "all or none" fluorescence stopped-flow DNA-unwinding assay [36,37] in buffer T at 25 °C (Fig. 2a). For this, we used an 18-bp duplex DNA (DNA II) containing a 3′-$(dT)_{20}$ tail with a Cy5 fluorophore attached to the long strand and Black Hole Quencher 2 (BHQ2) attached to the short strand. When in close proximity, BHQ2 quenches Cy5 fluorescence [38]; hence, DNA strand separation is accompanied by an increase in Cy5 fluorescence. DNA unwinding was initiated by mixing preformed UvrD–DNA or MutL–UvrD–DNA complexes with buffer T containing 1 mM ATP, 2 mM $MgCl_2$, and 2 μM protein trap. The protein trap, a 10-bp DNA hairpin (DNA X) possessing a 3′-$(dT)_{40}$ ssDNA tail, binds to any free UvrD or UvrD that dissociates during unwinding, thus preventing any re-initiation of DNA unwinding (see Supplementary Fig. 2) and ensuring that any unwinding is due to UvrD that is pre-bound to the DNA (single-round conditions).

We first performed single-round DNA-unwinding experiments in the presence of a 2.5-fold excess of DNA (125 nM) over UvrD (50 nM) with and without MutL. The resulting DNA-unwinding time courses (Fig. 2b) display the expected lag phase due to the fact that UvrD-catalyzed DNA unwinding occurs in multiple steps with similar rate constants, resulting in the formation of partially unwound intermediates prior to complete unwinding of double-stranded (ds) DNA [13,36,37]. We note that MutL alone does not support DNA unwinding (Fig. 2b). In the absence of MutL, <2% of the DNA substrate was unwound by UvrD (Fig. 2b), likely due to the small percentage of

Table 1. Kinetic parameters for MutL activated DNA unwinding by UvrD monomers

[ATP]	$\bar{t}$ (s)	*n* (steps)	*k* (s^{-1})	$m = L/n$ (bp/step)	$r = L/\bar{t}$ (bp/s)
5 μM	1.54 ± 0.05	4.1 ± 0.4	2.6 ± 0.3	4.4 ± 0.4	11.7 ± 0.4
15 μM	0.78 ± 0.02	5.1 ± 0.6	6.7 ± 0.9	3.5 ± 0.4	23.0 ± 0.7
50 μM	0.48 ± 0.01	5.9 ± 0.7	12.2 ± 1.7	3.1 ± 0.4	37.6 ± 1.1

Best-fit parameters (best fit ± s.e.) determined from maximum-likelihood estimation analysis (see Methods) of the data in Fig. 1c to Supplementary Scheme 1 (Eq. (1)).

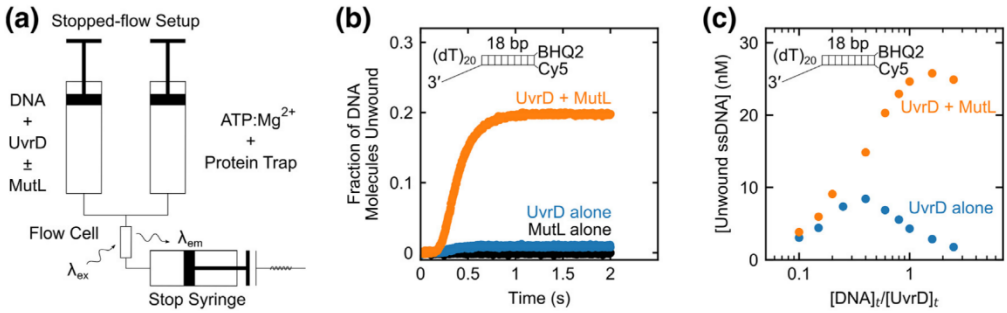

Fig. 2. DNA substrate inhibition of UvrD-catalyzed DNA unwinding is relieved by MutL. (a) Schematic of the stopped-flow DNA-unwinding experiment. In one syringe, UvrD is pre-incubated with DNA labeled with Cy5 and BHQ2, with or without MutL in buffer T at 25 °C. UvrD–DNA–(±MutL) complex is rapidly mixed with ATP, $MgCl_2$, and a protein trap to initiate DNA unwinding. DNA strand separation is accompanied by an enhancement in Cy5 fluorescence signal. (b) DNA-unwinding time courses from experiments performed at 125 nM 3′-$(dT)_{20}$-ds18-BHQ2/Cy5 with 50 nM UvrD alone (blue), 625 nM MutL dimer alone (black), or 50 nM UvrD plus 625 nM MutL dimer (orange). (c) Multiple DNA-unwinding experiments were performed at constant 50 nM UvrD over a range of DNA concentrations in the presence (orange circles) or in the absence (blue circles) of saturating MutL (5-fold molar excess of MutL dimer over DNA), and the total unwinding amplitudes were plotted as a function of $[DNA]_t/[UvrD]_t$.

UvrD dimers present. However, at saturating MutL concentrations (625-nM dimer) (see Supplementary Fig. 3a, b) the same concentration of UvrD unwound ~20% of the DNA substrate (Fig. 2b). We note that in the Tris buffer that we used for the DNA-unwinding studies performed above MutL exists as a mixture of dimers and higher oligomeric species [39].

Next, we performed a series of single-round experiments at constant total UvrD concentration (50 nM) as a function of increasing DNA substrate concentration in the presence and absence of saturating MutL (Fig. 2c). With UvrD alone, we observe the expected DNA substrate inhibition. However, this DNA substrate inhibition is eliminated when excess MutL is included with UvrD. The amount of unwound ssDNA increases with increasing DNA substrate concentration until a plateau is reached at $[DNA]_t/[UvrD]_t \cong 0.8$. These results support the conclusion that MutL stably activates the helicase activity of a UvrD monomer.

3′ ssDNA tail requirements for formation of a productive MutL–UvrD complex

We next investigated the effect of 3′ ssDNA tail length on MutL stimulation of UvrD monomer helicase activity. Single-round stopped-flow DNA-unwinding experiments were performed using DNA substrates (DNA II) with an 18-bp duplex and varying 3′-$(dT)_N$ tail lengths from N = 6 to 40 nt. By performing experiments in the presence of saturating MutL (625-nM dimer) and in DNA excess (125 nM) over UvrD (50 nM), we ensure that DNA molecules bind only one UvrD monomer. The time courses of DNA unwinding and the dependence of the total unwinding amplitudes on 3′ ssDNA tail length, N, are shown in Fig. 3a and b, respectively. No unwinding is detected for DNA substrates with $N \leq 8$, whereas a sharp increase in DNA-unwinding amplitude is observed for 3′ ssDNA tail lengths from 10 to 14 nt, with no further increase in amplitude for $N > 14$ nt.

Crystal structures of UvrD monomer in complex with partial duplex DNA suggest that UvrD contacts ~5 nt on the 3′ ssDNA tail [40]. Unwinding competition experiments indicate that UvrD shows some specificity for a 3′ ssDNA/dsDNA junction with 3′ tail lengths as short as $N = 4$ nt [13]. Thus, if MutL does not require any contact with the ssDNA tail, we would expect to detect unwinding of DNA substrates with 3′ ssDNA tail lengths as short as $N = 4$–8 nt. Hence, the results above suggest that MutL interacts with at least some portion of the 3′ ssDNA tail in order to activate a UvrD monomer.

MutL stimulates the helicase activity of a UvrD dimer

We next examined the effect of MutL over a range of UvrD and DNA concentration ratios that will populate both UvrD monomers and dimers on the DNA [11–13]. Single-round stopped-flow DNA-unwinding experiments were performed at constant DNA concentration (50 nM) as a function of UvrD concentration with and without MutL. The fraction of DNA molecules unwound is plotted as a function of UvrD to DNA ratio for UvrD alone (Fig. 3c) or UvrD plus saturating MutL (250-nM dimer) (Fig. 3d). For UvrD alone, no unwinding is observed for DNA substrates with $N < 12$ nt since a 3′ ssDNA tail with $N \geq 12$ nt is needed to form a stable UvrD dimer–DNA complex [13]. In contrast, in the presence of MutL, UvrD can unwind DNA substrates with 3′ tail lengths as short as 10 nt (Fig. 3d) since a 10-nt tail is

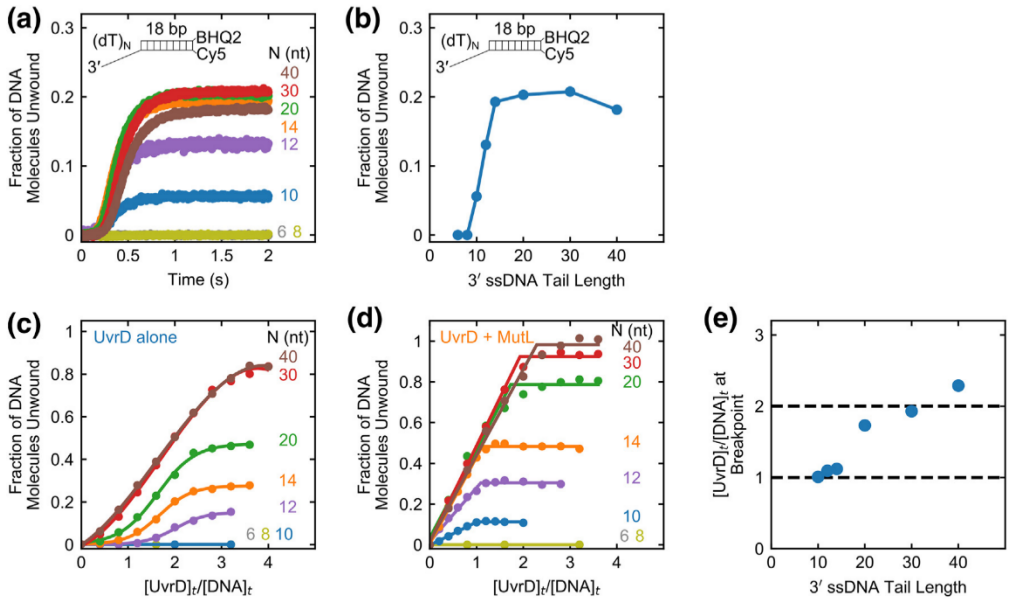

Fig. 3. Effect of 3′ ssDNA tail length on the stimulation of UvrD monomer helicase by MutL. (a) Stopped-flow DNA-unwinding time courses monitoring Cy5 fluorescence performed at 50 nM UvrD, 625 nM MutL dimer, and 125 nM 3′-$(dT)_N$-ds18-BHQ2/Cy5, with the indicated 3′-ssDNA tail lengths, *N* in nucleotides. (b) The total unwinding amplitude plotted as a function of 3′ ssDNA tail length (*N*). (c, d) The fraction of DNA molecules unwound, obtained under stoichiometric-binding conditions, is plotted as a function of the ratio of $[UvrD]_t/[DNA]_t$ for a series of stopped-flow experiments with DNA of the indicated 3′-$(dT)_N$. Experiments were performed by varying the [UvrD] for a constant DNA concentration (50 nM) with (c) UvrD alone or (d) UvrD plus 250 nM MutL dimer. (e) Breakpoints from the plots in panel d are plotted as a function of 3′ ssDNA tail length (*N*).

sufficient to stabilize a MutL–UvrD monomer–DNA complex consistent with the single-molecule and stopped-flow experiments discussed above.

In the absence of MutL, the amplitudes of DNA unwinding display a sigmoidal dependence on $[UvrD]_t/[DNA]_t$ with a breakpoint at $[UvrD]_t/[DNA]_t \cong 2$–3 depending on the 3′-$(dT)_N$ length (Fig. 3c). This reflects the fact that DNA-unwinding activity requires at least a UvrD dimer bound per DNA substrate [13]. However, in the presence of MutL, the DNA-unwinding amplitudes increase linearly with $[UvrD]_t/[DNA]_t$ for each DNA substrate (Fig. 3d) with a breakpoint that increases from one UvrD per DNA for *N* = 10-, 12-, and 14-nt tails to two UvrD per DNA for *N* = 20-, 30-, and 40-nt tails (Fig. 3e). This indicates that on DNA substrates possessing 3′-$(dT)_N$ tails with *N* = 10, 12, or 14 nt, MutL activates a UvrD monomer. However, for DNA substrates possessing longer 3′-$(dT)_N$ tails of $N \geq 20$ nt, MutL can stimulate the helicase activity of a UvrD dimer. We note that MutL eliminates the DNA substrate inhibition for the DNA substrates that can accommodate a UvrD dimer (*N* = 30 and 40 nt).

MutL increases UvrD DNA-unwinding processivity

DNA unwinding catalyzed by UvrD dimers has limited processivity [16,36]. Since we have shown that MutL stimulates the helicase activity of UvrD monomers and dimers under single-round conditions, this suggests the formation of a stable UvrD–MutL complex that can move along the DNA, that is, that MutL might function as a processivity factor, keeping UvrD tethered to the DNA.

To test this hypothesis, we performed a series of single-round stopped-flow experiments on 50 nM DNA substrates (DNA II–VIII) with varying duplex lengths (*L* = 18, 21, 25, 32, 40, 50, and 80 bp) to measure the unwinding processivity of UvrD alone (160 nM) on 3′-$(dT)_{20}$ tailed DNA substrates (Fig. 4a), UvrD (160 nM) plus MutL (375 nM dimer) on 3′-$(dT)_{20}$ tailed DNA substrates (Fig. 4b), and UvrD (160 nM) plus MutL (375 nM dimer) on 3′-$(dT)_{14}$ tailed DNA substrates (Fig. 4c). Note that a shorter 3′-$(dT)_{14}$ tail is sufficient to bind only one UvrD monomer in the presence of MutL (see Fig. 3e). These time courses all display lag phases that increase with duplex length as expected for an “all or none” unwinding assay [36,37]. We analyzed the time courses (Fig. 4a–c) using the *n*-step sequential unwinding model in Supplementary Scheme 2 (Eq. (3)). The best fit parameters obtained from the non-linear least-squares (NLLS) analysis are given in Table 2.

The total DNA-unwinding amplitude decreases with increasing duplex length (Fig. 4d). We analyzed

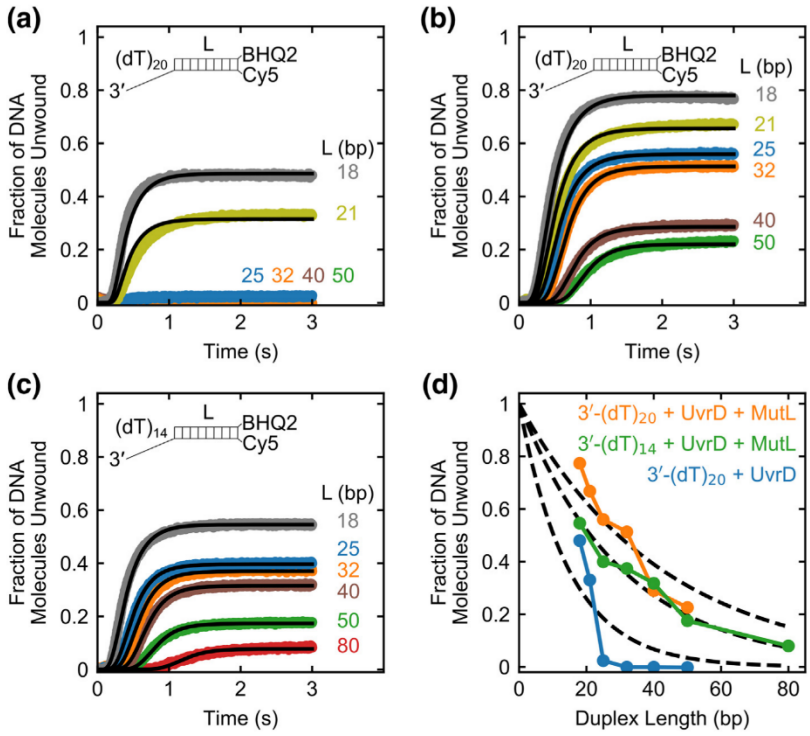

Fig. 4. MutL increases the processivity of UvrD-catalyzed DNA unwinding. Stopped-flow DNA-unwinding time courses monitoring Cy5 fluorescence are shown for a series of DNA substrates with the indicated duplex lengths, L (base pairs). (a) Experiments performed with 50 nM 3′-$(dT)_{20}$ tailed DNA substrates with 160 nM UvrD alone. (b) Experiments performed with 50 nM 3′-$(dT)_{20}$ tailed DNA substrates at 160 nM UvrD plus 375 nM MutL dimer. (c) Experiments performed with 50 nM 3′-$(dT)_{14}$ tailed DNA substrates at 160 nM UvrD plus 375 nM MutL dimer. Solid lines are simulations using Eq. (3) and best-fit parameters obtained from global NLLS analysis of the unwinding time courses (Table 2). (d) Fraction of DNA molecules unwound plotted as a function of duplex length (L) for 50 nM 3′-$(dT)_{20}$ tailed DNA with 160 nM UvrD alone (blue), 50 nM 3′-$(dT)_{20}$ tailed DNA with 160 nM UvrD plus 375 nM MutL dimer (orange), 50 nM 3′-$(dT)_{14}$ tailed DNA with 160 nM UvrD plus 375 nM MutL dimer (green). The dashed lines show the best fit of each data set to Eq. (4) with the values of processivity P in Table 2.

these data using Eq. (4), which assumes that DNA unwinding is catalyzed by a single monodisperse population of helicases to obtain estimates of the unwinding processivity, P, and the average number of DNA base pairs unwound per protein binding event, $\langle N_{bp} \rangle$, for UvrD alone and UvrD in complex with MutL (Table 2). This analysis indicates that UvrD in complex with MutL on the DNA substrates with either a 3′-$(dT)_{14}$ tail or 3′-$(dT)_{20}$ tail on average unwinds 2- to 3-fold more DNA base pairs compared to UvrD alone on 3′-$(dT)_{20}$ tailed DNA substrates (Table 2). The data for unwinding of DNA with a 3′-$(dT)_{14}$ tail show a good fit to Eq. (4) with $P = 0.910 \pm 0.003$. However, the fit for the DNA with a 3′-$(dT)_{20}$ tail is not as good. This may be due to the possible presence of a mixture of active UvrD species (UvrD dimers and UvrD dimer–MutL complexes), each of which may have different

Table 2. Kinetic parameters for DNA unwinding by UvrD alone and UvrD–MutL complexes

Sample	m (bp/step)	k_{obs} (s^{-1})	k_c (s^{-1})	mk_{obs} (bp/s)	P	$\langle N_{bp} \rangle$ (bp)
3′-$(dT)_{20}$ + UvrD	1.0 ± 0.2	78 ± 15	4.6 ± 0.1	80 ± 30	0.935 ± 0.012	15 ± 3
3′-$(dT)_{20}$ + UvrD + MutL	2.32 ± 0.05	29.5 ± 0.6	3.95 ± 0.02	68 ± 3	0.977 ± 0.002	42 ± 4
3′-$(dT)_{14}$ + UvrD + MutL	2.90 ± 0.05	26.9 ± 0.5	4.54 ± 0.02	78 ± 3	0.968 ± 0.001	31 ± 1

Best-fit parameters (best fit ± s.e.) determined from NLLS analysis (see Methods) of the data in Fig. 4a–c to Supplementary Scheme 2 (Eq. (3)).

processivities. Since these are single-round experiments that prevent re-binding of free UvrD, these results rule out a model in which MutL continuously loads free UvrD onto the DNA, but indicate that MutL serves to increase the DNA-unwinding processivity of UvrD.

A single MutL dimer activates a UvrD monomer

We next sought to determine how many MutL dimers are required to activate a UvrD monomer. For these experiments, we used analytical ultracentrifugation and stopped-flow fluorescence techniques to determine the minimum stoichiometry of a MutL–UvrD–DNA complex that shows DNA-unwinding activity. We performed these experiments in buffer M20/20, which is different from buffer T used in the experiments described above. We have previously shown that MutL exists as a mixture of dimers and higher oligomeric species in buffer T [39]. However, we have also shown that a MutL dimer is stable in buffer M20/20 that contains PO_4^{3-}, and this buffer inhibits formation of the higher oligomeric forms of MutL [39] (hydrodynamic properties of $MutL_2$ are shown in Supplementary Table 1). In buffer M20/20, one MutL dimer binds to one 3′-$(dT)_{20}$-ds18 DNA molecule with an apparent binding constant [39] $K = (3.4 \pm 0.4) \times 10^5$ M^{-1}. However, the DNA-unwinding activity of UvrD is lower in buffer M20/20 than in buffer T, which is why we used buffer T in the DNA-unwinding experiments described above.

Sedimentation velocity and equilibrium approaches were used to examine the stoichiometry of MutL–UvrD–DNA complexes in buffer M20/20 at 25 °C. We used an 18-bp duplex DNA (DNA IX) possessing a 3′-$(dT)_{10}$ tail which is short enough to allow binding of only one UvrD monomer to the DNA [13] (see also Fig. 3d). A partial specific volume of $\bar{\upsilon}_{DNA} = 0.563 \pm 0.002$ ml/g was measured for 3′-$(dT)_{10}$-ds18 DNA (DNA IX) by conducting sedimentation equilibrium experiments at 25 °C in buffer M20/20 (see Methods and Supplementary Fig. 4a). We used a UvrD variant, possessing a single Cys (UvrDΔCys-A100C) [41] that was labeled with Cy3. This UvrD-Cy3 variant retains both ssDNA translocase and DNA helicase activities [15,16]. Sedimentation velocity experiments of UvrD monitoring 555 nm (Supplementary Fig. 4b) showed a single symmetrical peak at 2.15 ± 0.02 S, the position of which was independent of concentration, indicating that UvrD was homogeneous and in a single assembly state. Sedimentation equilibrium experiments of UvrD-Cy3 (1 μM) at four rotor speeds (12, 15, 18, and 22k rpm) showed absorbance profiles that were well described by single exponentials (Fig. 5a). Initial analysis of the absorbance profiles using a partial specific volume for UvrD ($\bar{\upsilon}_{UvrD,calc} = 0.7308$ ml/g) calculated from its amino acid composition (see Methods) indicated molecular mass of 82.3 ± 1.2 kg/mol for UvrD-Cy3 consistent with monomeric UvrD-Cy3 (84.672 kg/mol). Using these sedimentation equilibrium data and constraining the molecular mass to the known value of 84.672 kg/mol for UvrD-Cy3 monomer, we estimated a more accurate partial specific volume ($\bar{\upsilon}_{UvrD-Cy3,\,exp} = 0.737 \pm 0.003$ ml/g) for the UvrD-Cy3 monomer in buffer M20/20 at 25 °C. Values of $s_{20,\,w}$ and f/f_0 for UvrD-Cy3 are given in Supplementary Table 1.

All remaining sedimentation experiments were performed in buffer M20/20 at 25 °C monitoring absorbance at 555 nm. At this wavelength, only the complexes that contain UvrD-Cy3 are detectable. Sedimentation velocity experiments were performed at four UvrD-Cy3 concentrations (0.6, 0.75, 0.85, and 1 μM) and a constant DNA concentration (1 μM). The resulting $c(s)$ distributions show a single symmetrical peak at 2.63 ± 0.02 S (Supplementary Fig. 4c), the position of which did not change with UvrD concentration, indicating a distinct UvrD–DNA species. A peak corresponding to free UvrD monomer (2.15 S) was absent, indicating that UvrD-Cy3 binds to the DNA stoichiometrically in buffer M20/20. To determine the molecular mass of the UvrD–DNA complex, we performed sedimentation equilibrium experiments with an equimolar mixture of UvrD-Cy3 (1 μM) and 3′-$(dT)_{10}$-ds18 (1 μM) at four rotor speeds (12, 15, 18, and 22k rpm). The absorbance profiles fit well to a single exponential (Fig. 5b) giving a best-fit molecular mass of 92.4 ± 1.4 kg/mol using a partial specific volume for the UvrD–DNA complex of 0.712 ml/g calculated as a weight average of the experimentally determined partial specific volumes of UvrD-Cy3 and 3′-$(dT)_{10}$-ds18 in buffer M20/20 at 25 °C. This molecular mass is consistent with, although slightly lower than, that expected for a UvrD monomer–DNA complex (98.717 kg/mol). By constraining the molecular mass of the complex to its known value, we calculated a partial specific volume, $\bar{\upsilon}_{UvrD-DNA,exp} = 0.727 \pm 0.003$ ml/g. Values of $s_{20,w}$ and f/f_0 for UvrD-Cy3–DNA complex are given in Supplementary Table 1.

We next performed sedimentation equilibrium experiments of a MutL–UvrD-Cy3–DNA complex using a 2.5-fold molar excess of MutL dimer (2.5 μM) over UvrD-Cy3 (1 μM) and 3′-$(dT)_{10}$-ds18 (1 μM) at four rotor speeds (9, 12, 15, and 18k rpm). The absorbance profiles were well described by a two-exponential fit (Fig. 5c) indicating the presence of two species containing UvrD-Cy3, with one species corresponding to UvrD-Cy3–DNA and the other to MutL–UvrD-Cy3–DNA. No improvement in the quality of the fit was obtained by including a third exponential. By constraining the molecular mass of the lower-molecular-weight species to that of the UvrD-Cy3 monomer–DNA complex (98.717 kg/mol), we obtained a best-fit value of 235 ± 6 kg/mol for the molecular mass of the MutL–UvrD-Cy3–DNA species using a weight average partial specific volume of 0.734 ml/g for $(MutL)_2$–UvrD–DNA

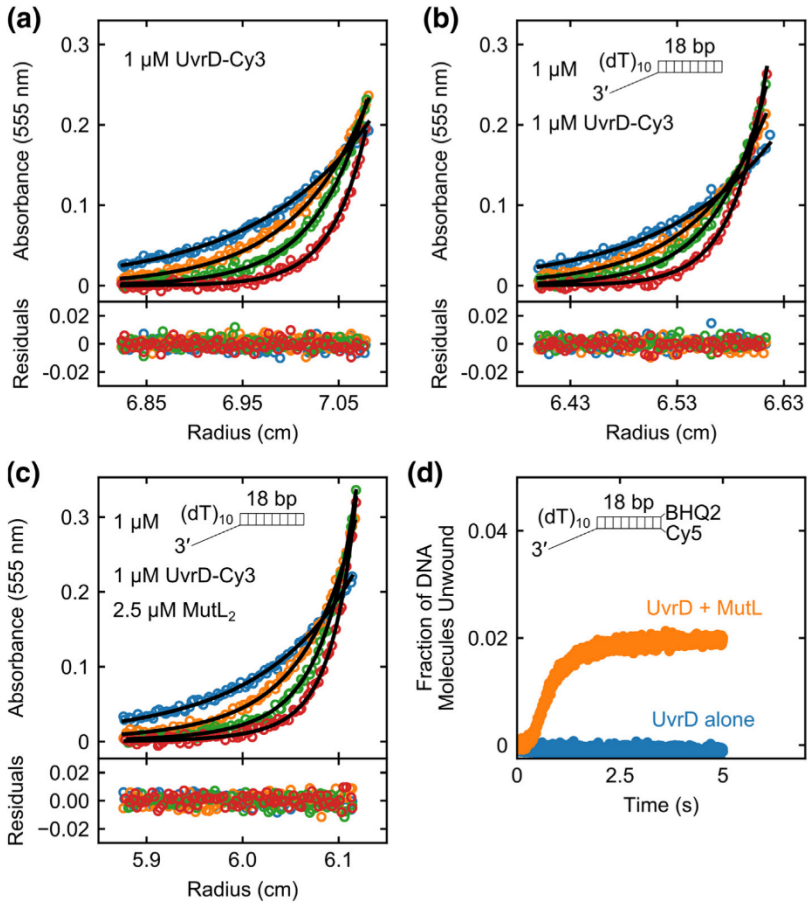

Fig. 5. A single MutL dimer can activate a UvrD monomer. Sedimentation equilibrium experiments monitoring the Cy3 absorbance of UvrD-Cy3 at 555 nm were performed in buffer M20/20 at 25 °C. (a) UvrD-Cy3 alone (1 μM) shows a single species corresponding to a monomer at four rotor speeds [12k rpm (blue); 15k rpm (orange); 18k rpm (green); 22k rpm (red)]. (b) UvrD-Cy3 (1 μM) plus 3′-$(dT)_{10}$-ds18 (1 μM) shows a single species corresponding to a UvrD-Cy3 monomer–DNA complex at four rotor speeds [12k rpm (blue); 15k rpm (orange); 18k rpm (green); 22k rpm (red)]. (c) UvrD-Cy3 (1 μM), 3′-$(dT)_{10}$-ds18 (1 μM), and MutL (2.5 μM dimer) mixture shows two species containing UvrD-Cy3 at four rotor speeds [9k rpm (blue); 12k rpm (orange); 15k rpm (green); 18k rpm (red)]. The two species correspond to a (UvrD-Cy3 monomer–DNA) complex and a (MutL dimer–UvrD-Cy3 monomer–DNA) complex. Smooth curves are simulations using best-fit parameters with residuals shown below the plots as described in the text. (d) Stopped-flow DNA-unwinding time courses with 100 nM 3′-$(dT)_{10}$-ds18-BHQ2/Cy5 DNA in buffer M20/20 at 25 °C were performed with 100 nM UvrD alone (blue) or 100 nM UvrD plus 250 nM MutL dimer (orange).

complex calculated from the partial specific volumes of UvrD-Cy3, $MutL_2$, and 3′-$(dT)_{10}$-ds18 in buffer M20/20 at 25 °C (see Methods and Supplementary Table 1). This molecular mass agrees well with the expected molecular mass for a MutL dimer–UvrD-Cy3 monomer–DNA complex (M = 234.540 kg/mol). Therefore, we conclude that the higher-molecular-mass species in buffer M20/20 contains only one MutL dimer and one UvrD-Cy3 monomer-bound to the DNA.

We next examined the DNA-unwinding activity associated with the $MutL_2$–UvrD–DNA complex at the same molar ratios (2.5:1:1) used in the sedimentation experiments under the identical solution conditions (buffer M20/20) at 25 °C. Based on the sedimentation experiments, this MutL–UvrD–DNA solution contains a mixture of DNA bound with a single UvrD monomer and DNA bound with a single UvrD monomer and a single MutL dimer. In single-round DNA-unwinding experiments performed at 100 nM 3′-$(dT)_{10}$-ds18-BHQ2/Cy5 (DNA II) pre-mixed with 100 nM UvrD plus 250 nM MutL dimer, we observe significant DNA unwinding (Fig. 5d). No DNA unwinding was detected in the absence of MutL

(Fig. 5d) consistent with there being no unwinding activity for the UvrD monomer–DNA complexes that are also present in the mixture. These results indicate that a single MutL dimer is sufficient to activate the helicase activity of a UvrD monomer.

MutL activation of UvrD helicase is specific

E. coli Rep is an SF1A helicase/translocase that shares ~40% sequence similarity with UvrD. Similar to UvrD, Rep monomers can translocate on ssDNA in an ATP-dependent manner (Supplementary Fig. 5a) but must form at least a dimer in order to activate its helicase activity [23–25,42] (Supplementary Fig. 5b). We therefore examined whether MutL is able to activate the helicase activity of a Rep monomer. These experiments were performed with an excess of DNA substrate over Rep so that no more than one Rep monomer is bound per DNA molecule [23]. Single-round unwinding experiments were performed using 50 nM 3′-$(dT)_{20}$-ds18-BHQ2/Cy5 (DNA II) and 25 nM Rep alone or 25 nM Rep plus 250 nM MutL dimer in buffer T at 25 °C (Supplementary Fig. 5c). No stimulation of Rep-catalyzed DNA unwinding by MutL was observed under these conditions, indicating that MutL stimulation is specific for UvrD reflecting a specific protein–protein interaction.

We next tested whether particular regions of UvrD are important for activation by MutL. The SF1A helicases, UvrD, Rep, and PcrA all possess a relatively disordered C-terminal tail that is the least conserved region among these helicases, and the C-terminal tail of UvrD has been reported to interact with MutL [31] as well as with RNA polymerase [43]. Hence, we examined UvrDΔ73 mutant, in which the last 73 C-terminal amino acids of UvrD are deleted, to see whether the C-terminal region of UvrD is important for activation by MutL. UvrDΔ73 retains helicase and ssDNA translocase activities [41], but monomeric UvrDΔ73 shows no helicase activity [11,13]. Surprisingly, MutL is able to activate the helicase activity of monomeric UvrDΔ73 (Supplementary Fig. 5d), indicating that the C-terminal tail of UvrD is not essential for activation by MutL.

Discussion

UvrD possesses both ssDNA translocase and DNA helicase activities and functions in multiple DNA metabolic processes *in vivo*. These include methyl-directed mismatch DNA repair [2], nucleotide excision repair [3], replication restart [4,5,7,44], recombination to remove RecA filaments from DNA [9,10], and transcriptional control through interactions with RNA polymerase [45–47]. Although it is often assumed that the DNA helicase activity of UvrD is required for all of these functions, this is not necessarily true. For some functions, it may be that ssDNA translocase activity alone is sufficient as in its role to displace RecA filaments from ssDNA [1,10,48,49]. Hence, it is of interest to understand how helicase activity *versus* ssDNA translocase activity might be regulated. In this regard, it has been shown that functioning by itself *in vitro*, UvrD monomers are capable of rapid and processive ssDNA translocation but are ineffective as DNA helicases, requiring dimerization for helicase activation [11–14,19]. Hence, UvrD self-assembly is one way to separate and thus regulate its helicase and translocase activities. Such regulation is likely important *in vivo* since an unregulated helicase would likely be detrimental to the cell. In bacteria, UvrD-like helicases generally function as components of larger molecular machines [1,26,30,50,51]. Therefore, it is important to understand how these cellular partners regulate the various activities of UvrD.

MutL activates the UvrD monomer helicase and stimulates the UvrD dimer helicase

We show here that the latent UvrD monomer helicase activity can be activated through specific interactions with the accessory protein MutL. Although activation of UvrD helicase activity *in vitro* requires dimerization [1,11–13,16,17,19], monomers of UvrD-like helicases contain all that is needed for helicase activity but are auto-inhibited and require activation. Evidence for that comes from the studies of Rep and PcrA helicases. Activation of Rep monomer helicase activity can be accomplished through deletion of its 2B sub-domain [23,42] or covalent crosslinking of the 2B sub-domain in a closed conformation [34]. Monomeric PcrA can be activated through interaction with an accessory protein, RepD [26]. In addition, limited helicase activity (<20 bp) has been observed for UvrD monomers when the DNA is under tension [16]. Interestingly, we find that MutL also stimulates the activity of UvrD dimers beyond that observed for UvrD dimers on their own [12,13,17]. Hence, the possibility remains that both UvrD monomers and dimers might both have functional roles *in vivo*.

MutL stimulation of UvrD is specific since we show here that MutL does not activate a Rep monomer, although Rep is similar in structure to UvrD. This is consistent with previous multiple turnover unwinding studies [29]. The main regions that differ between Rep and UvrD are the C-terminal disordered tails and the 2B sub-domain. Based on yeast two-hybrid system experiments, it was suggested that the C-terminal domain of MutL and both the N- and C-termini of UvrD are important for the interaction [31]. However, in our experiment, a truncated UvrDΔ73 mutant lacking its C-terminal tail was activated by MutL, indicating that the unstructured C-terminal tail of UvrD is dispensable for this activity. Interestingly, in an analogous way, it was reported that the C-terminal tail of UvrD interacts with UvrB, but the truncated UvrDΔ73 version is still functional in nucleotide excision repair [52].

MutL functions as a processivity factor

Our single-round DNA-unwinding studies demonstrate that MutL increases the DNA-unwinding processivity of UvrD, although this increase is moderate (2- to 3-fold increase; see Table 2). Such an increase can be explained by an increase in the rate of unwinding, mk_{obs}, and/or a decrease in the dissociation rate, k_d, of UvrD from DNA (Eq. (5)). Our results indicate that activation of UvrD monomer by MutL does not significantly affect the rate of unwinding compared to UvrD dimers [13,15,19,36] (Tables 1 and 2), suggesting that MutL acts to decrease the dissociation rate of UvrD from DNA. We infer from these results that MutL moves along the DNA in a complex with UvrD during unwinding, although we lack direct evidence for this. MutL is known to bind DNA with a preference for ssDNA [32,39,53–55]. Based on the effects of 3′ ssDNA tail length, it appears that MutL requires contacts with the 3′ ssDNA tail of the DNA in order to form a productive complex with a UvrD monomer on the DNA. We also show that a single MutL dimer is sufficient to activate UvrD monomer helicase activity. MutL is comprised of a C-terminal dimerization domain [54] and an N-terminal ATPase domain which dimerizes upon ATP binding [53,56]. Dimerization of the N-terminal domain leads to formation of a cavity in the MutL dimer, which can allow it to encircle the DNA substrate. Based on these observations, we propose a model where MutL clamps around the DNA and moves with UvrD during DNA unwinding.

In previous studies, Mechanic *et al.* [32] concluded that MutL functions to continually load multiple UvrD molecules onto a DNA substrate rather than to increase the DNA-unwinding processivity of UvrD. A key experiment in their study involved the addition of a protein trap 30 s after initiation of multiple turnover unwinding of 148-bp blunt duplex DNA. This trap caused a cessation of further DNA unwinding. The authors argued that if MutL increased processivity then DNA unwinding would continue due to any UvrD that was already bound to the DNA. However, this would occur only if the processivity of unwinding were much greater than the moderate increase that we observe in our experiments. We also note that the rate-limiting step in such multiple turnover unwinding of fully duplex DNA is the rate of initiation and not the rate of unwinding [57]. The actual rate of unwinding is relatively fast (on average it takes ~2 s to unwind a 148-bp duplex DNA). Therefore, even though MutL increases UvrD processivity, addition of a trap would still inhibit unwinding re-initiation and thus any detectable unwinding. Hence, our observations and those of Mechanic *et al.* [32] appear to be consistent.

The limited DNA-unwinding processivity of an MutL–UvrD complex might be explained by a molecular switch model proposed for MutL where the DNA binding affinity of MutL is modulated by ATP binding and ATP hydrolysis [53,55,58]. The processivity of this complex would be limited by the slow ATP hydrolysis rate of MutL. Notably, an MutL–E29A mutant that binds but does not hydrolyze ATP was shown to have greater stimulatory effect on UvrD compared to wild-type MutL [58] consistent with this interpretation.

In mismatch repair, UvrD initiates DNA unwinding from a nick and proceeds past the mismatch, which can be as far removed as 1–2 kb in length [27]. The moderate increase in the DNA-unwinding processivity of UvrD that we observe in the presence of MutL is inadequate to fully account for the unwinding of such long stretches of DNA. Hence, the processivity of UvrD may be further enhanced through interactions with other proteins, such as MutS. It was shown that MutS and MutL enhance unwinding of a nicked DNA by UvrD in the presence of a mismatch [29]. Furthermore, it was shown that MutS, MutL, and mismatch-dependent unwinding by UvrD starts at the nick and unwinding is biased toward the shorter path between the nick and the mismatch [27], suggesting that helicase activity of UvrD can be influenced by multiple proteins.

It has been shown that homologous recombination is inhibited by DNA mismatch repair [59], which requires MutL and UvrD. It has also been reported that MutL and MutS [60], as well as UvrD [46] are required for transcription-coupled repair of DNA, and it has been suggested that UvrD facilitates RNA polymerase backtracking during transcription-coupled repair [46]. Hence, it is possible that MutL activation of UvrD helicase activity might also play a role in these processes.

Methods

Buffers and reagents

Buffers were prepared with reagent grade chemicals using distilled, deionized (Milli-Q system; Millipore Corp., Bedford, MA) water. Spectrophotometric grade glycerol was from Alfa Aesar (Ward Hill, MA). Buffer T is 10 mM Tris–HCl (pH 8.3) at 25 °C, 20 mM NaCl, 20% (v/v) glycerol, and 1 mM 2-mercaptoethanol. Buffer M20/20 is 40.5 mM K_2HPO_4, 9.5 mM KH_2PO_4 (pH 7.4 at 25 °C), 20 mM NaCl, 20% (v/v) glycerol, and 1 mM 2-mercaptoethanol. Imaging buffer is 10 mM Tris–HCl (pH 8.3) at 25 °C, 20 mM NaCl, 20% (v/v) glycerol, 2 mM $MgCl_2$, 3 mM Trolox, 0.8% (w/v) dextrose, 20 units/ml glucose oxidase, and 20 units/ml catalase. ATP concentrations were determined spectrophotometrically using an extinction coefficient of $\varepsilon_{259} = 15.4 \times 10^3\ M^{-1}\ cm^{-1}$.

Proteins

MutL protein was expressed and purified as described [39]. Concentrations of MutL monomer were

determined spectrophotometrically in 20 mM Tris–HCl (pH 7.5) at 25 °C, 6 M Gdn-HCl using extinction coefficient of $\varepsilon_{280} = 5.39 \times 10^4\ M^{-1}\ cm^{-1}$. MutL protein was stored in buffer M [40.5 mM K_2HPO_4, 9.5 mM KH_2PO_4 [pH 7.4 at 25 °C], 50 mM KCl, 0.1 mM EDTA, 1 mM 2-mercaptoethanol] at −80 °C. wtUvrD, biotin–UvrD, UvrDΔCys(A100C), and UvrDΔ73 were expressed and purified as described previously [19,41,61]. The UvrD monomer concentrations were determined spectrophotometrically in 10 mM Tris (pH 8.1), 200 mM NaCl, 20% (v/v) glycerol using an extinction coefficient of $\varepsilon_{280} = 1.06 \times 10^5\ M^{-1}\ cm^{-1}$. The UvrD protein was stored in minimal storage buffer [20 mM Tris–HCl (pH 8.3 at 25 °C), 200 mM NaCl, 50% (v/v) glycerol] at −20 °C for up to 6 months without any loss of helicase activity. The single-cysteine variant UvrDΔCys(A100C) was labeled with Cy3 maleimide (GE Healthcare) [41]. The Cy3 labeling efficiency of UvrDΔCys(A100C) was around 70% and was determined spectrophotometrically using extinction coefficients of 150,000 $M^{-1}\ cm^{-1}$ at 550 nm for Cy3 dye. Rep protein was purified as described [62] and its concentration determined spectrophotometrically using $\varepsilon_{280} = 7.68 \times 10^4\ M^{-1}\ cm^{-1}$.

DNA

The oligodeoxynucleotides were synthesized using an ABI model 391 (Applied Biosystems, Foster City, CA), and purified as described [63]. The concentrations of DNA strands were determined by spectrophotometric analysis as described previously [64]. The oligonucleotide sequences of DNA strands used in these studies are given in Supplementary Table 2. DNA duplexes were prepared by mixing equimolar concentrations of two complementary strands in 10 mM Tris (pH 8.1) and 0.1 M NaCl, followed by heating to 95 °C for 5 min and slow cooling to room temperature in water bath.

Single-molecule total internal reflection fluorescence microscopy experiments

Single-molecule experiments were performed on an Olympus IX71 microscope (model IX2_MPI-TIRTL) as described [65,66]. Experiments were performed in imaging buffer at 25 °C. The Cy3 fluorophore was excited with a 532-nm laser, and the fluorescence emissions of Cy3 and Cy5 were recorded at a 32-ms resolution (30.3-ms exposure time) for 3–4 min on EM-CCD camera. The FRET efficiency was calculated from the ratio of corrected Cy3 and Cy5 signals as described [66,67].

The biotin–UvrD (20 μl of 250 pM) was immobilized onto the NeutrAvidin–polyethylene glycol surface for 5 min and then was washed to remove the excess of biotin–UvrD. Under this condition, UvrD is monomeric as confirmed from the fluorescence intensities and photobleaching steps. Unwinding reactions were initiated by flowing 1 nM DNA (DNA I), indicated concentration of ATP, 2 mM $MgCl_2$, and if necessary 50 nM MutL dimer in imaging buffer. Dwell times of DNA bound to a UvrD monomer were analyzed using one-step dissociation model described by the probability density function of an exponential distribution, $k_d e^{-k_d t}$, where k_d is the dissociation rate constant. To analyze the distribution of DNA-unwinding times, t, we used the simplest model presented in Supplementary Scheme 1, where the helicase proceeds through n irreversible rate-limiting steps to produce fully unwound ssDNA. This model is described by the probability density function of a gamma distribution [35,37] as given in Eq. (1):

$$F(t) = \frac{k^n t^{n-1} e^{-kt}}{\Gamma(n)}, \tag{1}$$

where k is the stepping rate and n is the number of steps. Fitting parameters were estimated utilizing maximum likelihood estimation method implemented in the Python `scipy.stats` module. Standard errors were estimated using a bootstrap method. The average unwinding rate is $r = L/\bar{t}$, where L is the duplex DNA length in bp and $\bar{t}$ is the average unwinding duration time and the kinetic step size is $m = L/n$.

Stopped-flow fluorescence experiments

All fluorescence stopped-flow experiments were carried out at 25 °C using an Applied Photophysics SX.18MV stopped-flow instrument (Applied Photophysics Ltd., Leatherhead, UK). DNA was preincubated with UvrD in buffer T for 5 min and then mixed with MutL if necessary and loaded into one syringe of the stopped-flow instrument. The solution of 1 mM ATP, 2 mM $MgCl_2$, and 2 μM of 10-bp DNA hairpin possessing a 3′-$(dT)_{40}$ ssDNA tail (DNA X) in buffer T was loaded into the other syringe of the stopped-flow instrument, and both solutions were incubated for an additional 5 min at 25 °C prior to mixing. Cy5 fluorophore was excited using 625-nm LED (Applied Photophysics Ltd.), and its fluorescence emission was monitored at wavelengths >665 nm using a long-pass filter (Oriel Corp., Stradford, CT). The kinetic traces shown represent an average of at least 10 individual measurements. Trap tests were carried out by including the DNA substrate with the ATP and DNA hairpin solution. When mixed with UvrD or UvrD plus MutL, no unwinding signal was observed, indicating that DNA hairpin trapped all of the free UvrD (Supplementary Fig. 2).

To quantify the fraction of DNA molecules unwound for each time point, $f_{ss}(t)$, the fluorescence signal, $S(t)$, was calibrated using Eq. (2):

$$f_{ss}(t) = \frac{S(t) - S_0}{S_{max} - S_0} \tag{2}$$

where S_0 is the baseline fluorescence immediately after addition of ATP and S_{max} is the maximum fluorescence signal determined by mocking unwinding reaction by using DNA strand with Cy5 fluorophore in the absence of BHQ2-modified complementary strand and all the other reaction components.

Single-round DNA-unwinding time courses were analyzed using Supplementary Scheme 2 described by Eq. (3) [37]:

$$f_{ss}(t) = A_T \mathcal{L}^{-1} F_{ss}(s) = A_T \mathcal{L}^{-1} \left(\frac{k_c k_{obs}^{L/m}}{s(k_c + s)(k_{obs} + s)^{L/m}} \right), \quad (3)$$

where $f_{ss}(t)$ is the fraction of ssDNA molecules formed, $F_{ss}(s)$ is the Laplace transform of $f_{ss}(t)$, $\mathcal{L}^{-1}$ is the inverse Laplace transform operator, s is the Laplace variable, A_T is the total DNA-unwinding amplitude, k_c is the rate constant for the additional step not involved in unwinding, k_u is the unwinding rate constant for n repeating steps, k_d is the dissociation rate constant, L is the duplex region length, m is the kinetic step size, $k_{obs} = k_u + k_d$ and $n = L/m$. Global NLLS fitting of the unwinding time courses was performed using Python `lmfit` module. The numerical inversion routine of the Laplace transform is based on Cody–Meinardus–Varga approximations of Talbot's method [68].

On the basis of the mechanism in Supplementary Scheme 2, the unwinding amplitude is described by Eq. (4) [37]:

$$A_T = \left(\frac{k_u}{k_u + k_d} \right)^{L/m} = P^L, \quad (4)$$

where the processivity of DNA unwinding, P, is the probability that the helicase will unwind the next base pair rather than dissociate from the DNA [37]. The processivity, P, is related to the average number of base pairs unwound, N_{bp}, by Eq. (5) [37]:

$$\langle N_{bp} \rangle = -\frac{1}{\ln(P)} \cong \frac{m(k_u + k_d)}{k_d} = \frac{m k_{obs}}{k_d} \quad (5)$$

where the approximation holds when $k_u \gg k_d$.

Experiments to examine Rep monomer translocation along ssDNA were performed in a stopped-flow apparatus as described [14,23]. Rep (50 nM) was pre-incubated with 5′-F-$(dT)_N$ ssDNA (100 nM) in buffer T for 5 min at 25 °C and then rapidly mixed with buffer T containing 1 mM ATP, 2 mM $MgCl_2$, and 8 mg/ml heparin. Fluorescein fluorescence was excited using a 490 nm LED (Applied Photophysics Ltd.), and its fluorescence emission was monitored at wavelengths >520 nm using a long-pass filter (Oriel Corp.). ssDNA translocation time courses were analyzed as described [23].

Analytical ultracentrifugation

Dialyzed proteins were clarified by centrifugation at 14,000 rpm for 15 min at 4 °C. Sedimentation equilibrium and velocity experiments were performed using a ProteomeLab XL-A analytical ultracentrifuge equipped with an An50Ti rotor (Beckman Coulter, Fullerton, CA) at 25 °C. Absorbance signal for Cy3 labeled UvrDΔCys(A100C) was collected by scanning the sample cells at 555-nm wavelength.

Samples for sedimentation equilibrium (110 μl) were loaded into the three channels of an Epon charcoal-filled six-channel centerpieces with 130 μl of buffer M20/20 in the reference chambers. Absorbance data were collected by scanning the sample cells at intervals of 0.003 cm in the step mode with 5 averages per step. Samples were sedimented to equilibrium at the indicated rotor speeds, starting with the lowest and finishing with the highest rotor speed. The baseline offset was determined by increasing the rotor speed to 42,000 rpm at the end of the run to pellet the solutes and then measuring the residual absorbance in the solution column.

The resulting absorbance profiles, A_r, were analyzed by using NLLS fitting to Eq. (6) as implemented in SEDPHAT [69],

$$A_r = \sum_{i=1}^{n} A_{r_0,i} \cdot \exp\left[M_i(1-\bar{u}_i\rho)\frac{\omega^2}{2RT}\left(r^2 - r_0^2\right)\right] + b_r, \quad (6)$$

where r is the distance from the center of rotation, r_0 is an arbitrary reference radius, ω is angular velocity, T is absolute temperature, R is the gas constant, M_i is the molecular mass of component i, $\bar{u}_i$ is partial specific volume of component i, ρ is buffer density, $A_{r_0,i}$ is the absorbance of component i at the reference position, and b_r is a radial-dependent baseline offset. Buffer density, ρ, was calculated from buffer composition using SEDNTERP [70]. Using the calculated partial specific volume of component i, the molecular mass of component i (M_i) can be estimated. Alternatively, a more accurate value of the partial specific volume of macromolecule i can be determined if the true molecular mass of the macromolecule is known and constrained.

Partial specific volumes for UvrD-Cy3 ($\bar{u}_{UvrD-Cy3} = 0.7308$ ml/g) and MutL ($\bar{u}_{MutL} = 0.7414$ ml/g) at 25 °C were calculated from the amino acid composition according to Eq. (7) using SEDNTERP [70] as well as the weight-average partial specific volumes for complexes:

$$\bar{u} = \frac{\left(\sum_{i=1}^{n} n_i M_i \bar{u}_i\right)}{\sum_{i=1}^{n} n_i M_i} \quad (7)$$

where M_i and $\bar{u}_i$ are the molecular mass and viscosity of component i.

In sedimentation velocity experiments, the sample (380 μl) and buffer (392 μl) were loaded into each sector of an Epon charcoal-filled two-sector centerpiece. Experiments were performed at 25 °C and 42,000 rpm. Absorbance data were collected by scanning the sample cells at intervals of 0.003 cm. The continuous sedimentation coefficient distribution, $c(s)$, was calculated using SEDFIT [71]. Calculated s values were converted to $s_{20,w}$ according to Eq. (8):

$$s_{20,w} = s_{\exp}\frac{\eta_{\exp}}{\eta_{20,w}}\left(\frac{1-\bar{\upsilon}_{20}\rho_{20,w}}{1-\bar{\upsilon}_{25}\rho_{\exp}}\right) \quad (8)$$

where $\rho_{20,w}$ and $\eta_{20,w}$ are density and viscosity of the water at 20 °C, $\rho_{\exp}$ and $\eta_{\exp}$ are density and viscosity of the buffer at 25 °C, and $\bar{\upsilon}_{20}$ and $\bar{\upsilon}_{25}$ are partial specific volumes of macromolecule at 20 °C and 25 °C. Buffer density, ρ, and viscosity, η, were calculated from buffer composition using SEDNTERP [70].

The ratio, f/f_0, of the frictional coefficient of the macromolecule, f, to the frictional coefficient of an unhydrated sphere of equivalent mass, f_0, was calculated using Eq. (9) [72]:

$$\frac{f}{f_0} = \left[\frac{M^2(1-\bar{\upsilon}\rho)^3}{162\pi^2 s^3\eta^3 N_A^2\bar{\upsilon}}\right]^{\frac{1}{3}} \quad (9)$$

where M and $\bar{\upsilon}$ are the molecular mass and partial specific volume of the macromolecule, η and ρ are the viscosity and density of the buffer, s is the measured sedimentation coefficient and N_A is Avogadro's number.

Acknowledgments

We thank Alex Kozlov and Eric Tomko for assistance, as well as all members of the Lohman laboratory for comments and suggestions, and Thang Ho for oligodeoxynucleotides. This work was supported by the National Institutes of Health (GM045948 to T.M.L).

Author Contributions: Y.A.O. and T.M.L. designed the experiments. Y.A.O. purified the protein; carried out the single-molecule TIRF, stopped-flow fluorescence, and analytical ultracentrifugation experiments; and analyzed the data. B.N. contributed to protein purification and single-molecule TIRF experiments. N.M.A. contributed to preliminary data and analytical ultracentrifugation experiments. T.M.L. supervised the study. Y.A.O. and T.M.L wrote the manuscript.

Competing Interests: The authors declare no competing interests.

Appendix A. Supplementary data

Supplementary data to this article can be found online at https://doi.org/10.1016/j.jmb.2018.08.022.

Received 5 June 2018;
Received in revised form 3 August 2018;
Accepted 23 August 2018
Available online 30 August 2018

Keywords:
DNA mismatch repair;
single-molecule fluorescence;
processivity;
protein assembly;
SF1A helicase

Current address: Gilead Sciences Inc., 333 Lakeside Drive, Foster City, CA 94404.

Abbreviations used:
ssDNA, single-stranded DNA; TIRF, total internal reflectance fluorescence.

References

[1] T.M. Lohman, E.J. Tomko, C.G. Wu, Non-hexameric DNA helicases and translocases: mechanisms and regulation, Nat. Rev. Mol. Cell Biol. 9 (2008) 391–401.
[2] R.R. Iyer, A. Pluciennik, V. Burdett, P.L. Modrich, DNA mismatch repair: functions and mechanisms, Chem. Rev. 106 (2006) 302–323.
[3] A. Sancar, DNA excision repair, Annu. Rev. Biochem. 65 (1996) 43–81.
[4] J. Atkinson, P. McGlynn, Replication fork reversal and the maintenance of genome stability, Nucleic Acids Res. 37 (2009) 3475–3492.
[5] R.C. Heller, K.J. Marians, Non-replicative helicases at the replication fork, DNA Repair (Amst) 6 (2007) 945–952.
[6] C. Bruand, S.D. Ehrlich, UvrD-dependent replication of rolling-circle plasmids in *Escherichia coli*, Mol. Microbiol. 35 (2000) 204–210.
[7] M.J. Flores, N. Sanchez, B. Michel, A fork-clearing role for UvrD, Mol. Microbiol. 57 (2005) 1664–1675.
[8] H.M. Arthur, R.G. Lloyd, Hyper-recombination in uvrD mutants of *Escherichia coli* K-12, Mol Gen Genet 180 (1980) 185–191.
[9] X. Veaute, S. Delmas, M. Selva, J. Jeusset, E. Le Cam, I. Matic, et al., UvrD helicase, unlike Rep helicase, dismantles RecA nucleoprotein filaments in *Escherichia coli*, EMBO J. 24 (2005) 180–189.
[10] V. Petrova, S.H. Chen, E.T. Molzberger, E. Tomko, S. Chitteni-Pattu, H. Jia, et al., Active displacement of RecA filaments by UvrD translocase activity, Nucleic Acids Res. 43 (2015) 4133–4149.
[11] N.K. Maluf, T.M. Lohman, Self-association equilibria of *Escherichia coli* UvrD helicase studied by analytical ultracentrifugation, J. Mol. Biol. 325 (2003) 889–912.
[12] N.K. Maluf, J.A. Ali, T.M. Lohman, Kinetic mechanism for formation of the active, dimeric UvrD helicase–DNA complex, J. Biol. Chem. 278 (2003) 31930–31940.

[13] N.K. Maluf, C.J. Fischer, T.M. Lohman, A dimer of *Escherichia coli* UvrD is the active form of the helicase in vitro, J. Mol. Biol. 325 (2003) 913–935.
[14] C.J. Fischer, N.K. Maluf, T.M. Lohman, Mechanism of ATP-dependent translocation of *E. coli* UvrD monomers along single-stranded DNA, J. Mol. Biol. 344 (2004) 1287–1309.
[15] K.S. Lee, H. Balci, H. Jia, T.M. Lohman, T. Ha, Direct imaging of single UvrD helicase dynamics on long single-stranded DNA, Nat. Commun. 4 (2013) 1878.
[16] M.J. Comstock, K.D. Whitley, H. Jia, J. Sokoloski, T.M. Lohman, T. Ha, et al., Protein structure. Direct observation of structure–function relationship in a nucleic acid-processing enzyme, Science 348 (2015) 352–354.
[17] J.A. Ali, N.K. Maluf, T.M. Lohman, An oligomeric form of *E. coli* UvrD is required for optimal helicase activity, J. Mol. Biol. 293 (1999) 815–834.
[18] H. Yokota, Y.A. Chujo, Y. Harada, Single-molecule imaging of the oligomer formation of the nonhexameric *Escherichia coli* UvrD helicase, Biophys. J. 104 (2013) 924–933.
[19] B. Nguyen, Y. Ordabayev, J.E. Sokoloski, E. Weiland, T.M. Lohman, Large domain movements upon UvrD dimerization and helicase activation, Proc. Natl. Acad. Sci. U. S. A. 114 (2017) 12178–12183.
[20] M.S. Dillingham, D.B. Wigley, M.R. Webb, Demonstration of unidirectional single-stranded DNA translocation by PcrA helicase: measurement of step size and translocation speed, Biochemistry 39 (2000) 205–212.
[21] M.S. Dillingham, D.B. Wigley, M.R. Webb, Direct measurement of single-stranded DNA translocation by PcrA helicase using the fluorescent base analogue 2-aminopurine, Biochemistry 41 (2002) 643–651.
[22] A. Niedziela-Majka, M.A. Chesnik, E.J. Tomko, T.M. Lohman, *Bacillus stearothermophilus* PcrA monomer is a single-stranded DNA translocase but not a processive helicase in vitro, J. Biol. Chem. 282 (2007) 27076–27085.
[23] K.M. Brendza, W. Cheng, C.J. Fischer, M.A. Chesnik, A. Niedziela-Majka, T.M. Lohman, Autoinhibition of *Escherichia coli* Rep monomer helicase activity by its 2B subdomain, Proc. Natl. Acad. Sci. U. S. A. 102 (2005) 10076–10081.
[24] W. Cheng, J. Hsieh, K.M. Brendza, T.M. Lohman, *E. coli* Rep oligomers are required to initiate DNA unwinding in vitro, J. Mol. Biol. 310 (2001) 327–350.
[25] T. Ha, I. Rasnik, W. Cheng, H.P. Babcock, G.H. Gauss, T.M. Lohman, et al., Initiation and re-initiation of DNA unwinding by the *Escherichia coli* Rep helicase, Nature 419 (2002) 638–641.
[26] L.T. Chisty, C.P. Toseland, N. Fili, G.I. Mashanov, M.S. Dillingham, J.E. Molloy, et al., Monomeric PcrA helicase processively unwinds plasmid lengths of DNA in the presence of the initiator protein RepD, Nucleic Acids Res. 41 (2013) 5010–5023.
[27] V. Dao, P. Modrich, Mismatch-, MutS-, MutL-, and helicase II-dependent unwinding from the single-strand break of an incised heteroduplex, J. Biol. Chem. 273 (1998) 9202–9207.
[28] C. Spampinato, P. Modrich, The MutL ATPase is required for mismatch repair, J. Biol. Chem. 275 (2000) 9863–9869.
[29] M. Yamaguchi, V. Dao, P. Modrich, MutS and MutL activate DNA helicase II in a mismatch-dependent manner, J. Biol. Chem. 273 (1998) 9197–9201.
[30] S.W. Matson, A.B. Robertson, The UvrD helicase and its modulation by the mismatch repair protein MutL, Nucleic Acids Res. 34 (2006) 4089–4097.
[31] M.C. Hall, J.R. Jordan, S.W. Matson, Evidence for a physical interaction between the *Escherichia coli* methyl-directed mismatch repair proteins MutL and UvrD, EMBO J. 17 (1998) 1535–1541.
[32] L.E. Mechanic, B.A. Frankel, S.W. Matson, *Escherichia coli* MutL loads DNA helicase II onto DNA, J. Biol. Chem. 275 (2000) 38337–38346.
[33] T. Ha, A.G. Kozlov, T.M. Lohman, Single-molecule views of protein movement on single-stranded DNA, Annu. Rev. Biophys. 41 (2012) 295–319.
[34] S. Arslan, R. Khafizov, C.D. Thomas, Y.R. Chemla, T. Ha, Protein structure. Engineering of a superhelicase through conformational control, Science 348 (2015) 344–347.
[35] K.C. Neuman, O.A. Saleh, T. Lionnet, G. Lia, J.F. Allemand, D. Bensimon, et al., Statistical determination of the step size of molecular motors, J. Phys. Condens. Matter 17 (2005) S3811–S3820.
[36] J.A. Ali, T.M. Lohman, Kinetic measurement of the step size of DNA unwinding by *Escherichia coli* UvrD helicase, Science 275 (1997) 377–380.
[37] A.L. Lucius, N.K. Maluf, C.J. Fischer, T.M. Lohman, General methods for analysis of sequential "n-step" kinetic mechanisms: application to single turnover kinetics of helicase-catalyzed DNA unwinding, Biophys. J. 85 (2003) 2224–2239.
[38] S.A. Marras, F.R. Kramer, S. Tyagi, Efficiencies of fluorescence resonance energy transfer and contact-mediated quenching in oligonucleotide probes, Nucleic Acids Res. 30 (2002) e122.
[39] A. Niedziela-Majka, N.K. Maluf, E. Antony, T.M. Lohman, Self-assembly of *Escherichia coli* MutL and its complexes with DNA, Biochemistry 50 (2011) 7868–7880.
[40] J.Y. Lee, W. Yang, UvrD helicase unwinds DNA one base pair at a time by a two-part power stroke, Cell 127 (2006) 1349–1360.
[41] H. Jia, S. Korolev, A. Niedziela-Majka, N.K. Maluf, G.H. Gauss, S. Myong, et al., Rotations of the 2B sub-domain of *E. coli* UvrD helicase/translocase coupled to nucleotide and DNA binding, J. Mol. Biol. 411 (2011) 633–648.
[42] W. Cheng, K.M. Brendza, G.H. Gauss, S. Korolev, G. Waksman, T.M. Lohman, The 2B domain of the *Escherichia coli* Rep protein is not required for DNA helicase activity, Proc. Natl. Acad. Sci. U. S. A. 99 (2002) 16006–16011.
[43] K. Sanders, C.L. Lin, A.J. Smith, N. Cronin, G. Fisher, V. Eftychidis, et al., The structure and function of an RNA polymerase interaction domain in the PcrA/UvrD helicase, Nucleic Acids Res. 45 (2017) 3875–3887.
[44] B. Michel, H. Boubakri, Z. Baharoglu, M. Lemasson, R. Lestini, Recombination proteins and rescue of arrested replication forks, DNA Repair (Amst) 6 (2007) 967–980.
[45] E.J. Gwynn, A.J. Smith, C.P. Guy, N.J. Savery, P. McGlynn, M.S. Dillingham, The conserved C-terminus of the PcrA/UvrD helicase interacts directly with RNA polymerase, PLoS One 8 (2013), e78141. .
[46] V. Epshtein, V. Kamarthapu, K. McGary, V. Svetlov, B. Ueberheide, S. Proshkin, et al., UvrD facilitates DNA repair by pulling RNA polymerase backwards, Nature 505 (2014) 372–377.
[47] P. McGlynn, N.J. Savery, M.S. Dillingham, The conflict between DNA replication and transcription, Mol. Microbiol. 85 (2012) 12–20.
[48] E.J. Tomko, C.J. Fischer, A. Niedziela-Majka, T.M. Lohman, A nonuniform stepping mechanism for *E. coli* UvrD monomer translocation along single-stranded DNA, Mol. Cell 26 (2007) 335–347.

[49] E.J. Tomko, H. Jia, J. Park, N.K. Maluf, T. Ha, T.M. Lohman, 5′-Single-stranded/duplex DNA junctions are loading sites for *E. coli* UvrD translocase, EMBO J. 29 (2010) 3826–3839.
[50] P. Soultanas, M.S. Dillingham, F. Papadopoulos, S.E. Phillips, C.D. Thomas, D.B. Wigley, Plasmid replication initiator protein RepD increases the processivity of PcrA DNA helicase, Nucleic Acids Res. 27 (1999) 1421–1428.
[51] J. Atkinson, C.P. Guy, C.J. Cadman, G.F. Moolenaar, N. Goosen, P. McGlynn, Stimulation of UvrD helicase by UvrAB, J. Biol. Chem. 284 (2009) 9612–9623.
[52] L. Manelyte, C.P. Guy, R.M. Smith, M.S. Dillingham, P. McGlynn, N.J. Savery, The unstructured C-terminal extension of UvrD interacts with UvrB, but is dispensable for nucleotide excision repair, DNA Repair (Amst) 8 (2009) 1300–1310.
[53] C. Ban, M. Junop, W. Yang, Transformation of MutL by ATP binding and hydrolysis: a switch in DNA mismatch repair, Cell 97 (1999) 85–97.
[54] A. Guarne, S. Ramon-Maiques, E.M. Wolff, R. Ghirlando, X. Hu, J.H. Miller, et al., Structure of the MutL C-terminal domain: a model of intact MutL and its roles in mismatch repair, EMBO J. 23 (2004) 4134–4145.
[55] A. Robertson, S.R. Pattishall, S.W. Matson, The DNA binding activity of MutL is required for methyl-directed mismatch repair in *Escherichia coli*, J. Biol. Chem. 281 (2006) 8399–8408.
[56] C. Ban, W. Yang, Crystal structure and ATPase activity of MutL: implications for DNA repair and mutagenesis, Cell 95 (1998) 541–552.
[57] G.T. Runyon, T.M. Lohman, Kinetics of *Escherichia coli* helicase II-catalyzed unwinding of fully duplex and nicked circular DNA, Biochemistry 32 (1993) 4128–4138.
[58] A.B. Robertson, S.R. Pattishall, E.A. Gibbons, S.W. Matson, MutL-catalyzed ATP hydrolysis is required at a post-UvrD loading step in methyl-directed mismatch repair, J. Biol. Chem. 281 (2006) 19949–19959.
[59] K.C. Tham, N. Hermans, H.H. Winterwerp, M.M. Cox, C. Wyman, R. Kanaar, et al., Mismatch repair inhibits homeologous recombination via coordinated directional unwinding of trapped DNA structures, Mol. Cell 51 (2013) 326–337.
[60] I. Mellon, G.N. Champe, Products of DNA mismatch repair genes mutS and mutL are required for transcription-coupled nucleotide–excision repair of the lactose operon in *Escherichia coli*, Proc. Natl. Acad. Sci. U. S. A. 93 (1996) 1292–1297.
[61] G.T. Runyon, I. Wong, T.M. Lohman, Overexpression, purification, DNA binding, and dimerization of the *Escherichia coli* uvrD gene product (helicase II), Biochemistry 32 (1993) 602–612.
[62] T.M. Lohman, K. Chao, J.M. Green, S. Sage, G. Runyon, Large-scale purification and characterization of the *Escherichia coli rep* gene product, J. Biol. Chem. 264 (1989) 10139–10147.
[63] I. Wong, K.L. Chao, W. Bujalowski, T.M. Lohman, DNA-induced dimerization of the *Escherichia coli* rep helicase. Allosteric effects of single-stranded and duplex DNA, J. Biol. Chem. 267 (1992) 7596–7610.
[64] A.L. Lucius, C. Jason Wong, T.M. Lohman, Fluorescence stopped-flow studies of single turnover kinetics of *E. coli* RecBCD helicase-catalyzed DNA unwinding, J. Mol. Biol. 339 (2004) 731–750.
[65] E. Antony, A.G. Kozlov, B. Nguyen, T.M. Lohman, *Plasmodium falciparum* SSB tetramer binds single-stranded DNA only in a fully wrapped mode, J. Mol. Biol. 420 (2012) 284–295.
[66] B. Nguyen, J. Sokoloski, R. Galletto, E.L. Elson, M.S. Wold, T.M. Lohman, Diffusion of human replication protein A along single-stranded DNA, J. Mol. Biol. 426 (2014) 3246–3261.
[67] C. Joo, T. Ha, Single molecule FRET with total internal reflection microscopy, in: P.R. Selvin, T. Ha (Eds.), Single Molecule techniques: A Laboratory Manual, Cold Spring Harbor Laboratory Press, NY, Cold Spring Harbor, NY 2008, pp. 3–36.
[68] L.N. Trefethen, J.A.C. Weideman, T. Schmelzer, Talbot quadratures and rational approximations, BIT Numer. Math. 46 (2006) 653–670.
[69] J. Vistica, J. Dam, A. Balbo, E. Yikilmaz, R.A. Mariuzza, T.A. Rouault, et al., Sedimentation equilibrium analysis of protein interactions with global implicit mass conservation constraints and systematic noise decomposition, Anal. Biochem. 326 (2004) 234–256.
[70] T.M. Laue, B.D. Shah, T.M. Ridgeway, S.L. Pelletier, Computer-Aided Interpretation of Analytical Sedimentation Data for Proteins, Royal Society of Chemistry, Cambridge, UK, 1992.
[71] J. Dam, P. Schuck, Calculating sedimentation coefficient distributions by direct modeling of sedimentation velocity concentration profiles, Methods Enzymol. 384 (2004) 185–212.
[72] C. Tanford, Physical Chemistry of Macromolecules, Wiley, NY, 1961.

Supplementary Information

Regulation of UvrD Helicase Activity by MutL

Yerdos A. Ordabayev, Binh Nguyen, Anita Niedziela-Majka and Timothy M. Lohman

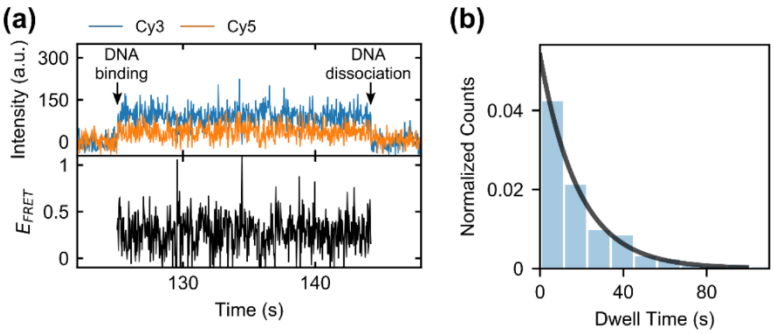

Supplementary Fig. 1. DNA binding to and dissociation from surface immobilized biotin-UvrD monomers. (a) Example of a time trace for binding to and dissociation of DNA (1 nM) from a surface-immobilized UvrD monomer at 5 μM ATP in imaging buffer at 25 °C. (b) Histogram of the dwell times of DNA bound to UvrD and a single exponential fit (black line) indicating a dissociation rate constant of 0.054 ± 0.002 s^{-1}.

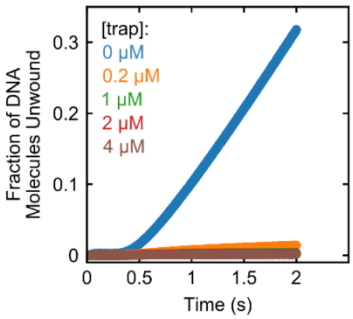

Supplementary Fig. 2. Protein trap test. Stopped-flow experiments were performed with 160 nM UvrD and 250 nM MutL dimer in one syringe and mixing vs. 50 nM 3′-$(dT)_{20}$-ds18-BHQ2/Cy5, 1 mM ATP, 2 mM $MgCl_2$, plus varying concentrations of 10-bp DNA hairpin with a 3′-$(dT)_{40}$ ssDNA tail (protein trap) (0 μM (blue); 0.2 μM (orange); 1 μM (green); 2 μM (red); 4 μM (brown)) in buffer T at 25 °C.

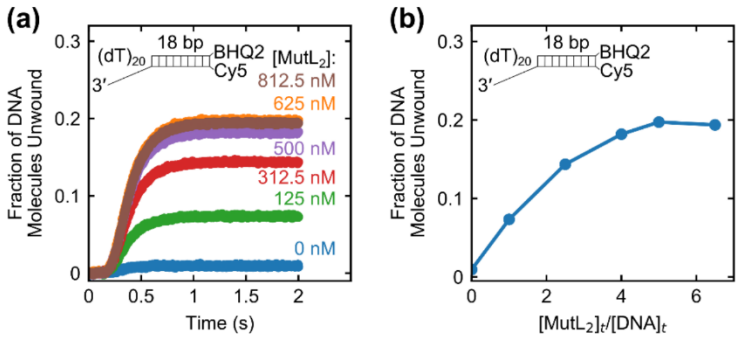

Supplementary Fig. 3. Effects of MutL concentration on UvrD activation. (a) Stopped-flow DNA unwinding time courses performed with 125 nM 3′-$(dT)_{20}$-ds18-BHQ2/Cy5 and 50 nM UvrD as a function of MutL dimer concentration (0 nM (blue); 125 nM (green); 312.5 nM (red); 500 nM (purple); 625 nM (orange); 812.5 nM (brown)) in buffer T at 25 °C. (b) Fraction of DNA molecules unwound plotted as a function of $[MutL_2]_t/[DNA]_t$.

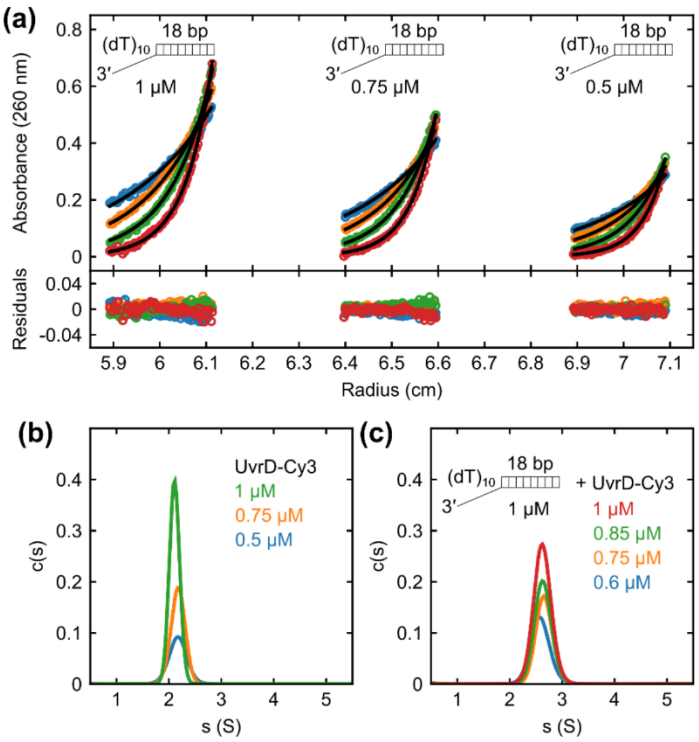

Supplementary Fig. 4. UvrD-Cy3 binds to 3′-$(dT)_{10}$-ds18 as a monomer in buffer M20/20. (a) Sedimentation equilibrium experiments of 3′-$(dT)_{10}$-ds18 (0.5 μM, 0.75 μM, 1 μM) were performed in buffer M20/20 at 25 °C. Global analysis of absorbance profiles at 260 nm shows a single species at four rotor speeds (18k rpm (blue); 22k rpm (orange); 27k rpm (green); 33k rpm (red)). Smooth curves are simulations using best fit parameters with residuals shown below the plots. (b,c) Sedimentation velocity experiments monitoring the Cy3 absorbance of UvrD-Cy3 at 555 nm were performed at 42k rpm in buffer M20/20 at 25 °C. (b) Continuous sedimentation coefficient distributions $c(s)$ of UvrD-Cy3 at three concentrations (0.5 μM (blue); 0.75 μM (orange); 1 μM (green)) show a single peak at 2.15 ± 0.02 S. (c) $c(s)$ distributions of UvrD-Cy3 at four concentrations (0.6 μM (blue); 0.75 μM (orange); 0.85 μM (green); 1 μM (red)) in complex with 3′-$(dT)_{10}$-ds18 (1 μM) show a single peak at 2.63 ± 0.02 S.

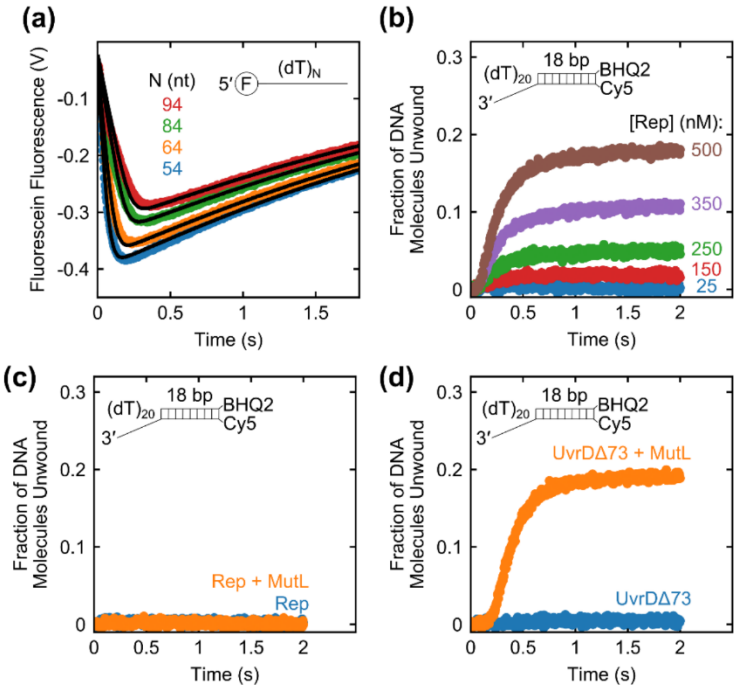

Supplementary Fig. 5. MutL specifically stimulates UvrD helicase. (a) Time courses for stopped-flow ssDNA translocation experiments performed with Rep (50 nM) and a series of 5′-F-$(dT)_N$ (N = 54, 64, 84, 94 nt) (100 nM) to ensure that no more than one Rep monomer is bound per DNA. The macroscopic translocation rate (mk_t) of a Rep monomer determined from NLLS analysis (see Methods) is 293±16 nt/s. (b,c,d) Stopped-flow DNA unwinding time courses for experiments performed with 3′-$(dT)_{20}$-ds18-BHQ2/Cy5 in buffer T at 25 °C (b) DNA (50 nM) was pre-incubated with Rep at varying concentrations (25 nM (blue); 150 nM (red); 250 nM (green); 350 nM (purple); 500 nM (brown)). Helicase activity is observed only for [Rep] >> [DNA]. (c) DNA (50 nM) was pre-incubated with 25 nM Rep (blue) or 25 nM Rep plus 250 nM MutL dimer (orange), favoring Rep monomer bound to the DNA. (d) DNA was pre-incubated with 25 nM UvrDΔ73 (blue) or 25 nM UvrDΔ73 plus 250 nM MutL dimer (orange).

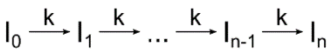

Supplementary Scheme 1

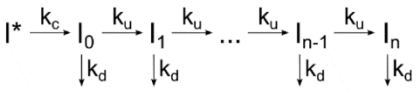

Supplementary Scheme 2

Supplementary Table 1. Hydrodynamic properties of 3′-(dT)$_{10}$-ds18, UvrD-Cy3, MutL$_2$, and their complexes in buffer M20/20

Species	M (kg/mol)	$\bar{\upsilon}_{calc}$[b] (ml/g)	$s_{20,w}$ (S)	f/f_0	$M_{predicted}$ (kg/mol)	$\bar{\upsilon}_{exp}$[c] (ml/g)
3′-(dT)$_{10}$-ds18	14.044	-	-	-	-	0.563 ± 0.002
UvrD-Cy3	84.672	0.7308	4.66 ± 0.05	1.46 ± 0.02	82.3 ± 1.2	0.737±0.003
MutL$_2$[a]	135.824	0.7414	4.88 ± 0.04	1.88 ± 0.02	130.2 ± 6.9	0.750 ± 0.010
UvrD-DNA	98.717	0.712	5.63 ± 0.03	1.40 ± 0.01	92.4 ± 1.4	0.727 ± 0.003
MutL$_2$-UvrD-DNA	234.540	0.734	-	-	235 ± 6	0.734 ± 0.005

[a] Niedziela-Majka *et al.*[1]
[b] Calculated from the amino acid composition using SEDNTERP[2] for UvrD-Cy3 and MutL$_2$ as well as weight-average partial specific volumes for UvrD-DNA and MutL$_2$-UvrD-DNA complexes according to Eq. (7)
[c] Estimated from sedimentation equilibrium analysis by constraining to the known molecular mass of the species

Supplementary Table 2. DNA substrate sequences

dsDNA pairs	Length (nt)	Oligonucleotide sequence
I	19	5′-(Y) GCC CTG CTG CCG ACC AAC-3′
I	39	5′-(X) GTT GGT CGG CAG CAG GGC $(dT)_{20}$-3′
II	19	5′-GCC CTG CTG CCG ACC AAC (Q)-3′
II	19 + N	5′-(Y) GTT GGT CGG CAG CAG GGC $(dT)_N$-3′
III	22	5′-GCC CTG CTG CCG ACC AAC GAT (Q)-3′
III	42	5′-(Y) ATC GTT GGT CGG CAG CAG GGC $(dT)_{20}$-3′
IV	26	5′-GCC CTG CTG CCG ACC AAC GAT GGT T (Q)-3′
IV	26 + N	5′-(Y) AAC CAT CGT TGG TCG GCA GCA GGG C $(dT)_N$-3′
V	33	5′-GCC CTG CTG CCG ACC AAC GAT GGT TAC ATT CC (Q)-3′
V	33 + N	5′-(Y) GGA ATG TAA CCA TCG TTG GTC GGC AGC AGG GC $(dT)_N$-3′
VI	41	5′-GCC CTG CTG CCG ACC AAC GAT GGT TAC ATT CCC GCT GCT G (Q)-3′
VI	41 + N	5′-(Y) CAG CAG CGG GAA TGT AAC CAT CGT TGG TCG GCA GCA GGG C $(dT)_N$-3′
VII	51	5′-GCC CTG CTG CCG ACC AAC GAT GGT TAC ATT CCC GCT GCT GCT AGT GCA GG(Q)-3′
VII	51 + N	5′-(Y) CCT GCA CTA GCA GCA GCG GGA ATG TAA CCA TCG TTG GTC GGC AGC AGG GC $(dT)_N$-3′
VIII	81	5′-GCC CTG CTG CCG ACC AAC GAT GGT TAC ATT CCC GCT GCT GCT AGT CGA GGT AGC GTT CAC GTC GCA TTC GAC GCT CGA CG (Q)-3′
VIII	95	5′ -(Y) CGT CGA GCG TCG AAT GCG ACG TGA ACG CTA CCT CGA CTA GCA GCA GCG GGA ATG TAA CCA TCG TTG GTC GGC AGC AGG GC $(dT)_{14}$-3′
IX	18	5′-GCC CTG CTG CCG ACC AAC-3′
IX	28	5′-GTT GGT CGG CAG CAG GGC $(dT)_{10}$-3′
X	65	5′-GCC TCG CTG CTT TTT GCA GCG AGG C $(dT)_{40}$-3′

X = Cy3; Y = Cy5; Q = BHQ2

1. Niedziela-Majka, A., Maluf, N.K., Antony, E. & Lohman, T.M. Self-assembly of Escherichia coli MutL and its complexes with DNA. *Biochemistry* **50**, 7868-80 (2011).
2. Laue, T.M., Shah, B.D, Ridgeway, T.M. and Pelletier, S.L. *Computer-aided interpretation of analytical sedimentation data for proteins.*, 90-125 (Royal Society of Chemistry, Cambridge, UK, 1992).

Chapter III

UvrD Helicase Activation by MutL Involves Closing of its 2B sub-domain

Preface to the Chapter

In this chapter I discuss the effect of MutL on the rotational conformational state of the 2B sub-domain of UvrD and associated activation of the UvrD helicase activity. Using single molecule and ensemble FRET experiments I showed that MutL binding to UvrD monomer-DNA complex induces partial closing of the 2B sub-domain. In order to determine the functional relevance of this conformational change, I designed and performed two sets of parallel pre-steady state kinetic experiments under identical solution conditions monitoring the helicase activity *and* conformational changes in the 2B sub-domain of UvrD upon binding of MutL to the pre-formed UvrD monomer-DNA complex. The results of these experiments are well-described by the four-state mixed kinetic model where UvrD activation can proceed either through the conformational selection (CS) pathway or the induced fit (IF) pathway. The analysis of the fractional net fluxes through each pathway shows that under the experimentally used MutL concentrations the CS pathway is favored (>90%) over the IF pathway (<10%). Furthermore, I showed that MutL does not activate the chimeric UvrD(Rep2B) monomer helicase activity, suggesting that MutL simulation is regulated specifically by the UvrD 2B sub-domain. This manuscript has been submitted to the Proceedings of the National Academy of Sciences and is currently under review.

UvrD Helicase Activation by MutL Involves Closing of its 2B sub-domain

Yerdos A. Ordabayev, Binh Nguyen, Alexander G. Kozlov, Haifeng Jia, Timothy M. Lohman*

Department of Biochemistry and Molecular Biophysics

Washington University School of Medicine

660 S. Euclid Ave., Box 8231

St. Louis, MO 63110

Running title: MutL induced conformational changes upon UvrD helicase activation

Key words: helicase, single molecule fluorescence, activation, mismatch repair, conformational selection

Classification: Biological Sciences

*Address correspondence to:

Department of Biochemistry and Molecular Biophysics

Washington University School of Medicine

660 S. Euclid Ave., Box 8231

St. Louis, MO 63110

E-mail: lohman@biochem.wustl.edu

Tel: (314)-362-4393

Fax: (314)-362-7183

Abstract

Escherichia coli UvrD is a superfamily 1 helicase/translocase that functions in DNA repair, replication, and recombination. Although a UvrD monomer can translocate along single stranded DNA, self-assembly or interaction with an accessory protein is needed to activate its helicase activity *in vitro*. Our previous studies have shown that an *E. coli* MutL dimer can activate the UvrD monomer helicase *in vitro,* but the mechanism for this is not known. The UvrD 2B sub-domain is rotationally flexible and can access a range of rotational conformational states. Using single molecule FRET experiments, we show that the 2B sub-domain of a UvrD monomer bound to DNA exists in equilibrium between open and closed states, but predominantly in an open conformation. However, MutL binding to a UvrD monomer-DNA complex promotes an intermediate, partially closed state. Parallel studies of the kinetics of MutL-induced activation of the UvrD helicase and the kinetics of MutL-induced changes in the UvrD 2B sub-domain shows that MutL activation involves a transition from an open to a closed 2B sub-domain mainly via conformational selection. We further show that MutL is unable to activate the helicase activity of a chimeric UvrD containing the 2B sub-domain of the structurally similar Rep helicase. Hence, MutL activation of the monomeric UvrD helicase is regulated specifically by the 2B sub-domain.

Significance

UvrD helicase plays essential roles in multiple DNA metabolic processes including methyl-directed mismatch repair. UvrD monomers can translocate along single-stranded DNA, but requires self-assembly or interaction with an accessory factor to activate processive DNA unwinding *in vitro*. A MutL protein dimer can activate the monomeric UvrD helicase, however, the mechanism of activation is not known. The 2B sub-domain of UvrD is regulatory and can

freely rotate among multiple rotational sub-states. Using single molecule and stopped-flow fluorescence approaches, we show that binding of MutL to a UvrD-DNA substrate complex induces an intermediate rotational 2B conformation that is on pathway to form an active helicase. The results show the important role of the 2B sub-domain in regulating helicase activity.

Introduction

Escherichia coli UvrD is an SF1A DNA helicase/translocase involved in methyl-directed mismatch DNA repair (1), nucleotide excision repair (2), replication restart (3, 4), recombination (5, 6), and transcriptional control through interactions with RNA polymerase (7-9). *E. coli* UvrD and the structurally similar SF1A helicases, *E. coli* Rep and *Bacillus stearothermophilus* PcrA, share two core ATPase sub-domains, 1A and 2A, and two less conserved auxiliary subdomains, 1B and 2B (10). The monomeric forms of UvrD-like helicases are processive single-stranded DNA translocases (11-18) but have little to no helicase activity by themselves *in vitro* (13, 19-24). In the absence of accessory proteins, UvrD, Rep and PcrA must assemble to form at least a dimer in order to activate helicase activity (13, 19-23). Crystal structures as well as single molecule and ensemble FRET studies show that the 2B sub-domains of UvrD (25-27), Rep (28, 29), and PcrA (30-33) can populate open and closed conformations that differ by rotations of the 2B sub-domain from 130 to 160 degrees. The helicase activity of the Rep monomer is auto-inhibited by its 2B sub-domain since removal of the 2B sub-domain activates Rep monomer helicase activity (19, 34, 35) demonstrating that a Rep monomer possesses all that is needed for both translocase and helicase activities. This important finding coupled with the rotational flexibility of the 2B sub-domain led to the hypothesis that the 2B sub-domain is regulatory and that its rotational conformational state can modulate helicase activity (19, 24, 34). Indeed, single molecule studies of UvrD have shown that DNA unwinding activity correlates with the closed conformation of the 2B sub-domain (36). Crosslinking of the 2B sub-domain of Rep into a closed configuration also activates Rep monomer helicase activity (32). Studies of the PcrA helicase have shown that the *B. stearothermophilus* RepD protein activates PcrA helicase

activity (37). Finally, a recent study has shown that upon formation of a UvrD dimer the 2B sub-domain of the lead UvrD subunit is shifted to a more closed state (27).

The helicase activity of UvrD can be activated through interactions with the MutL protein (38, 39) that is required for methyl-directed mismatch repair (40) and we have recently shown that a single MutL dimer is sufficient to activate the UvrD monomer helicase and increase its processivity as well as stimulate the helicase activity of a UvrD dimer (41). However, the molecular basis for this activation is not known. Here, we use single-molecule and ensemble fluorescence resonance energy transfer (FRET) experiments to demonstrate that MutL binding to a UvrD-DNA complex leads to a closing of the rotational conformational state of the UvrD 2B sub-domain and that the closing is on the pathway to activation of DNA unwinding activity by the MutL-UvrD monomer complex. We also show that UvrD activation by MutL is specific for the UvrD 2B sub-domain.

Results

The 2B sub-domain of UvrD adopts a more open conformation upon binding to a partial duplex DNA

A crystal structure of a UvrD monomer complexed with a 3′-$(dN)_7$ partial duplex DNA (18-28 bp) shows the 2B sub-domain in a very closed state with the 2B sub-domain in direct contact with duplex DNA (25). However, ensemble and single-molecule FRET studies in solution (26, 27) show that UvrD monomers bound to a 3′-$(dT)_{20}$-duplex DNA substrate of 18 bp display a distribution of 2B sub-domain rotational conformational states that center on a more open state. We investigated the distribution of 2B sub-domain conformation states for UvrD bound to a partial ss-ds DNA using single-molecule FRET. The rotational conformational state of the 2B sub-domain

was probed using a double-cysteine UvrD mutant, UvrDΔCys-(A100C, A473C), referred to as UvrD-DM-1B/2B, with Cysteines in the 1B sub-domain (A100C) and the 2B sub-domain (A473C) that we have characterized previously (26, 27) (Fig. 1A). The two Cys residues were labeled stochastically with a mixture of Cy3 (donor) and Cy5 (acceptor) fluorophores as described (26, 27). As predicted from the distances between residues A100 and A473 measured from the crystal structures of apo UvrD (26) and UvrD in complex with partial duplex DNA (25), and as shown previously in solution (26, 27), the Cy3/Cy5-labeled UvrD-DM-1B/2B construct yields a high FRET efficiency signal, E_{FRET}, when the 2B sub-domain is in its closed state and a low E_{FRET} signal when the 2B sub-domain is in an open state (Fig. 1A). Hence rotations of the 2B sub-domain relative to the other three sub-domains can be monitored as a change in FRET efficiency. Single-molecule FRET time traces were analyzed using a hidden Markov model to extract FRET states and transition rates between states as described in Methods.

To selectively observe only DNA-bound UvrD-DM-1B/2B molecules we immobilized an 18 bp duplex DNA with a flanking 3′-$(dT)_{20}$ tail, referred to as 3′-$(dT)_{20}$-ds18-biotin, to a coverslip through a biotin-neutravidin tag at the blunt-end of the duplex DNA (Fig. 1B). Cy3/Cy5-labeled UvrD-DM-1B/2B was added at low concentration (250 pM) in imaging buffer at 25°C. Binding and the 2B conformational state of the UvrD-DM-1B/2B was monitored by exciting Cy3 donor fluorescence with a 532 nm laser and detecting Cy3 and Cy5 fluorescence emission signals using an objective based TIRF microscope as described (42). Total fluorescence intensity and one step photobleaching/dissociation behavior indicate that UvrD-DM-1B/2B binds to DNA as a monomer under these conditions. Figure 1C shows an example smFRET trajectory of Cy3/Cy5-UvrD-DM-1B/2B bound to DNA in which the 2B sub-domain undergoes reversible transitions accompanied by anti-correlated changes in Cy3 and Cy5 fluorescence, between open ($E_{FRET}(S1) = 0.26 \pm 0.08$)

and closed (E_{FRET}(S3) = 0.75 ± 0.08) states with transition rates k_{13} = 0.224±0.012 s^{-1} and k_{31} = 0.72±0.05 s^{-1}. Total E_{FRET} distributions of 346 trajectories (Fig 1D) show that the 2B sub-domain of UvrD bound to 3′ tailed DNA predominantly occupies a more open state (S1).

Stopped-flow studies (Supplementary Fig. 1) show that binding of Cy3/Cy5-UvrD-DM-1B/2B to an excess of the same partial duplex DNA results in an anti-correlated increase in Cy3 fluorescence and decrease in Cy5 fluorescence (decrease in FRET) consistent with the 2B sub-domain of UvrD moving to a more open state upon DNA binding, consistent with the smFRET observation and in agreement with previous studies (26, 27).

MutL binding shifts the UvrD 2B sub-domain to a partially closed state

Upon addition of an excess of MutL (250 nM dimer) along with UvrD-DM-1B/2B (250 pM) to the surface immobilized 3′-$(dT)_{20}$-ds18-biotin DNA molecules in imaging buffer (Fig. 1E), we now observe UvrD monomers with three discrete E_{FRET} states (Figure 1F and 1G); the same S1 (E_{FRET}(S1)= 0.22 ± 0.11) and S3 (E_{FRET}(S3) = 0.76 ± 0.12) states as in the absence of MutL, but also a new S2 E_{FRET} state with intermediate FRET value (E_{FRET}(S2) = 0.45 ± 0.08) (Fig. 1F and 1G). Hidden Markov analysis shows transitions only between S1 and S2 states and between S2 and S3 states, yielding the transition rates, k_{12} = 0.165±0.032 s^{-1}, k_{21} = 0.21±0.05 s^{-1}, k_{23} = 0.19±0.03 s^{-1}, and k_{32} = 0.32±0.08 s^{-1}.

Kinetics of formation of the active MutL-UvrD-DNA complex

In a previous study (41) we showed that binding of a single MutL dimer to a UvrD monomer-DNA complex activates the UvrD monomer helicase activity. Here we performed two sets of stopped-flow experiments to examine the kinetics of UvrD activation by MutL and whether this correlates with 2B sub-domain movement. In the first set of experiments we

examined the kinetics of MutL binding and formation of an active MutL-UvrD-DNA complex by monitoring the unwinding of a fluorescently labeled DNA (3′-$(dT)_{20}$-ds18-BHQ2/Cy5 depicted in Figure 2A). In the duplex DNA, the fluorescence of Cy5 on one DNA strand is quenched by the black hole quencher, BHQ2, on the other strand (43). Hence, when the two strands of the duplex are unwound and separated, the Cy5 fluorescence increases (41). In a second set of independent, but otherwise identical experiments, we monitored the kinetics of the conformational changes in the monomeric UvrD 2B sub-domain that accompany MutL binding by using the Cy3/Cy5-UvrD-DM-1B/2B (Fig. 1A).

We first performed sequential-mixing stopped-flow experiments to monitor the kinetics of formation of an active monomeric UvrD-DNA helicase using fluorescently labeled DNA to monitor DNA unwinding upon addition of MutL (Fig. 2A) in buffer T at 25°C. Syringe A contained UvrD (100 nM) and 3′-$(dT)_{20}$-ds18-BHQ2/Cy5 (250 nM), syringe B contained excess MutL and syringe C contained 1 mM ATP, 2 mM $MgCl_2$, 2 μM protein trap (10 bp DNA hairpin possessing 3′-$(dT)_{40}$ tail). Under these conditions a UvrD monomer is bound to the DNA in syringe A (22, 41). Syringes A and B were rapidly mixed in the first step and allowed to incubate for a time (Δt), after which this mixture (A + B) was rapidly mixed with syringe C to initiate DNA unwinding by any active $(MutL)_2$-UvrD-DNA complex that assembled during the incubation period (Δt). The DNA hairpin in syringe C serves as a trap to prevent any rebinding of free UvrD to the DNA substrate. Since the rate of formation of the active $(MutL)_2$-UvrD-DNA complex is much slower than the rate of DNA unwinding, the final amplitude of the Cy5 fluorescence increase observed after mixing with syringe C (see Supplementary Figure 2), monitors formation of active $(MutL)_2$-UvrD helicase. From a series of experiments varying Δt

we obtain a time course for formation of active $(MutL)_2$-UvrD helicase (Supplementary Figure 2).

Figure 2B shows the time dependence of the fraction of DNA molecules unwound for three experiments performed at different MutL dimer concentrations (0.5, 0.75, 1.25 μM) (Supplementary Figures 2A-C). The time courses are biphasic and the reciprocal relaxation times, $1/\tau_2$ and $1/\tau_3$, determined by fitting from a two-exponential fit (Eq. (2)), are plotted in Figures 2C and 2D. The biphasic time courses suggest the presence of two populations of UvrD monomers bound to the DNA that can both be activated by MutL. The first population shows $1/\tau_2$ increases with increasing MutL concentration from ~3 s^{-1} to ~9 s^{-1}, suggesting activation by MutL binding to a UvrD-DNA complex. The second reciprocal relaxation time $1/\tau_3$ ~0.08-0.09 s^{-1}, changes little with $[MutL_2]$, suggesting that activation of this UvrD-DNA population is limited by a uni-molecular conformational change. The existence of two populations of UvrD on the DNA prior to the addition of MutL is consistent with the single molecule results in panel 1D.

Kinetics of MutL binding to UvrD-DNA complex and MutL binding induced 2B sub-domain conformational changes

In an independent set of otherwise identical stopped-flow experiments, we next monitored the time course of MutL-induced conformational changes in the 2B sub-domain of the monomeric UvrD-DNA complex (Fig. 3A). Cy3/Cy5-labeled UvrD-DM-1B/2B (100 nM) (Fig. 1A) was pre-equilibrated with excess of 3′-$(dT)_{20}$-ds18 (250 nM) in syringe A for 5 min and then rapidly mixed with MutL at a series of concentrations (0.5, 0.75, 1, 1.25, 1.5, and 1.75 μM MutL dimer) in syringe B. The Cy3 fluorescence was excited and both Cy3 and Cy5 fluorescence emissions were monitored. The time-courses in Figure 3B show the simultaneous changes in

both Cy3 donor and Cy5 acceptor fluorescence signals upon excitation of Cy3 fluorescence. Figures 3C-E plot the reciprocal relaxation times, $1/\tau_1$, $1/\tau_2$, and $1/\tau_3$, determined from a fit of the time courses in Figure 3B to three exponentials (Eq. (17)), as a function of the total MutL dimer concentration. The observation of three relaxation times in these experiments indicates the presence of at least three independent kinetic steps involving the labeled UvrD. We note that both $1/\tau_1$ and $1/\tau_2$ increase linearly with [$MutL_2$] indicating that the first two phases involve binding of MutL to the UvrD-DNA complex. However, $1/\tau_3$ decreases with increasing [$MutL_2$] indicating a conformational selection step as part of the pathway (44, 45).

Based on these observations we considered the four-state mechanism in Figure 4A. In this scheme, UvrD-DNA complexes exist in equilibrium between open and closed 2B sub-domain conformations ($U_OD \leftrightarrow U_CD$) and MutL dimer can bind to both conformations to form MU_OD and MU_CD, which are also in equilibrium. Although Figure 4A shows four states and four steps, we note that due to the closed thermodynamic cycle, only three kinetic steps are independent, consistent with the observation of three exponential phases.

We analyzed the fluorescence time courses by global non-linear least squares analysis (Supplementary Figure 3) according to Figure 4A using Eq. (8) as described in Supplementary Methods. The resulting best-fit values of all rate constants (Table 1) and relative molar fluorescence intensities (Table 2) were well constrained. We note that a well constrained set of rate constants could only be obtained by including the fluorescence intensities and fitting the full time courses. However, since the labeled UvrD in these stopped-flow studies is not uniformly labeled with both Cy3 and Cy5, but exists as a mixture of labeled species, one cannot assign much significance to the molar fluorescence intensities given in Table 2. The equilibrium constants for each step in scheme in Figure 4A are given in Table 2. These results indicate that

before MutL binding, the UvrD monomer predominantly exists in an open conformation in complex with DNA, but shifts to a more closed conformation upon MutL binding, consistent with the single molecule experiments above.

In Figures 4B-D we compare the experimental reciprocal relaxation times obtained from the fluorescence time-courses (Figure 3C, D, E) and those from the helicase activity time courses (Figure 2C, D) with the relaxation times computed from the best-fit values of the rate constants in Table 1 as described in Methods. The good agreement indicates that the mechanism and rate constants provide a good description of the data. Lastly, in Figure 4E we compare the experimental time courses for production of active MutL-UvrD helicase (Figure 2B) with the simulated concentration time courses for MU_CD production (continuous lines) (Figure 4E). The excellent agreement supports the conclusion that the $(MutL)_2$-UvrD-DNA complex with the 2B sub-domain in a partially closed conformation is the active form of the helicase.

Activation of UvrD by MutL is specific for the UvrD 2B sub-domain

We have shown that MutL does not activate Rep monomer helicase activity indicating that activation by MutL is specific to UvrD(41). Given the regulatory role of the 2B sub-domain and its low-sequence conservation among UvrD-like helicases we hypothesized that the 2B sub-domain might be involved in specific UvrD-MutL interactions. To test this idea, we designed a UvrD(Rep2B) chimera, in which the UvrD 2B sub-domain was replaced with the Rep 2B sub-domain. The UvrD(Rep2B) chimera retains both ssDNA translocase activity and helicase activity under conditions of excess protein that is comparable to wt UvrD. ssDNA translocation activity of UvrD(Rep2B) monomers (Supplementary Fig. S4A) was examined as described previously (15). The 3’ to 5’ macroscopic translocation rate is 152±6 nt/s, only slightly slower than for

wtUvrD monomer (191±3 nt/s) (15, 17) under the same conditions. DNA unwinding activity of UvrD(Rep2B) was determined using 3′-$(dT)_{20}$-ds18-BHQ2/Cy5 as described in Methods (Supplementary Figure S4B). The macroscopic rate of DNA unwinding is 88±7 bp/s, the same as for wtUvrD (80±30 bp/s) (41) under identical conditions.

We next examined whether the helicase activity of the chimeric UvrD(Rep2B) monomer can be stimulated by MutL. Single round unwinding experiments were performed with 50 nM 3′-$(dT)_{20}$-ds18-BHQ2/Cy5 and 25 nM UvrD(Rep2B) alone or plus 250 nM MutL dimer in buffer T at 25°C. No stimulation of monomeric UvrD(Rep2B) by MutL is observed under these conditions (Fig. 5A) in contrast to the stimulation of monomeric wtUvrD helicase by MutL under the same conditions (Fig. 5B). This suggests that MutL activation of the UvrD monomer helicase is specific for the UvrD 2B sub-domain.

Discussion

E. coli UvrD, *E. coli* Rep, and *B. stearothermophilus* PcrA are closely related SF1A helicases, detailed investigations of which have provided many key insights into their mechanism of ssDNA translocation and DNA unwinding. The monomeric forms of UvrD-like helicases can rapidly and processively translocate along ssDNA with a 3′ to 5′ directionality (11, 12, 15-17, 19, 24). However, significant DNA unwinding is observed *in vitro* only in the presence of an excess of enzyme over DNA or in the presence of accessory proteins indicating that the monomeric form is inactive as a helicase and requires activation either through self-assembly or interaction with an accessory protein(19-22, 46). Structural and functional studies of UvrD and the similar SF1A helicases, Rep and PcrA, have shown that they possess a rotationally flexible 2B sub-domain that can assume a wide range of conformational states depending on

solution conditions, DNA binding and assembly state and it has been suggested that the rotational conformational state of this sub-domain plays a regulatory role (24-28, 31).

We have shown that the helicase activity of a UvrD monomer can be activated upon binding a single MutL dimer (41). Here we show that activation of the UvrD monomer helicase by MutL is associated with a partial closing of the UvrD 2B sub-domain. A single molecule FRET experiment with FRET labeled UvrD shows that the 2B sub-domain of a UvrD monomer bound to a 3′-ssDNA-duplex displays dynamic transitions between an open and closed state. Upon binding MutL, a new intermediate, partially closed state becomes populated. Stopped-flow experiments show that under these same conditions, apo UvrD has a relatively closed state that becomes more open upon binding the 3′-ssDNA duplex. Upon binding of a MutL dimer, the 2B sub-domain assumes a partially closed conformation and we show that formation of this more closed state is on the pathway to forming the active helicase. This intermediate conformation is more similar to the open state of the Rep-ssDNA crystal structure(28) than to the fully closed state observed in a UvrD-DNA crystal structure(25).

Activation of the helicase activity of other UvrD-like enzymes has also been correlated with a more closed conformation of the 2B sub-domain. Rep monomer can be activated by covalent cross-linking of the 2B sub-domain in the closed form (32), UvrD dimerization shifts the 2B sub-domain of the lead UvrD monomer to a more closed state (27), PcrA transitions to a closed state upon RepD binding (32), and UvrD monomer in a closed state can unwind DNA when a pulling force is applied to the DNA (36). Whether these “closed” states are all equivalent is not known.

The mechanism that provides an excellent description of the relaxation times and kinetic time courses is given in Figure 4A. In this scheme, the 2B sub-domain of a UvrD monomer

bound to DNA exists in equilibrium between two conformations, open and closed. Both the single molecule data as well as the stopped-flow fluorescence data provide support for a pre-existing equilibrium between an open form, U_OD, and a closed form, U_CD. A MutL dimer can bind to either conformation and proceed to form the active MutL-UvrD helicase, MU_CD, via two pathways, one being an induced fit (IF) via step 4 and the other a conformational selection (CS) via step 3. We were able to determine all of the rate constants for the Figure 4A scheme. This required analysis of the complete fluorescence time courses. The relaxations times alone did not provide sufficient constraints to determine all of the rate constants. The kinetics of MutL binding and subsequent effects on the 2B sub-domain rotational conformation display three relaxation times, with the two slowest relaxation times being the same as the two relaxation times observed for formation of the active MutL-UvrD helicase. Hence, the fastest relaxation time, τ_1, which is dominated by the rate constants, k_1 and k_{-1}, reflecting MutL binding to the open UvrD-DNA complex, does not contribute significantly to the kinetics of formation of the active helicase. The second and third relaxation times contribute to active helicase formation and reflect the steps involving k_2, k_{-2} and k_3, k_{-3}, both of which involve the closed MU_CD state. We note that under the solution conditions used in our experiments, the MutL protein has a tendency to form higher order assemblies beyond a dimer (47), hence the bimolecular rate constants estimated here for MutL dimer binding to the UvrD-DNA complex, k_1 = (4.01±0.01) x 10^6 M^{-1} s^{-1} and k_3 = (5.82±0.01) x 10^6 M^{-1} s^{-1}, are likely underestimates.

Although there has been much discussion in the literature as to whether two step binding processes occur via a CS (steps 2 and 3) or IF pathway (44, 45, 48), as noted previously (49, 50) the answer is generally both (49, 50), with the relative flux through each pathway (Figure 6A) depending on the concentration of the binding ligand, in this case MutL. Using the rate constants

in Table 1, we can calculate the time courses for formation of all the UvrD species in Figure 4A as shown in Figure 6B, before addition of 1 μM MutL dimer, the dominant species is the open UvrD bound to DNA, U_OD. Although MutL can bind to both U_OD and U_CD, most of the MU_CD formed goes through the CS pathway (steps 2 and 3). In Figure 6C we plot the fractional equilibrium flux for the conformational selection pathway (49) and the fractional net flux through step 3 as a function of MutL concentration calculated using the rate constants in Table 1 as described in Methods. Under the conditions and MutL concentrations used in our experiments (black part of curve in Figure 6C), it is clear that formation of the active MutL-UvrD helicase occurs predominantly through step 3 (the CS pathway) (>90%), although there is a small component that proceeds via step 4 (the IF pathway) (<10%) (Figure 6B and C). However, at sufficiently high MutL concentrations, the IF pathway through step 4 will ultimately dominate.

Finally, although we have demonstrated that closing of the UvrD 2B sub-domain is on pathway to formation of an active MutL-UvrD helicase, we do not know why a partially closed form is associated with activation. It has been suggested based on crystal structures of monomers of UvrD (25) and PcrA (31) bound to a 3'-$(dN)_7$-duplex DNA that an interaction of the 2B sub-domain with duplex DNA is involved in DNA unwinding. However, neither UvrD nor PcrA can unwind such DNA as monomers (13, 15, 22) raising the issue that those structures might not represent the conformations of an active helicase. In fact, the single molecule experiments reported here suggest that the 2B sub-domain of the active MutL-UvrD helicase is only partially closed, i.e., intermediate between an open and closed state. In addition, in contrast to the proposed functional role of the 2B sub-domain in DNA unwinding (25, 31), deletion of the 2B sub-domain in Rep does not eliminate helicase activity, but rather activates Rep monomer helicase activity (19, 34, 51). Crosslinking of the 2B sub-domain of Rep into a closed form also

activates the Rep monomer, making it a very processive monomeric helicase(32). In that case it may be that the closed 2B sub-domain surrounds the DNA preventing dissociation.

Materials and Methods

Buffers, Proteins and DNA and all methods are provided in Supplementary Materials.

Acknowledgements

We thank Drs. Roberto Galletto, Eric Galburt and members of the Lohman lab for discussions and Thang Ho for oligodeoxynucleotides. This work was supported in part by NIH (GM045948 to TML).

References

1. Iyer RR, Pluciennik A, Burdett V, & Modrich PL (2006) DNA mismatch repair: functions and mechanisms. *Chem Rev* 106(2):302-323.
2. Sancar A (1996) DNA Excision Repair. *Annu.Rev.Biochem.* 65:43-81.
3. Atkinson J & McGlynn P (2009) Replication fork reversal and the maintenance of genome stability. *Nucleic Acids Res* 37(11):3475-3492.
4. Heller RC & Marians KJ (2007) Non-replicative helicases at the replication fork. *DNA Repair (Amst)* 6(7):945-952.
5. Veaute X*, et al.* (2005) UvrD helicase, unlike Rep helicase, dismantles RecA nucleoprotein filaments in *Escherichia coli*. *EMBO J* 24(1):180-189.
6. Petrova V*, et al.* (2015) Active displacement of RecA filaments by UvrD translocase activity. *Nucleic Acids Res* 43(8):4133-4149.
7. Gwynn EJ*, et al.* (2013) The Conserved C-Terminus of the PcrA/UvrD Helicase Interacts Directly with RNA Polymerase. *PLoS One* 8(10):e78141.
8. Epshtein V*, et al.* (2014) UvrD facilitates DNA repair by pulling RNA polymerase backwards. *Nature* 505(7483):372-377.
9. McGlynn P, Savery NJ, & Dillingham MS (2012) The conflict between DNA replication and transcription. *Mol Microbiol* 85(1):12-20.
10. Singleton MR, Dillingham MS, & Wigley DB (2007) Structure and Mechanism of Helicases and Nucleic Acid Translocases. *Annu Rev Biochem* 76:23-50.

11. Dillingham MS, Wigley DB, & Webb MR (2000) Demonstration of unidirectional single-stranded DNA translocation by PcrA helicase: measurement of step size and translocation speed. *Biochemistry* 39(1):205-212.
12. Dillingham MS, Wigley DB, & Webb MR (2002) Direct measurement of single-stranded DNA translocation by PcrA helicase using the fluorescent base analogue 2-aminopurine. *Biochemistry* 41(2):643-651.
13. Niedziela-Majka A, Chesnik MA, Tomko EJ, & Lohman TM (2007) Bacillus stearothermophilus PcrA Monomer Is a Single-stranded DNA Translocase but Not a Processive Helicase in Vitro. *J. Biol. Chem.* 282(37):27076-27085.
14. Kang YH, Lee CH, & Seo YS (Dna2 on the road to Okazaki fragment processing and genome stability in eukaryotes. *Crit Rev Biochem Mol Biol* 45(2):71-96.
15. Fischer CJ, Maluf NK, & Lohman TM (2004) Mechanism of ATP-dependent translocation of E.coli UvrD monomers along single-stranded DNA. *J Mol Biol* 344(5):1287-1309.
16. Tomko EJ, Fischer CJ, & Lohman TM (2012) Single-Stranded DNA Translocation of E. coli UvrD Monomer Is Tightly Coupled to ATP Hydrolysis. *J Mol Biol* 418(1-2):32-46.
17. Tomko EJ, Fischer CJ, Niedziela-Majka A, & Lohman TM (2007) A Nonuniform Stepping Mechanism for E. coli UvrD Monomer Translocation along Single-Stranded DNA. *Molecular Cell* 26(3):335-347.
18. Tomko EJ & Lohman TM (2017) Modulation of Escherichia coli UvrD Single-Stranded DNA Translocation by DNA Base Composition. *Biophys J* 113(7):1405-1415.
19. Brendza KM*, et al.* (2005) Autoinhibition of *Escherichia coli* Rep monomer helicase activity by its 2B subdomain. *Proc Natl Acad Sci U S A* 102(29):10076-10081.
20. Cheng W, Hsieh J, Brendza KM, & Lohman TM (2001) *E. coli* Rep oligomers are required to initiate DNA unwinding in vitro. *J. Mol. Biol.* 310(2):327-350.
21. Maluf NK, Ali JA, & Lohman TM (2003) Kinetic mechanism for formation of the active, dimeric UvrD helicase-DNA complex. *J. Biol. Chem.* 278(34):31930-31940.
22. Maluf NK, Fischer CJ, & Lohman TM (2003) A Dimer of *Escherichia coli* UvrD is the active form of the helicase in vitro. *J. Mol. Biol.* 325(5):913-935.
23. Lee KS, Balci H, Jia H, Lohman TM, & Ha T (2013) Direct imaging of single UvrD helicase dynamics on long single-stranded DNA. *Nat Commun* 4:1878.
24. Lohman TM, Tomko EJ, & Wu CG (2008) Non-hexameric DNA helicases and translocases: mechanisms and regulation. *Nat Rev Mol Cell Biol* 9(5):391-401.
25. Lee JY & Yang W (2006) UvrD Helicase Unwinds DNA One Base Pair at a Time by a Two-Part Power Stroke. *Cell* 127(7):1349-1360.
26. Jia H*, et al.* (2011) Rotations of the 2B sub-domain of E. coli UvrD helicase/translocase coupled to nucleotide and DNA binding. *J Mol Biol* 411(3):633-648.
27. Nguyen B, Ordabayev Y, Sokoloski JE, Weiland E, & Lohman TM (2017) Large domain movements upon UvrD dimerization and helicase activation. *Proc Natl Acad Sci U S A* 114(46):12178-12183.
28. Korolev S, Hsieh J, Gauss GH, Lohman TM, & Waksman G (1997) Major domain swiveling revealed by the crystal structures of complexes of E. coli Rep helicase bound to single-stranded DNA and ADP. *Cell* 90(4):635-647.
29. Myong S, Rasnik I, Joo C, Lohman TM, & Ha T (2005) Repetitive shuttling of a motor protein on DNA. *Nature* 437(7063):1321-1325.

30. Subramanya HS, Bird LE, Brannigan JA, & Wigley DB (1996) Crystal Structure of a DExx box DNA helicase. *Nature* 384:379-383.
31. Velankar SS, Soultanas P, Dillingham MS, Subramanya HS, & Wigley DB (1999) Crystal Structures of Complexes of PcrA DNA Helicase with a DNA Substrate Indicate an Inchworm Mechanism. *Cell* 97:75-84.
32. Arslan S, Khafizov R, Thomas CD, Chemla YR, & Ha T (2015) Protein structure. Engineering of a superhelicase through conformational control. *Science* 348(6232):344-347.
33. Park J*, et al.* (2010) PcrA Helicase Dismantles RecA Filaments by Reeling in DNA in Uniform Steps. *Cell* 142(4):544-555.
34. Cheng W*, et al.* (2002) The 2B Domain of the *Escherichia coli* Rep protein is not required for DNA helicase activity. *Proc. Natl. Acad. Sci., U.S.A.* 99:16006-16011.
35. Makurath MA, Whitley KD, Nguyen B, Lohman TM, & Chemla YR (2019) Regulation of Rep helicase unwinding by an auto-inhibitory subdomain. *Nucleic Acids Res*.
36. Comstock MJ*, et al.* (2015) Protein structure. Direct observation of structure-function relationship in a nucleic acid-processing enzyme. *Science* 348(6232):352-354.
37. Chisty LT*, et al.* (2013) Monomeric PcrA helicase processively unwinds plasmid lengths of DNA in the presence of the initiator protein RepD. *Nucleic Acids Res* 41(9):5010-5023.
38. Yamaguchi M, Dao V, & Modrich P (1998) MutS and MutL activate DNA helicase II in a mismatch-dependent manner. *J Biol Chem* 273(15):9197-9201.
39. Mechanic LE, Frankel BA, & Matson SW (2000) Escherichia coli MutL loads DNA helicase II onto DNA. *J Biol Chem* 275(49):38337-38346.
40. Lahue RS, Au KG, & Modrich P (1989) DNA mismatch correction in a defined system. *Science* 245:160-164.
41. Ordabayev YA, Nguyen B, Niedziela-Majka A, & Lohman TM (2018) Regulation of UvrD Helicase Activity by MutL. *J Mol Biol* 430(21):4260-4274.
42. Nguyen B*, et al.* (2014) Diffusion of human replication protein A along single-stranded DNA. *J Mol Biol* 426(19):3246-3261.
43. Marras SA, Kramer FR, & Tyagi S (2002) Efficiencies of fluorescence resonance energy transfer and contact-mediated quenching in oligonucleotide probes. *Nucleic Acids Res* 30(21):e122.
44. Galletto R, Jezewska MJ, & Bujalowski W (2005) Kinetics of allosteric conformational transition of a macromolecule prior to ligand binding: analysis of stopped-flow kinetic experiments. *Cell Biochem Biophys* 42(2):121-144.
45. Vogt AD & Di Cera E (2012) Conformational selection or induced fit? A critical appraisal of the kinetic mechanism. *Biochemistry* 51(30):5894-5902.
46. Ali JA, Maluf NK, & Lohman TM (1999) An oligomeric form of E. coli UvrD is required for optimal helicase activity. *J Mol Biol* 293(4):815-834.
47. Niedziela-Majka A, Maluf NK, Antony E, & Lohman TM (2011) Self-assembly of Escherichia coli MutL and its complexes with DNA. *Biochemistry* 50(37):7868-7880.
48. Gianni S, Dogan J, & Jemth P (2014) Distinguishing induced fit from conformational selection. *Biophys Chem* 189:33-39.
49. Hammes GG, Chang YC, & Oas TG (2009) Conformational selection or induced fit: a flux description of reaction mechanism. *Proc Natl Acad Sci U S A* 106(33):13737-13741.

50. Galburt EA & Rammohan J (2016) A Kinetic Signature for Parallel Pathways: Conformational Selection and Induced Fit. Links and Disconnects between Observed Relaxation Rates and Fractional Equilibrium Flux under Pseudo-First-Order Conditions. *Biochemistry* 55(50):7014-7022.
51. Makurath MA, Whitley KD, Nguyen B, Lohman TM, & Chemla YR (2019) Regulation of Rep helicase unwinding by an auto-inhibitory subdomain. *Nucleic Acids Res* 47(5):2523-2532.
52. Runyon GT, Wong I, & Lohman TM (1993) Overexpression, purification, DNA binding, and dimerization of the Escherichia coli uvrD gene product (helicase II). *Biochemistry* 32(2):602-612.
53. Wong I, Chao KL, Bujalowski W, & Lohman TM (1992) DNA-induced dimerization of the Escherichia coli rep helicase. Allosteric effects of single-stranded and duplex DNA. *J Biol Chem* 267(11):7596-7610.
54. Lucius AL, Jason Wong C, & Lohman TM (2004) Fluorescence stopped-flow studies of single turnover kinetics of *E.coli* RecBCD helicase-catalyzed DNA unwinding. *J. Mol. Biol.* 339(4):731-750.
55. Antony E, Kozlov AG, Nguyen B, & Lohman TM (2012) Plasmodium falciparum SSB tetramer binds single-stranded DNA only in a fully wrapped mode. *J Mol Biol* 420(4-5):284-295.
56. Joo C & Ha T (2008) Single Molecule FRET with Total Internal Reflection Microscopy. *Single Molecule techniques: A Laboratory Manual.*, eds Selvin PR & Ha T (Cold Spring Harbor Laboratory Press, NY, Cold Spring Harbor, NY), pp 3-36.
57. van de Meent JW, Bronson JE, Wiggins CH, & Gonzalez RL, Jr. (2014) Empirical Bayes methods enable advanced population-level analyses of single-molecule FRET experiments. *Biophys J* 106(6):1327-1337.
58. Efron B (1979) 1977 Rietz Lecture - Bootstrap Methods - Another Look at the Jackknife. *Ann Stat* 7(1):1-26.
59. Fischer CJ & Lohman TM (2004) ATP-dependent translocation of proteins along single-stranded DNA: models and methods of analysis of pre-steady state kinetics. *J Mol Biol* 344(5):1265-1286.
60. Bujalowski W & Jezewska MJ (2000) Kinetic Mechanism of the Single-stranded DNA Recognition by *Escherichia coli* Replicative Helicase DnaB Protein. Application of the Matrix Projection Operator Technique to Analyze Stopped-flow Kinetics. *J. Mol. Biol.* 295:831-852.

Table 1. Kinetic parameters for scheme in Figure 4A from global NLLS analysis

k_1 (M^{-1} s^{-1})	k_{-1} (s^{-1})	k_2 (s^{-1})	k_{-2} (s^{-1})	k_3 (M^{-1} s^{-1})	k_{-3} (s^{-1})	k_4 (s^{-1})	k_{-4}[a] (s^{-1})
$(4.01\pm0.01)\times10^6$	121.3±0.1	0.0380±0.0001	0.4076±0.0005	$(5.82\pm0.01)\times10^6$	0.433±0.001	$(9.54\pm0.01)\times10^{-2}$	$(2.49\pm0.01)\times10^{-3}$

[a] During the fit k_{-4} was constrained ($k_{-4} = (k_{-2}k_{-3}k_1k_4)/(k_2k_3k_{-1})$) to satisfy detailed balance

Table 2. Thermodynamic and spectroscopic[a] parameters for scheme in Figure 4A

K_1 (M^{-1})	K_2	K_3 (M^{-1})	K_4	ΔF_2^{Cy3} (U_CD)	ΔF_3^{Cy3} (MU_OD)	ΔF_4^{Cy3} (MU_CD)	ΔF_2^{Cy5} (U_CD)	ΔF_3^{Cy5} (MU_OD)	ΔF_4^{Cy5} (MU_CD)
$(3.31\pm0.01)\times10^4$	$(9.32\pm0.04)\times10^{-2}$	$(1.34\pm0.01)\times10^7$	38.3±0.2	-0.465±0.005	5.32±0.06	0.085±0.001	0.245±0.003	1.35±0.02	0.493±0.001

[a] Values relative to the Cy3 and Cy5 fluorescence intensities of the U_OD, F_1^{Cy3} and F_1^{Cy5}.

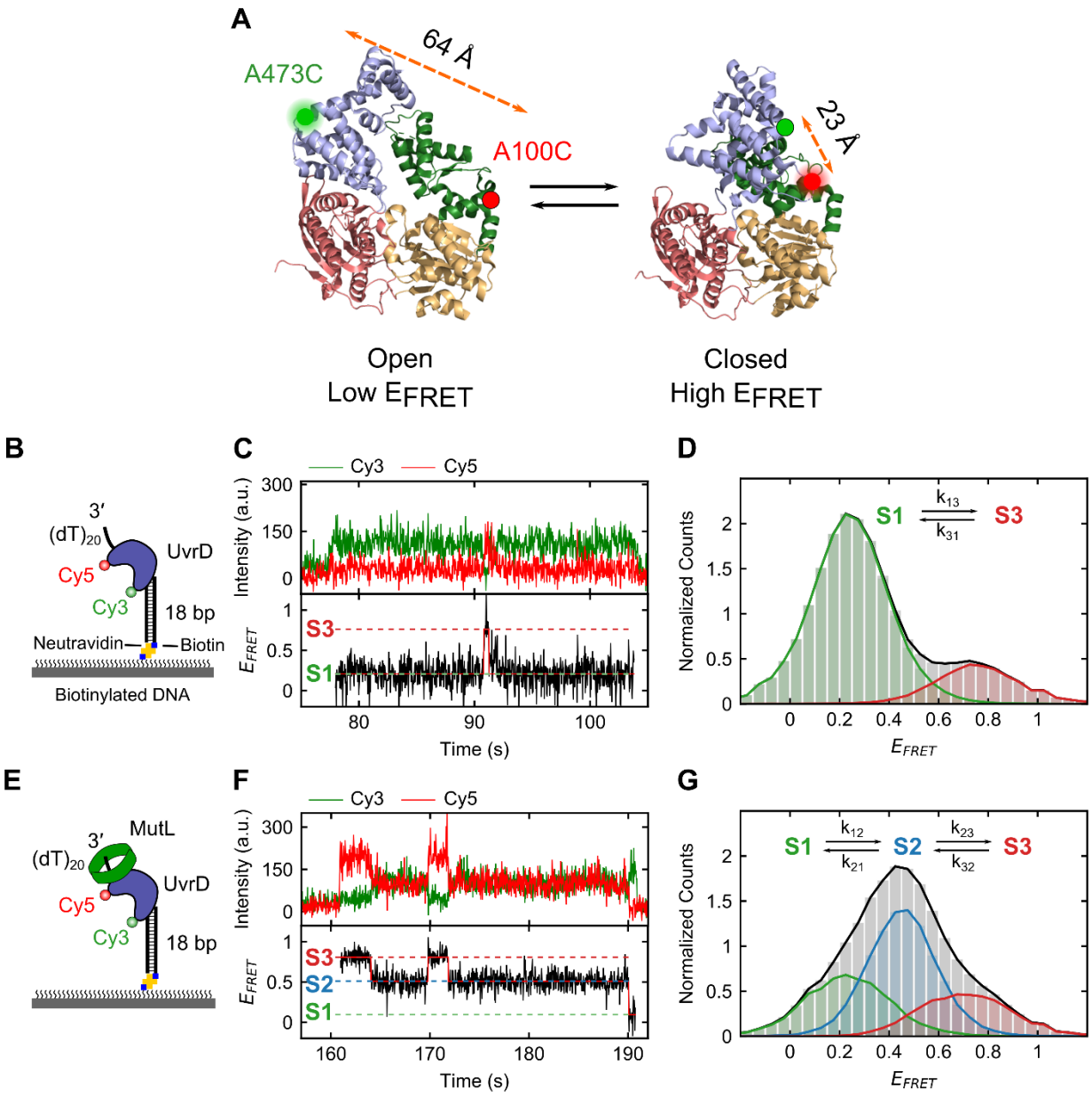

Figure 1. The 2B sub-domain of UvrD in complex with a DNA unwinding substrate shifts to a more closed conformation upon MutL binding. A, The 2B sub-domain rotation of Cy3/Cy5 labeled UvrD-DM-1B/2B can be monitored by a change in FRET. The labeling positions (A100C and A473C) and the distances between them are indicated in the apo UvrD structure (open state, low-E_{FRET}) and DNA bound UvrD structure (closed state, high-E_{FRET}). **B**, Depiction of Cy3/Cy5-labeled UvrD-DM-1B/2B binding to a 3′-$(dT)_{20}$-ds18-biotin DNA tethered on a PEG surface via biotin-Neutravidin linkage. **C**, Single molecule time trace showing binding of UvrD-DM-1B/2B to DNA and rotation of the 2B sub-domain between open (S1) and closed (S3) states. **D**, FRET histogram obtained from 346 traces. UvrD monomer bound to DNA exists in two states: S1 state with E_{FRET}=0.26±0.08 (18% of population) and S3 state with

E_{FRET}=0.75±0.08 (82% of population). **E**, Binding of MutL and Cy3/Cy5-UvrD-DM-1B/2B to a 3′-$(dT)_{20}$-ds18-biotin DNA on the surface. **F**, Single molecule FRET trajectory of Cy3/Cy5-UvrD-DM-1B/2B (250 pM) binding to the immobilized DNA in the presence of MutL (250 nM dimer). **G**, FRET histogram obtained from 70 traces. The UvrD monomer bound to DNA is observed in three states in the presence of MutL: S1 state with E_{FRET}=0.22±0.11 (29% of population), S2 state with E_{FRET}=0.45±0.08 (49% population), and S3 state with E_{FRET}=0.76±0.12 (22% of population).

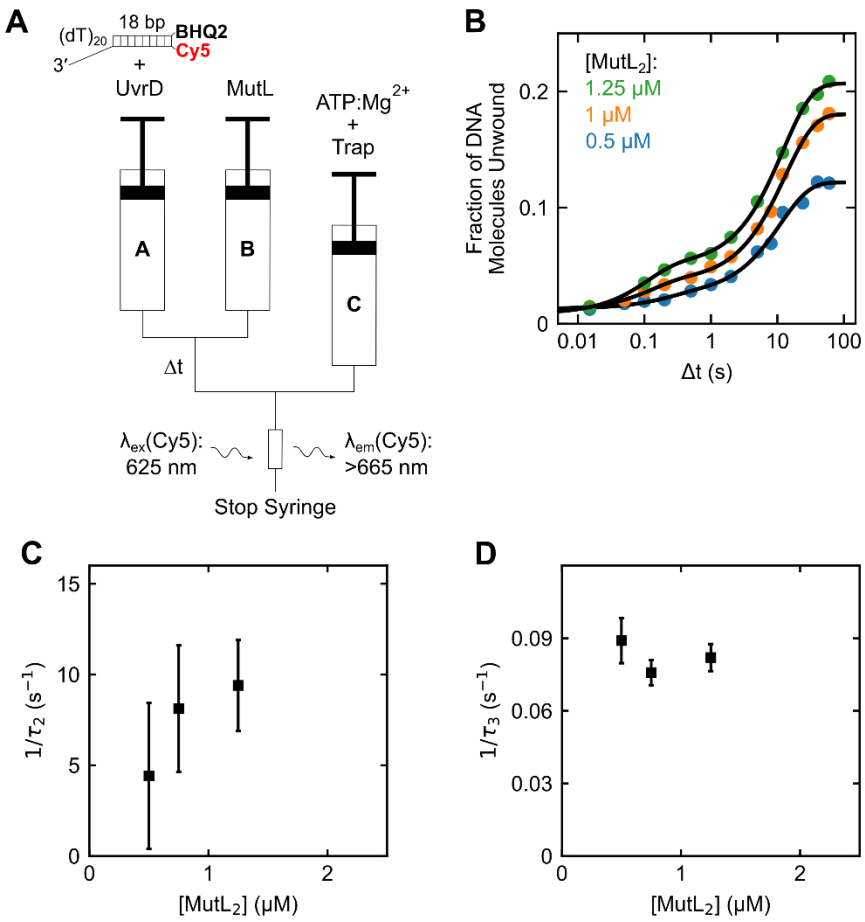

Figure 2. Kinetics of formation of the active MutL-UvrD-DNA helicase. A, Schematic representation of the sequential-mixing stopped-flow fluorescence experiment. Experiments were performed in buffer T at 25 °C. **B**, Each data point represents the fraction of DNA molecules unwound in a series of experiments performed with 100 nM UvrD, 250 nM 3′-$(dT)_{20}$-ds18-BHQ2/Cy5 DNA substrate and the indicated MutL concentration plotted as a function of Δt on a log time-scale. Continuous lines are simulations based on the best-fit values using Eq. (2). **C**,**D**, Reciprocal relaxation times ($1/\tau_2$ and $1/\tau_3$) obtained from non-linear least-squares fitting of time courses in panel **B** using Eq. (2).

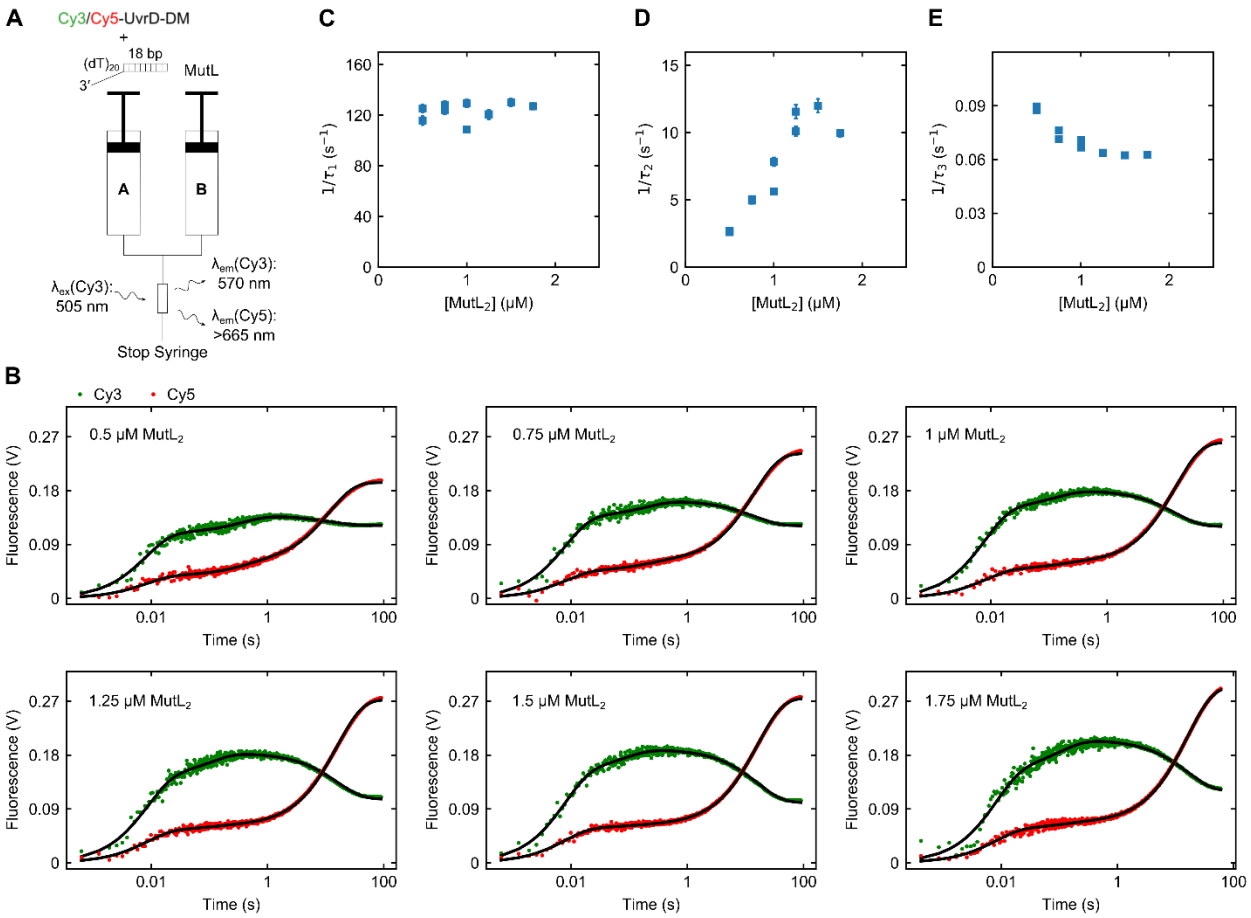

Figure 3. Kinetics of conformational changes in the UvrD 2B sub-domain upon MutL binding. A, Schematic representation of the stopped-flow experiment monitoring conformational changes in the 2B sub-domain upon binding of MutL to Cy3/Cy5-UvrD-DM-1B/2B monomer-DNA complex. Experiments were performed in buffer T at 25 °C. **B** Cy3 and Cy5 fluorescence time courses from experiments performed with 100 nM Cy3/Cy5-UvrD-DM-1B/2B pre-equilibrated with 250 nM 3′-$(dT)_{20}$-ds18 for 5 min and then rapidly mixed with MutL at the indicated concentration. Continuous lines are simulations based on the best-fit values using Eq. (17). **C-E**, The dependence of the reciprocal relaxation times ((C) $1/\tau_1$, (D) $1/\tau_2$, and (E) $1/\tau_3$) on the total [$MutL_2$]. The error bars are standard deviations from the NLLS fitting.

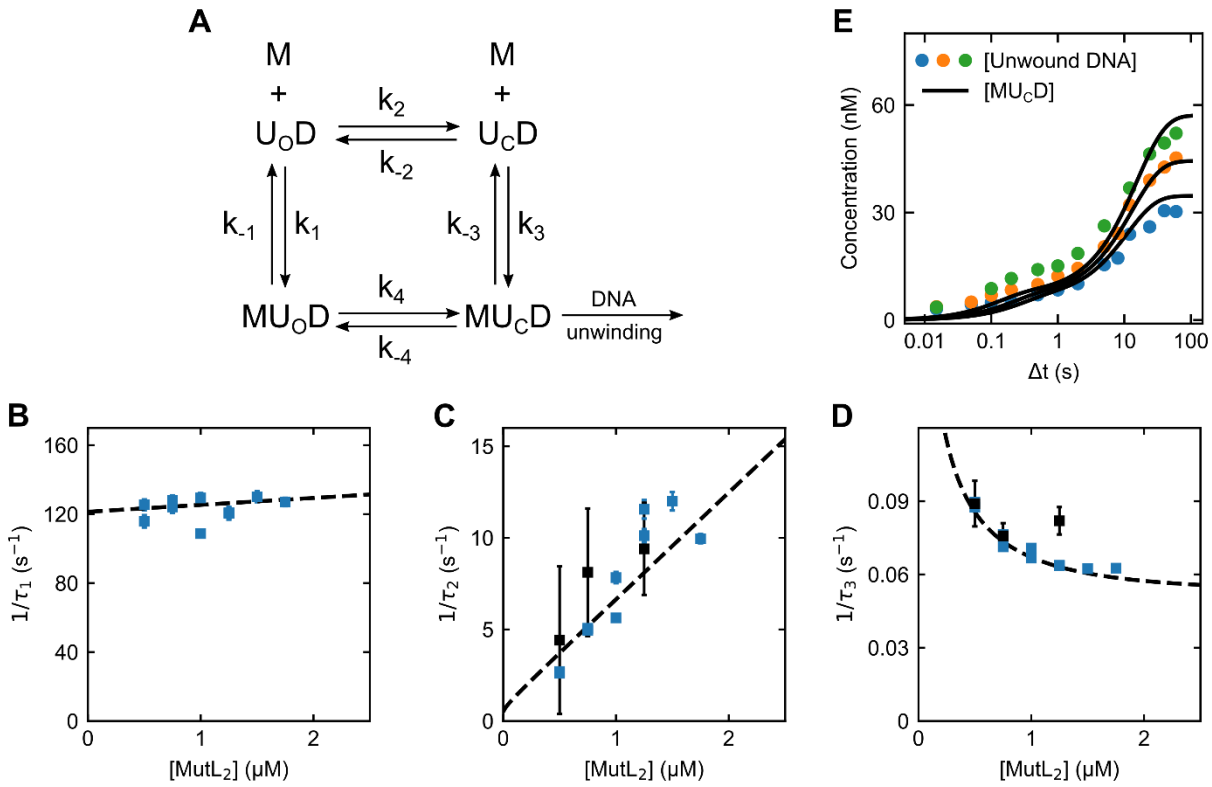

Figure 4. The kinetic mechanism for MutL binding to the UvrD-DNA complex.
A, Four states defined by the 2B sub-domain conformational state of UvrD and MutL (M) binding. **B-D**, Dashed lines show the dependence of the reciprocal relaxation times on the MutL concentration simulated from the scheme in panel A and the rate constants in Table 1 overlaid on the experimentally obtained values. **E**, Simulations of the time course for formation of the active MutL-UvrD helicase (*MU_CD*) overlaid on the experimental concentrations determined from the experiments in Figure 2B.

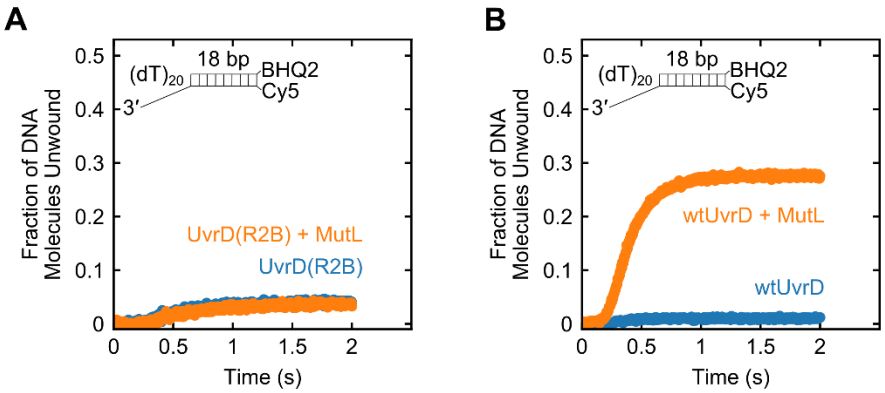

Figure 5. MutL stimulation of UvrD helicase activity is specific for the UvrD 2B sub-domain. A, Stopped-flow DNA unwinding experiments were performed with 3′-$(dT)_{20}$-ds18-BHQ2/Cy5 DNA substrate in buffer T at 25°C. **A**, Monomeric UvrD(Rep2B) shows little DNA unwinding activity and is not stimulated by MutL. DNA (50 nM) was pre-incubated with 25 nM UvrD(Rep2B) alone (blue) or 25 nM UvrD(Rep2B) plus 500 nM MutL dimer (orange). **B**, wtUvrD monomer shows helicase activity in the presence of MutL. DNA (50 nM) was pre-incubated with 25 nM UvrD alone (blue) or 25 nM UvrD plus 500 nM MutL dimer (orange).

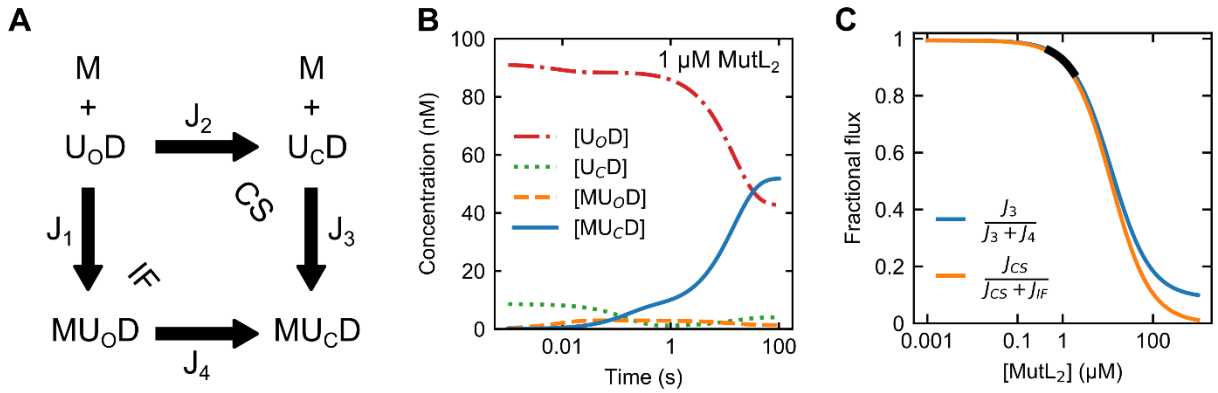

Figure 6. Species concentration profiles and fluxes at low and high [MutL]. A, Two alternative pathways exist for formation of MU_CD: conformational selection through steps 2 and 3, and induced fit through steps 1 and 4. **B**, Simulations of concentrations of each UvrD-DNA species for 1 μM MutL dimer based on the rate constants in Table 1 using Eq. (8). **C**, Fractional net flux through step 3 (blue) and fractional equilibrium forward flux (Eq. (22)) through the conformational selection pathway (orange) of the cycle are plotted as a function of MutL concentration for the best-fit values of the rate constants determined using Eq. (8). The black line is the range of MutL concentrations used in our study.

Supplementary information for:

UvrD Helicase Activation by MutL Involves Closing of its 2B sub-domain

Yerdos A. Ordabayev, Binh Nguyen, Alexander G. Kozlov, Haifeng Jia, Timothy M. Lohman*

Department of Biochemistry and Molecular Biophysics

Washington University School of Medicine

660 S. Euclid Ave., Box 8231

St. Louis, MO 63110

*Address correspondence to:

Department of Biochemistry and Molecular Biophysics

Washington University School of Medicine

660 S. Euclid Ave., Box 8231

St. Louis, MO 63110

E-mail: lohman@biochem.wustl.edu

Tel: (314)-362-4393

Fax: (314)-362-7183

Methods

Buffers and reagents

Buffers were made with reagent-grade chemicals and distilled water that was deionized using a Milli-Q purification system. Buffer T is 10 mM Tris-HCl (pH 8.3) at 25 °C, 20 mM NaCl, 20% (v/v) glycerol, and 1 mM 2-mercaptoethanol. Storage minimal buffer is 20 mM Tris-HCl (pH 8.3) at 25 °C, 200 mM NaCl, 50% (v/v) glycerol. Imaging buffer is 10 mM Tris-HCl (pH 8.3) at 25 °C, 20 mM NaCl, 20% (v/v) glycerol, 3 mM Trolox, 0.8% (w/v) dextrose, 20 units/ml glucose oxidase, and 20 units/ml catalase. ATP concentration was determined spectrophotometrically using an extinction coefficient of $\varepsilon_{259} = 15.4 \times 10^3\ M^{-1}\ cm^{-1}$.

Proteins

Wild-type UvrD and UvrDΔCys(A100C, A473C) were expressed and purified as described (26) and stored in minimal storage buffer at −20 °C. UvrD monomer concentrations were determined spectrophotometrically in 10 mM Tris (pH 8.1), 200 mM NaCl, 20% (v/v) glycerol using an extinction coefficient $\varepsilon_{280} = 1.06 \times 10^5\ M^{-1}\ cm^{-1}$. The double-cysteine variant UvrDΔCys(A100C, A473C) (UvrD-DM) was labeled stochastically with an equimolar mixture of Cy3 and Cy5 maleimides (GE Healthcare) followed by thrombin digestion to remove the 6XHis tag (26). The fluorophore labeling efficiency was determined as described (26) with a labeling efficiency of ~ 90%.

The 2B sub-domain of UvrD was replaced with the 2B sub-domain of Rep to make the chimeric UvrD(Rep2B) protein as follows. The plasmid for UvrD(Rep2B), pGG245-UvrD(Rep2B), was constructed using the two plasmids, pGG209LR3(wtUvrD) and pGG245(wtRep) as templates. Using standard molecular biology approaches. The final

sequence was confirmed by DNA sequencing. The end result is that 168 amino acids of UvrD from M379 – G545 were replaced with 167 amino acids of Rep from T375-G542. The UvrD(Rep2B) chimera contains 723 amino acids (82.5 kDa).

UvrD(Rep2B) protein was overexpressed in *E. coli* BL21(DE3) ΔUvrD containing pGroESL in Terrific Broth (supplemented with Kanamycin (50 μg/ml), chloramphenicol (35 μg/ml), tetracycline (12.5 μg/ml), thiamine (10 μg/ml), and thymine (4 μg/ml)). Cells were grown at 37°C until OD_{600}~0.8 - 1.0, followed by a shift to 25°C and addition of IPTG to 0.2 mM and growth for 3 hours. Purification of the UvrD(Rep2B) protein followed the procedure for wt UvrD (52) with the following modifications. The solubility of UvrD(Rep2B) after cell lysis was low and most protein was found in the cell pellet. The cell pellet was solubilized in 6 M GdnHCl, 50 mM Tris, 1 mM EDTA, 5 mM BME, pH 8.3, 25 °C and then dialyzed extensively vs. 20 mM Tris, 400 mM NaCl, 0.2 mM EDTA, 0.1 mM EGTA, 20 % (v/v) glycerol, 5 mM 2-ME, pH 8.3, 25 °C. The buffer was changed four times every 8 hours. The solution was centrifuged for 15 min at 13k rpm and the supernatant was saved. DNA was precipitated with Polymin P to 0.2% final concentration and the protein in the supernatant was precipitated with 40% ammonium sulfate. The ammonium sulfate pellet was slowly resuspended in Buffer G + 300 mM NaCl and the refolded UvrD(Rep2B) was further purified as described for wtUvrD (52).

DNA

The oligodeoxynucleotides were synthesized using a Mermaid 4 synthesizer (Plano, TX) with reagents from Glen Research (Sterling, VA), purified by electroelution from denaturing polyacrylamide gels, concentrations determined by spectrophotometric analysis as described (53,

54). The partial duplex DNA substrates used in this study consisted of an 18-bp duplex with a flanking 3′-$(dT)_{20}$ tail. The sequence of the short top-strand is 5′-GCCCTGCTGCCGACCAAC-3′ and the sequence of the bottom long-strand is 5′-GTTGGTCGGCAGCAGGGC$(dT)_{20}$-3′. Biotin tag on 3′-$(dT)_{20}$-ds18-biotin DNA was attached at the 3′-end of the short-strand, BHQ2 quencher dye and Cy5 dye on 3′-$(dT)_{20}$-ds18-BHQ2/Cy5 were attached at the 3′-end of the short-strand and the 5′-end of the long-strand, respectively. The sequence of the 3′ tailed DNA hairpin used as a protein trap is 5′-GCCTCGCTGCTTTTTGCAGCGAGGC$(dT)_{40}$-3′. DNA duplexes were prepared by annealing equimolar concentrations of the complementary strands in 10 mM Tris (pH 8.1) and 100 mM NaCl by heating to 95 °C for 5 min and then slowly cooling to room temperature.

Single-molecule total internal reflection fluorescence microscopy experiments

Single-molecule FRET experiments were carried out as described (42, 55) using an Olympus IX71 microscope (model IX2_MPI-TIRTL) with a 60× oil-immersed objective (N.A. 1.45). Movies of Cy3 and Cy5 fluorescence emissions were acquired on separated channels at a frame rate of 32 ms under continuous illumination of Cy3 fluorophore with a 532 nm laser. The ratio of the Cy3 and Cy5 intensities corrected for instrumental detection efficiency and leakage of the donor signal into the acceptor detection channel was used to calculate the approximate FRET efficiency (42, 56).

To study the 2B sub-domain conformation of DNA-bound UvrD we first attached DNA to the slide surface by incubating 100 pM biotinylated DNA for 5 min. The excess DNA was washed out. Then, 250 pM Cy3/Cy5-UvrD-DM-1B/2B alone or 250 pM Cy3/Cy5-UvrD-DM-1B/2B plus 250 nM MutL dimer in imaging buffer was injected. Stochastic labeling of UvrD-DM-1B/2B construct with two dyes produces a mixture of Cy3 and Cy5 labeled populations

(26). In order to analyze the FRET signal between 2B and 1B subdomains we only selected molecules labeled with both Cy3 and Cy5 dyes. Hidden Markov models were used to globally analyze FRET trajectories using an empirical Bayes method as implemented in ebFRET software (57). To obtain transition rates from state *i* to state *j*, k_{ij}, dwell times were fit to a single exponential distribution, $k_{ij}e^{-k_{ij}t}$, using the maximum likelihood estimation method implemented in the Python `scipy.stats` module. Standard errors were estimated using a bootstrap method (58) using custom script written in Python.

Stopped-flow fluorescence kinetic experiments

All stopped-flow experiments were performed in buffer T at 25 °C using an SX.18MV stopped-flow spectrofluorometer (Applied Photophysics Ltd., Leatherhead, UK).

Single-round DNA unwinding assay

DNA unwinding activity of UvrD under single-round conditions was monitored by the increase in Cy5 fluorescence emission upon complete unwinding of 3′-$(dT)_{20}$-ds18-Cy5/BHQ2 DNA substrate by UvrD as described (41). UvrD-DNA-MutL complex was pre-incubated in buffer T in the first reservoir syringe of the stopped-flow apparatus and then was rapidly mixed with the solution from the second reservoir syringe containing 1 mM ATP, 2 mM $MgCl_2$, and 2 μM 10-bp DNA hairpin possessing a 3′-$(dT)_{40}$ ssDNA tail in buffer T. Reaction progress was monitored by exciting Cy5 fluorophore using 625 nm LED and detecting its fluorescence emission using a >665 nm long-pass filter (Oriel Corp., Stradford, CT). Fluorescence time-courses for each experimental condition are averages of at least 10 repeated measurements.

The time courses of DNA unwinding were analyzed globally using n-step sequential model with an additional step preceding DNA unwinding (41):

$$f_{ss}(t) = A_T \mathcal{L}^{-1}\left(\frac{k_c k_{obs}^{\frac{L}{m}}}{s(k_c + s)(k_{obs} + s)^{\frac{L}{m}}}\right) \quad (1)$$

where $f_{ss}(t)$ is the fraction of ssDNA molecules produced, $\mathscr{L}^{-1}$ is the inverse Laplace transform operator, s is the Laplace variable, A_T is the total DNA unwinding amplitude, k_c is the rate constant for the additional step not involved in unwinding, k_{obs} is the observed unwinding rate constant for n repeating steps, L is the DNA duplex length in bp, and $n = L/m$.

Kinetics of formation of active MutL-UvrD-DNA complexes

Kinetics of formation of active MutL-UvrD-DNA helicase was monitored using the "sequential-mixing mode" of the stopped-flow. In the first-mixing step MutL in buffer T in one syringe is mixed with a UvrD-DNA complex in buffer T for a defined period of time, Δt, and then mixed with1 mM ATP, 2 mM $MgCl_2$, and 2 μM 10-bp DNA hairpin possessing a 3′-$(dT)_{40}$ ssDNA tail in buffer T. Progress of DNA unwinding was monitored by exciting the Cy5 fluorescence using a 625 nm LED and detecting its fluorescence emission using a >665 nm long-pass filter (Oriel Corp., Stamford, CT). Fluorescence time courses for each experimental condition are averages of at least 4 repeated measurements.

The biphasic time courses of formation of the active MutL-UvrD-DNA complexes were fit to a double-exponential function (Eq. (2)) to determine the relaxation times and amplitudes

$$f_{ss}(t) = A_0 + A_2\left(1 - e^{-\frac{t}{\tau_2}}\right) + A_3\left(1 - e^{-\frac{t}{\tau_3}}\right) \quad (2)$$

for each phase, where τ_2 and A_2 are the relaxation time and amplitude of the fast phase and τ_3 and A_3 are the relaxation time and amplitude of slow phase.

Kinetics of conformational changes in the 2B sub-domain

The kinetics of the 2B sub-domain conformational change upon binding of MutL to the UvrD-DNA complex was monitored using Cy3/Cy5 labeled UvrD-DM-1B/2B (26) in the stopped-flow. Cy3/Cy5 labeled UvrD-DM-1B/2B was pre-equilibrated with 3′-$(dT)_{20}$-ds18 in buffer T and loaded into one syringe and MutL in buffer T was loaded into the second syringe. Solutions in both syringes were incubated at 25 °C for 5 min and then rapidly mixed. Cy3 fluorescence was excited using a 505 nm LED and fluorescence emissions were monitored at 570 nm using an interference filter (Oriel Corp., Stamford, CT) for Cy3 and at >665 nm using a long-pass filter (Oriel Corp., Stamford, CT) for Cy5. Fluorescence time courses for each experimental condition are averages of at least 10 repeated measurements.

Kinetics of UvrD(Rep2B) monomer ssDNA translocation

The time course for UvrD(Rep2B) monomer translocation along ssDNA was monitored by the decrease in fluorescein fluorescence upon the arrival of UvrD(Rep2B) at the 5′-end of 5′-F-$(dT)_L$ and analyzed as described (15, 59). Fluorescein fluorescence was excited using 494 nm LED and emission was detected at >520 nm using a long-pass filter (Oriel Corp., Stamford, CT).

Fluorescein fluorescence time courses were analyzed using *n*-step sequential translocation with two-step dissociation model as previously described (15, 59):

$$f(t) = \frac{A}{1+nr}\mathcal{L}^{-1}\left(\frac{1}{s+k_c}\left(1+\frac{k_t r}{s+k_d}\left(1-\left(\frac{k_t}{s+k_t+k_d}\right)^n\right)\right)\left(1+\frac{f^*_{end}}{f_{end}}\frac{k_c}{(s+k_{end})}\right)\right) \quad (3)$$

Analysis of the time courses for MutL binding to UvrD-DNA complexes

The system of differential equations describing the time courses of the reactions in Figure 4A are given in Eq. (4):

$$\begin{aligned}
\frac{d[U_O D]}{dt} &= -k_2[U_O D] - k_1[U_O D][M] + k_{-2}[U_C D] + k_{-1}[MU_O D] \\
\frac{d[U_C D]}{dt} &= k_2[U_O D] - k_{-2}[U_C D] - k_3[U_C D][M] + k_{-3}[MU_C D] \\
\frac{d[MU_O D]}{dt} &= k_1[U_O D][M] - (k_{-1} + k_4)[MU_O D] + k_{-4}[MU_C D] \\
\frac{d[MU_C D]}{dt} &= k_3[U_C D][M] + k_4[MU_O D] - (k_{-3} + k_{-4})[MU_C D] \\
\frac{d[M]}{dt} &= -k_1[U_O D][M] - k_3[U_C D][M] + k_{-1}[MU_O D] + k_{-3}[MU_C D]
\end{aligned} \tag{4}$$

with the initial concentrations at time $t = 0$ given in Eq. (5),

$$\begin{aligned}
[U_O D]_0 &= \frac{[U]_{Tot}}{(1 + K_2)} \\
[U_C D]_0 &= \frac{[U]_{Tot} K_2}{(1 + K_2)} \\
[MU_O D]_0 &= 0 \\
[MU_C D]_0 &= 0 \\
[M]_0 &= [M]_{Tot}
\end{aligned} \tag{5}$$

where $[U]_{Tot}$ is the total concentration of the initial UvrD-DNA complex, $[M]_{Tot}$ is the total initial MutL dimer concentration, and $K_2 = k_2/k_{-2}$ is the equilibrium constant for the conformational transition ($U_O D \leftrightarrow U_C D$). We used the Python `scipy.integrate.odeint` module to numerically integrate this system of differential equations given the initial concentrations.

Analysis of the fluorescence stopped-flow experiments monitoring the fluorescence changes of the Cy3/Cy5-UvrD-DM-1B/2B upon binding MutL was performed as follows. There are eight molar fluorescence intensities, F_1^{Cy3}, F_2^{Cy3}, F_3^{Cy3}, and F_4^{Cy3} for Cy3 and F_1^{Cy5}, F_2^{Cy5}, F_3^{Cy5}, and F_4^{Cy5} for Cy5 characterizing $U_O D$, $U_C D$, $MU_O D$, and $MU_C D$, respectively. The Cy3 and Cy5 fluorescence signals of the system at time t, $F^{Cy3}(t)$ and $F^{Cy5}(t)$, are defined in Eq. (6),

$$F^{Cy3}(t) = F_1^{Cy3}[U_O D] + F_2^{Cy3}[U_C D] + F_3^{Cy3}[MU_O D] + F_4^{Cy3}[MU_C D] + F_0^{Cy3}$$
$$F^{Cy5}(t) = F_1^{Cy5}[U_O D] + F_2^{Cy5}[U_C D] + F_3^{Cy5}[MU_O D] + F_4^{Cy5}[MU_C D] + F_0^{Cy5} \quad (6)$$

where F_0^{Cy3} and F_0^{Cy5} are the values at t=0 for Cy3 and Cy5 fluorescence.

Introducing Eq. (7) for the mass conservation of UvrD into Eq. (6), yields Eq. (8).

$$[U]_{Tot} = [U_O D] + [U_C D] + [MU_O D] + [MU_C D] \quad (7)$$

$$F^{Cy3}(t) = \left(F_2^{Cy3} - F_1^{Cy3}\right)[U_C D] + \left(F_3^{Cy3} - F_1^{Cy3}\right)[MU_O D] + \left(F_4^{Cy3} - F_1^{Cy3}\right)[MU_C D] + const$$
$$F^{Cy5}(t) = \left(F_2^{Cy5} - F_1^{Cy5}\right)[U_C D] + \left(F_3^{Cy5} - F_1^{Cy5}\right)[MU_O D] + \left(F_4^{Cy5} - F_1^{Cy5}\right)[MU_C D] + const \quad (8)$$

Global nonlinear least squares (NLLS) fitting of the fluorescence time courses (Supplemental Figure 3) to Eq. (8) with globally constrained rate constants satisfying detailed balance (i.e., $(k_1 k_4)/(k_{-1} k_{-4}) = (k_2 k_3)/(k_{-2} k_{-3})$) and the Cy3 and Cy5 molar fluorescence intensities was performed in Python using custom script.

Analysis of the relaxation times

We analyzed the relaxation kinetics of the fluorescence changes using the matrix projection operator method (60). Under pseudo-first order conditions with respect to MutL concentration, the system of differential equations describing the time courses of the UvrD-DNA species can be expressed in matrix notation as in Eqs. (9) and (10).

$$\begin{pmatrix} \frac{d[U_O D]}{dt} \\ \frac{d[U_C D]}{dt} \\ \frac{d[MU_O D]}{dt} \\ \frac{d[MU_C D]}{dt} \end{pmatrix} = \begin{pmatrix} -k_2 - k_1[M] & k_{-2} & k_{-1} & 0 \\ k_2 & -k_{-2} - k_3[M] & 0 & k_{-3} \\ k_1[M] & 0 & -k_{-1} - k_4 & k_{-4} \\ 0 & k_3[M] & k_4 & -k_{-3} - k_{-4} \end{pmatrix} \begin{pmatrix} [U_O D] \\ [U_C D] \\ [MU_O D] \\ [MU_C D] \end{pmatrix} \quad (9)$$

or

$$\frac{dU}{dt} = \boldsymbol{MU} \tag{10}$$

where $\boldsymbol{M}$ is the coefficient matrix, and $\boldsymbol{U}$ is the vector of concentrations.

Using the matrix projection operators, $\boldsymbol{Q_i}$, the solution of Eq. (9) is given by Eq. (11) (60). The quantities λ_1, λ_2, and λ_3 are non-zero eigenvalues of the coefficient matrix $\boldsymbol{M}$ at a

$$\boldsymbol{U} = \boldsymbol{Q_0 U_0} + \boldsymbol{Q_1 U_0} \exp(\lambda_1 t) + \boldsymbol{Q_2 U_0} \exp(\lambda_2 t) + \boldsymbol{Q_3 U_0} \exp(\lambda_3 t) \tag{11}$$

given ligand concentration which can be determined either numerically using the Python `numpy.linalg.eigvals` module or analytically (Appendix A). $\boldsymbol{U_0}$ is the column vector of the initial concentrations of UvrD species before MutL binding and is given in Eq. (12).

$$\boldsymbol{U_0} = \begin{pmatrix} \dfrac{[U]_{Tot}}{1 + K_2} \\ \dfrac{[U]_{Tot} K_2}{1 + K_2} \\ 0 \\ 0 \end{pmatrix} \tag{12}$$

$\boldsymbol{Q_i}$ is defined as in Eq. (13), where $\boldsymbol{I}$ is the identity matrix of the same size as $\boldsymbol{M}$.

$$\boldsymbol{Q_i} = \frac{\prod_{j=0, j\neq i}^{3} (\boldsymbol{M} - \lambda_j \boldsymbol{I})}{\prod_{j=0, j\neq i}^{3} (\lambda_i - \lambda_j)} \tag{13}$$

We note that $\boldsymbol{Q_i U_0}$ are column vectors and Eq. (11) can be re-written as Eqs. (14) or (15).

$$\boldsymbol{U} = \boldsymbol{S_0} + \boldsymbol{S_1}\left(1 - \mathrm{e}^{-\mathrm{t}/\tau_1}\right) + \boldsymbol{S_2}\left(1 - \mathrm{e}^{-\mathrm{t}/\tau_2}\right) + \boldsymbol{S_3}\left(1 - \mathrm{e}^{-\mathrm{t}/\tau_3}\right) \tag{14}$$

and

$$\begin{pmatrix}[U_O D]\\ [U_C D]\\ [MU_O D]\\ [MU_C D]\end{pmatrix} = \begin{pmatrix}S_{10}\\ S_{20}\\ S_{30}\\ S_{40}\end{pmatrix} + \begin{pmatrix}S_{11}\\ S_{21}\\ S_{31}\\ S_{41}\end{pmatrix}\left(1 - e^{-\frac{t}{\tau_1}}\right) + \begin{pmatrix}S_{12}\\ S_{22}\\ S_{32}\\ S_{42}\end{pmatrix}\left(1 - e^{-\frac{t}{\tau_2}}\right) + \begin{pmatrix}S_{13}\\ S_{23}\\ S_{33}\\ S_{43}\end{pmatrix}\left(1 - e^{-\frac{t}{\tau_3}}\right) \quad (15)$$

where $1/\tau_i = -\lambda_i$ is the reciprocal relaxation time of the *i*-th relaxation process, $\boldsymbol{S_i} = -\boldsymbol{Q_i U_0}$ is the column vector of the amplitudes corresponding to the *i*-th relaxation process, and $\boldsymbol{S_0} = (\boldsymbol{Q_0} + \boldsymbol{Q_1} + \boldsymbol{Q_2} + \boldsymbol{Q_3})\boldsymbol{U_0} \equiv \boldsymbol{U_0}$ is the column vector of the initial concentrations.

Based on Eq. (7) we obtain the relationships in Eq. (16).

$$\begin{aligned} S_{10} + S_{20} + S_{30} + S_{40} &= [U]_{Tot} \\ S_{11} + S_{21} + S_{31} + S_{41} &= 0 \\ S_{12} + S_{22} + S_{32} + S_{42} &= 0 \\ S_{13} + S_{23} + S_{33} + S_{43} &= 0 \end{aligned} \quad (16)$$

By multiplying the row vector of molar fluorescence intensities, $\boldsymbol{F} = (F_1 \quad F_2 \quad F_3 \quad F_4)$, and the column vectors of the concentrations (15) and introducing (16) we obtain Eq. (17) for the time dependence of the total fluorescence, $F(t)$,

$$F(t) = A_0 + A_1\left(1 - \mathrm{e}^{-\frac{\mathrm{t}}{\tau_1}}\right) + A_2\left(1 - \mathrm{e}^{-\frac{\mathrm{t}}{\tau_2}}\right) + A_3\left(1 - \mathrm{e}^{-\frac{\mathrm{t}}{\tau_3}}\right) \quad (17)$$

where A_0 is the fluorescence of the UvrD species at $t = 0$. A_1, A_2, and A_3 are the amplitudes of each individual relaxation process defined as in Eq. (18).

$$
\begin{aligned}
A_0 &= \begin{pmatrix} F_1 & F_2 - F_1 & F_3 - F_1 & F_4 - F_1 \end{pmatrix} \begin{pmatrix} [U]_{Tot} \\ S_{20} \\ S_{30} \\ S_{40} \end{pmatrix} \\
A_1 &= \begin{pmatrix} F_2 - F_1 & F_3 - F_1 & F_4 - F_1 \end{pmatrix} \begin{pmatrix} S_{21} \\ S_{31} \\ S_{41} \end{pmatrix} \\
A_2 &= \begin{pmatrix} F_2 - F_1 & F_3 - F_1 & F_4 - F_1 \end{pmatrix} \begin{pmatrix} S_{22} \\ S_{32} \\ S_{42} \end{pmatrix} \\
A_3 &= \begin{pmatrix} F_2 - F_1 & F_3 - F_1 & F_4 - F_1 \end{pmatrix} \begin{pmatrix} S_{23} \\ S_{33} \\ S_{43} \end{pmatrix}
\end{aligned}
\tag{18}
$$

All computations were performed in Python using `numpy`, `scipy`, and `lmfit` modules.

Flux analysis

The net flux, dJ_i/dt, through a reaction step *i* is defined as the difference between forward and backward reaction rates:

$$
\begin{aligned}
\frac{dJ_1}{dt} &= k_1[M][U_OD] - k_{-1}[MU_OD] \\
\frac{dJ_2}{dt} &= k_2[U_OD] - k_{-2}[U_CD] \\
\frac{dJ_3}{dt} &= k_3[M][U_CD] - k_{-3}[MU_CD] \\
\frac{dJ_4}{dt} &= k_4[MU_OD] - k_{-4}[MU_CD]
\end{aligned}
\tag{19}
$$

Expressions for transient net flux were integrated numerically to obtain the net flux accumulated over time (integrated flux), $J(t)$. The integrated fluxes at time $t = 0$ were defined as $J_i(0) = 0$ for $1 \leq i \leq 4$.

In order to determine which pathway to formation of the active helicase, MU_CD, is dominant under our experimental conditions we calculated the relative contributions of flux

through each step to the production of MU_CD. Incorporating Eq. (19) into Eq. (3), one obtains Eq. (20).

$$\begin{aligned}
\frac{d[U_OD]}{dt} &= -\frac{dJ_1}{dt} - \frac{dJ_2}{dt} \\
\frac{d[U_CD]}{dt} &= \frac{dJ_2}{dt} - \frac{dJ_3}{dt} \\
\frac{d[MU_OD]}{dt} &= \frac{dJ_1}{dt} - \frac{dJ_4}{dt} \\
\frac{d[MU_CD]}{dt} &= \frac{dJ_3}{dt} + \frac{dJ_4}{dt} \\
\frac{d[M]}{dt} &= -\frac{dJ_1}{dt} - \frac{dJ_3}{dt}
\end{aligned} \tag{20}$$

Upon integrating Eq.(20), we obtain Eq. (21) relating the integrated fluxes through each step to the concentrations of each species in Figure 4A.

$$\begin{aligned}
[U_OD] &= [U_OD]_0 - J_1 - J_2 \\
[U_CD] &= [U_CD]_0 + J_2 - J_3 \\
[MU_OD] &= J_1 - J_4 \\
[MU_CD] &= J_3 + J_4 \\
[M] &= [M]_0 - J_2 - J_3
\end{aligned} \tag{21}$$

The relative contributions to the production of MU_CD of the conformational selection (CS) pathway is $J_3/(J_3 + J_4)$ and of the induced fit (IF) pathway is $J_4/(J_3 + J_4)$.

The forward equilibrium flux through the CS and IF pathways are given by Eq. (22) (49).

$$\begin{aligned}
J_{CS} &= \left(\frac{1}{k_2[U_OD]} + \frac{1}{k_3[U_CD][M]}\right)^{-1} \\
J_{IF} &= \left(\frac{1}{k_1[U_OD][M]} + \frac{1}{k_4[MU_OD]}\right)^{-1}
\end{aligned} \tag{22}$$

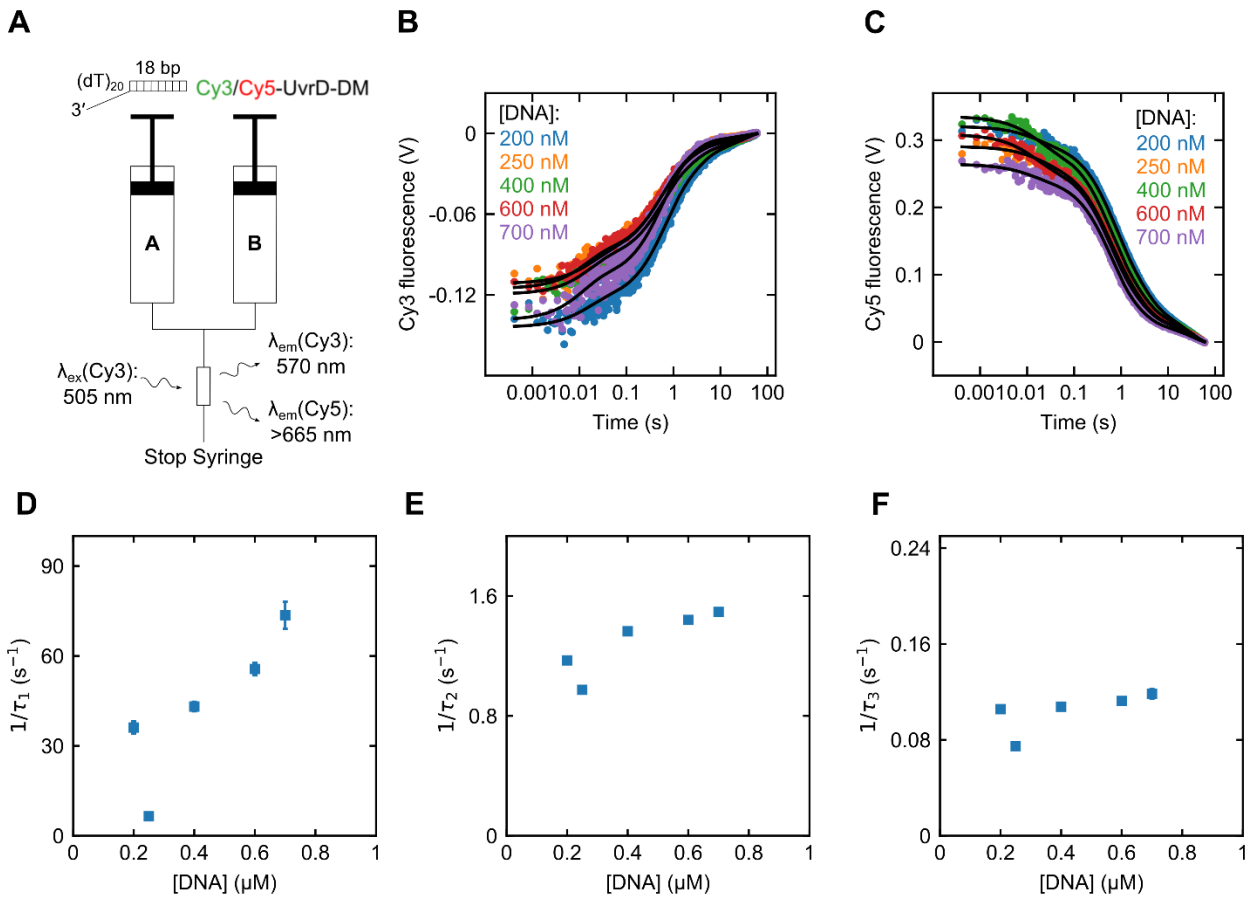

Supplementary Figure 1. A, Schematic representation of the stopped-flow experiment monitoring conformational changes in the 2B sub-domain upon interaction of Cy3/Cy5-UvrD-DM-1B/2B with 3′-(dT)20-ds18 DNA substrate. Experiments were performed in buffer T at 25 °C. **B,C**, Cy3 (B) and Cy5 (C) fluorescence time courses from experiments performed with 100 nM Cy3/Cy5-UvrD-DM-1B/2B rapidly mixed with 3′-(dT)20-ds18 DNA at the indicated concentration. Continuous lines are simulations based on the best-fit values using Eq. (17). **D-F**, The dependence of the reciprocal relaxation times ((D) $1/\tau_1$, (E) $1/\tau_2$, and (F) $1/\tau_3$) on the total DNA concentration. The error bars are standard deviations from the NLLS fitting.

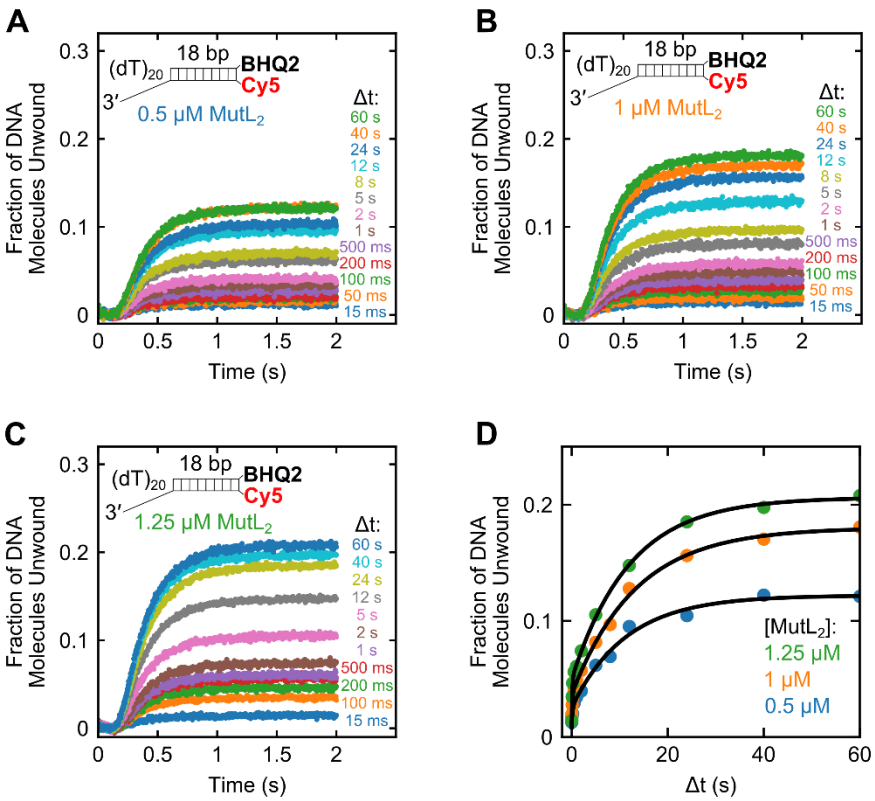

Supplementary Figure 2. A-C, DNA unwinding time courses obtained from sequential-mixing stopped-flow assay (Figure 2A). Experiments were performed with: (A) 100 nM UvrD, 250 nM 3′-$(dT)_{20}$-ds18-BHQ2/Cy5 DNA substrate, and 0.5 μM MutL dimer; (B) 100 nM UvrD, 250 nM 3′-$(dT)_{20}$-ds18-BHQ2/Cy5 DNA substrate, and 0.75 μM MutL dimer; and (C) 100 nM UvrD, 250 nM 3′-$(dT)_{20}$-ds18-BHQ2/Cy5 DNA substrate, and 1.25 μM MutL dimer. **D**, DNA unwinding amplitudes obtained from a series of experiments (A-C) plotted as a function of Δt on a linear time-scale. Continuous lines are simulations based on the best-fit values using Eq. (2).

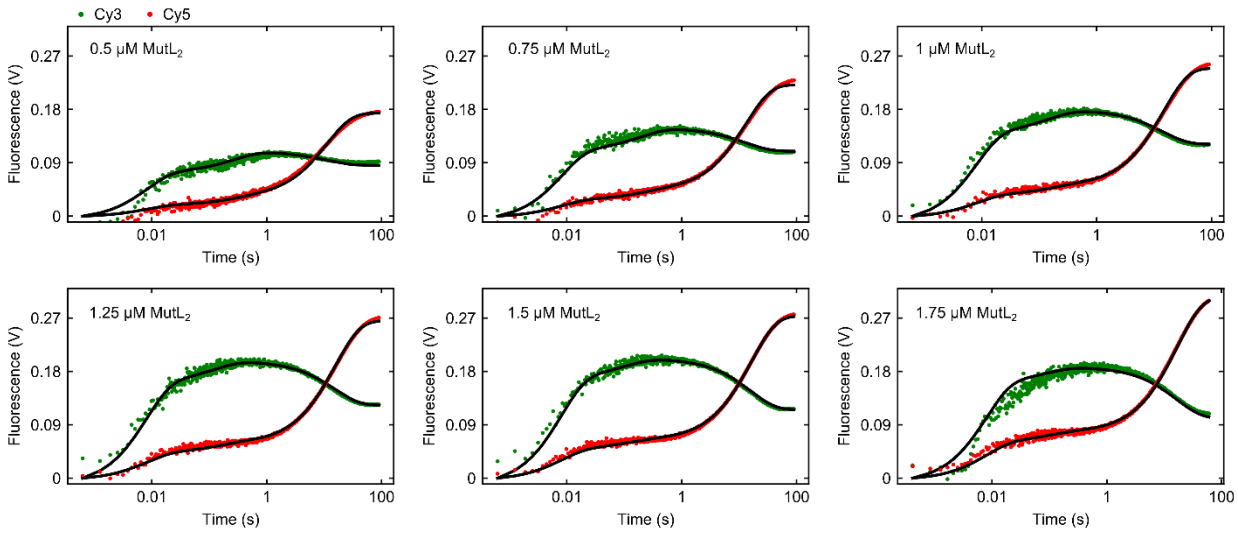

Supplementary Figure 3. Cy3 and Cy5 fluorescence time courses from experiments performed with 100 nM Cy3/Cy5-UvrD-DM-1B/2B pre-equilibrated with 250 nM 3′-$(dT)_{20}$-ds18 for 5 min and then rapidly mixed with MutL at the indicated concentration (Figure 3B). Continuous lines are simulations based on the best-fit values in Tables 1 and 2 using Eq. (8).

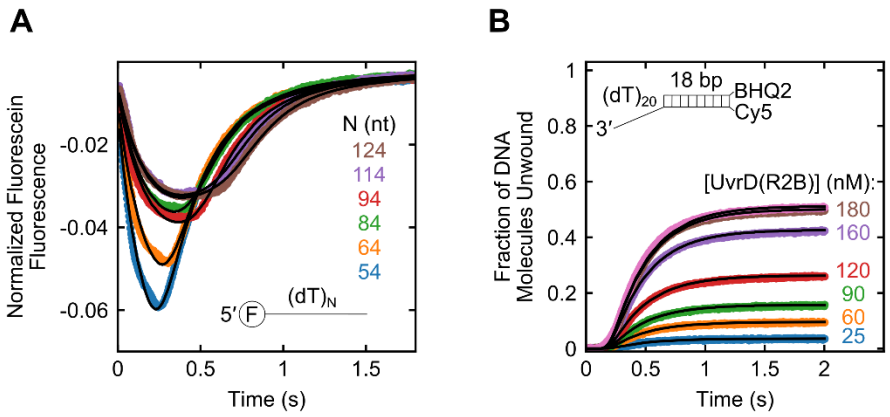

Supplementary Figure 4. ssDNA translocase and helicase activities of UvrD(Rep2B). All **s**topped-flow experiments were performed in buffer T at 25°C. **A**, Stopped-flow time courses for the chimeric UvrD(Rep2B) (50 nM) and a series of 5′-F-$(dT)_N$ (N = 54, 64, 84, 94, 114, 124 nt) (100 nM) showing ssDNA translocation activity with macroscopic translocation rate (mk_t) of 152±5 nt/s. Continuous lines are simulations based on the best-fit values using Eq. (3). **B**, Stopped-flow DNA unwinding time courses for experiments performed with 3′-$(dT)_{20}$-ds18-BHQ2/Cy5 (50 nM) and varying concentrations of UvrD(Rep2B). The chimeric UvrD(Rep2B) shows DNA unwinding activity when in excess over DNA with macroscopic unwinding rate of 88±7 bp/s. Simulations based on the best-fit values using Eq. (1) are shown as continuous lines.

Appendix

Analytical expressions of eigenvalues of the coefficient matrix ***M*** were obtained using the Python SymPy library for symbolic mathematics.

λ_1 =

```
-k1*m/3 - k2/3 - k3*m/3 - k4/3 - kr1/3 - kr2/3 - kr3/3 - kr4/3 - (27*k1
*k3*k4*m**2/2 + 27*k1*k3*kr4*m**2/2 + 27*k1*k4*kr2*m/2 + 27*k1*k4*kr3*m/2
+ 27*k1*kr2*kr3*m/2 + 27*k1*kr2*kr4*m/2 + 27*k2*k3*k4*m/2 + 27*k2*k3*kr1*m
/2 + 27*k2*k3*kr4*m/2 + 27*k2*k4*kr3/2 + 27*k2*kr1*kr3/2 + 27*k2*kr1*kr4/2
+ 27*k3*kr1*kr4*m/2 + 27*k4*kr2*kr3/2 + 27*kr1*kr2*kr3/2 + 27*kr1*kr2*kr4/
2 + sqrt((27*k1*k3*k4*m**2 + 27*k1*k3*kr4*m**2 + 27*k1*k4*kr2*m + 27*k1*k4
*kr3*m + 27*k1*kr2*kr3*m + 27*k1*kr2*kr4*m + 27*k2*k3*k4*m + 27*k2*k3*kr1*
m + 27*k2*k3*kr4*m + 27*k2*k4*kr3 + 27*k2*kr1*kr3 + 27*k2*kr1*kr4 + 27*k3*
kr1*kr4*m + 27*k4*kr2*kr3 + 27*kr1*kr2*kr3 + 27*kr1*kr2*kr4 + 2*(k1*m + k2
+ k3*m + k4 + kr1 + kr2 + kr3 + kr4)**3 - (9*k1*m + 9*k2 + 9*k3*m + 9*k4 +
9*kr1 + 9*kr2 + 9*kr3 + 9*kr4)*(k1*k3*m**2 + k1*k4*m + k1*kr2*m + k1*kr3*m
+ k1*kr4*m + k2*k3*m + k2*k4 + k2*kr1 + k2*kr3 + k2*kr4 + k3*k4*m + k3*kr1
*m + k3*kr4*m + k4*kr2 + k4*kr3 + kr1*kr2 + kr1*kr3 + kr1*kr4 + kr2*kr3 +
kr2*kr4))**2 - 4*(-3*k1*k3*m**2 - 3*k1*k4*m - 3*k1*kr2*m - 3*k1*kr3*m - 3*
k1*kr4*m - 3*k2*k3*m - 3*k2*k4 - 3*k2*kr1 - 3*k2*kr3 - 3*k2*kr4 - 3*k3*k4*
m - 3*k3*kr1*m - 3*k3*kr4*m - 3*k4*kr2 - 3*k4*kr3 - 3*kr1*kr2 - 3*kr1*kr3
- 3*kr1*kr4 - 3*kr2*kr3 - 3*kr2*kr4 + (k1*m + k2 + k3*m + k4 + kr1 + kr2 +
kr3 + kr4)**2)**3)/2 + (k1*m + k2 + k3*m + k4 + kr1 + kr2 + kr3 + kr4)**3
- (9*k1*m + 9*k2 + 9*k3*m + 9*k4 + 9*kr1 + 9*kr2 + 9*kr3 + 9*kr4)*(k1*k3*m
**2 + k1*k4*m + k1*kr2*m + k1*kr3*m + k1*kr4*m + k2*k3*m + k2*k4 + k2*kr1
+ k2*kr3 + k2*kr4 + k3*k4*m + k3*kr1*m + k3*kr4*m + k4*kr2 + k4*kr3 + kr1*
kr2 + kr1*kr3 + kr1*kr4 + kr2*kr3 + kr2*kr4)/2)**(1/3)/3 - (-3*k1*k3*m**2
- 3*k1*k4*m - 3*k1*kr2*m - 3*k1*kr3*m - 3*k1*kr4*m - 3*k2*k3*m - 3*k2*k4 -
3*k2*kr1 - 3*k2*kr3 - 3*k2*kr4 - 3*k3*k4*m - 3*k3*kr1*m - 3*k3*kr4*m - 3*k
4*kr2 - 3*k4*kr3 - 3*kr1*kr2 - 3*kr1*kr3 - 3*kr1*kr4 - 3*kr2*kr3 - 3*kr2*k
r4 + (k1*m + k2 + k3*m + k4 + kr1 + kr2 + kr3 + kr4)**2)/(3*(27*k1*k3*k4*m
**2/2 + 27*k1*k3*kr4*m**2/2 + 27*k1*k4*kr2*m/2 + 27*k1*k4*kr3*m/2 + 27*k1*
kr2*kr3*m/2 + 27*k1*kr2*kr4*m/2 + 27*k2*k3*k4*m/2 + 27*k2*k3*kr1*m/2 + 27*
k2*k3*kr4*m/2 + 27*k2*k4*kr3/2 + 27*k2*kr1*kr3/2 + 27*k2*kr1*kr4/2 + 27*k3
*kr1*kr4*m/2 + 27*k4*kr2*kr3/2 + 27*kr1*kr2*kr3/2 + 27*kr1*kr2*kr4/2 + sqr
t((27*k1*k3*k4*m**2 + 27*k1*k3*kr4*m**2 + 27*k1*k4*kr2*m + 27*k1*k4*kr3*m
+ 27*k1*kr2*kr3*m + 27*k1*kr2*kr4*m + 27*k2*k3*k4*m + 27*k2*k3*kr1*m + 27*
k2*k3*kr4*m + 27*k2*k4*kr3 + 27*k2*kr1*kr3 + 27*k2*kr1*kr4 + 27*k3*kr1*kr4
*m + 27*k4*kr2*kr3 + 27*kr1*kr2*kr3 + 27*kr1*kr2*kr4 + 2*(k1*m + k2 + k3*m
+ k4 + kr1 + kr2 + kr3 + kr4)**3 - (9*k1*m + 9*k2 + 9*k3*m + 9*k4 + 9*kr1
+ 9*kr2 + 9*kr3 + 9*kr4)*(k1*k3*m**2 + k1*k4*m + k1*kr2*m + k1*kr3*m + k1*
kr4*m + k2*k3*m + k2*k4 + k2*kr1 + k2*kr3 + k2*kr4 + k3*k4*m + k3*kr1*m +
k3*kr4*m + k4*kr2 + k4*kr3 + kr1*kr2 + kr1*kr3 + kr1*kr4 + kr2*kr3 + kr2*k
r4))**2 - 4*(-3*k1*k3*m**2 - 3*k1*k4*m - 3*k1*kr2*m - 3*k1*kr3*m - 3*k1*kr
4*m - 3*k2*k3*m - 3*k2*k4 - 3*k2*kr1 - 3*k2*kr3 - 3*k2*kr4 - 3*k3*k4*m - 3
*k3*kr1*m - 3*k3*kr4*m - 3*k4*kr2 - 3*k4*kr3 - 3*kr1*kr2 - 3*kr1*kr3 - 3*k
r1*kr4 - 3*kr2*kr3 - 3*kr2*kr4 + (k1*m + k2 + k3*m + k4 + kr1 + kr2 + kr3
+ kr4)**2)**3)/2 + (k1*m + k2 + k3*m + k4 + kr1 + kr2 + kr3 + kr4)**3 - (9
*k1*m + 9*k2 + 9*k3*m + 9*k4 + 9*kr1 + 9*kr2 + 9*kr3 + 9*kr4)*(k1*k3*m**2
+ k1*k4*m + k1*kr2*m + k1*kr3*m + k1*kr4*m + k2*k3*m + k2*k4 + k2*kr1 + k2
```

```
*kr3 + k2*kr4 + k3*k4*m + k3*kr1*m + k3*kr4*m + k4*kr2 + k4*kr3 + kr1*kr2
+ kr1*kr3 + kr1*kr4 + kr2*kr3 + kr2*kr4)/2)**(1/3))
```

λ_2 =
```
-k1*m/3 - k2/3 - k3*m/3 - k4/3 - kr1/3 - kr2/3 - kr3/3 - kr4/3 - (-1/2
+ sqrt(3)*I/2)*(27*k1*k3*k4*m**2/2 + 27*k1*k3*kr4*m**2/2 + 27*k1*k4*kr2*m/
2 + 27*k1*k4*kr3*m/2 + 27*k1*kr2*kr3*m/2 + 27*k1*kr2*kr4*m/2 + 27*k2*k3*k4
*m/2 + 27*k2*k3*kr1*m/2 + 27*k2*k3*kr4*m/2 + 27*k2*k4*kr3/2 + 27*k2*kr1*kr
3/2 + 27*k2*kr1*kr4/2 + 27*k3*kr1*kr4*m/2 + 27*k4*kr2*kr3/2 + 27*kr1*kr2*k
r3/2 + 27*kr1*kr2*kr4/2 + sqrt((27*k1*k3*k4*m**2 + 27*k1*k3*kr4*m**2 + 27*
k1*k4*kr2*m + 27*k1*k4*kr3*m + 27*k1*kr2*kr3*m + 27*k1*kr2*kr4*m + 27*k2*k
3*k4*m + 27*k2*k3*kr1*m + 27*k2*k3*kr4*m + 27*k2*k4*kr3 + 27*k2*kr1*kr3 +
27*k2*kr1*kr4 + 27*k3*kr1*kr4*m + 27*k4*kr2*kr3 + 27*kr1*kr2*kr3 + 27*kr1*
kr2*kr4 + 2*(k1*m + k2 + k3*m + k4 + kr1 + kr2 + kr3 + kr4)**3 - (9*k1*m +
9*k2 + 9*k3*m + 9*k4 + 9*kr1 + 9*kr2 + 9*kr3 + 9*kr4)*(k1*k3*m**2 + k1*k4*
m + k1*kr2*m + k1*kr3*m + k1*kr4*m + k2*k3*m + k2*k4 + k2*kr1 + k2*kr3 + k
2*kr4 + k3*k4*m + k3*kr1*m + k3*kr4*m + k4*kr2 + k4*kr3 + kr1*kr2 + kr1*kr
3 + kr1*kr4 + kr2*kr3 + kr2*kr4))**2 - 4*(-3*k1*k3*m**2 - 3*k1*k4*m - 3*k1
*kr2*m - 3*k1*kr3*m - 3*k1*kr4*m - 3*k2*k3*m - 3*k2*k4 - 3*k2*kr1 - 3*k2*k
r3 - 3*k2*kr4 - 3*k3*k4*m - 3*k3*kr1*m - 3*k3*kr4*m - 3*k4*kr2 - 3*k4*kr3
- 3*kr1*kr2 - 3*kr1*kr3 - 3*kr1*kr4 - 3*kr2*kr3 - 3*kr2*kr4 + (k1*m + k2 +
k3*m + k4 + kr1 + kr2 + kr3 + kr4)**2)**3)/2 + (k1*m + k2 + k3*m + k4 + kr
1 + kr2 + kr3 + kr4)**3 - (9*k1*m + 9*k2 + 9*k3*m + 9*k4 + 9*kr1 + 9*kr2 +
9*kr3 + 9*kr4)*(k1*k3*m**2 + k1*k4*m + k1*kr2*m + k1*kr3*m + k1*kr4*m + k2
*k3*m + k2*k4 + k2*kr1 + k2*kr3 + k2*kr4 + k3*k4*m + k3*kr1*m + k3*kr4*m +
k4*kr2 + k4*kr3 + kr1*kr2 + kr1*kr3 + kr1*kr4 + kr2*kr3 + kr2*kr4)/2)**(1/
3)/3 - (-3*k1*k3*m**2 - 3*k1*k4*m - 3*k1*kr2*m - 3*k1*kr3*m - 3*k1*kr4*m -
3*k2*k3*m - 3*k2*k4 - 3*k2*kr1 - 3*k2*kr3 - 3*k2*kr4 - 3*k3*k4*m - 3*k3*kr
1*m - 3*k3*kr4*m - 3*k4*kr2 - 3*k4*kr3 - 3*kr1*kr2 - 3*kr1*kr3 - 3*kr1*kr4
- 3*kr2*kr3 - 3*kr2*kr4 + (k1*m + k2 + k3*m + k4 + kr1 + kr2 + kr3 + kr4)*
*2)/(3*(-1/2 + sqrt(3)*I/2)*(27*k1*k3*k4*m**2/2 + 27*k1*k3*kr4*m**2/2 + 27
*k1*k4*kr2*m/2 + 27*k1*k4*kr3*m/2 + 27*k1*kr2*kr3*m/2 + 27*k1*kr2*kr4*m/2
+ 27*k2*k3*k4*m/2 + 27*k2*k3*kr1*m/2 + 27*k2*k3*kr4*m/2 + 27*k2*k4*kr3/2 +
27*k2*kr1*kr3/2 + 27*k2*kr1*kr4/2 + 27*k3*kr1*kr4*m/2 + 27*k4*kr2*kr3/2 +
27*kr1*kr2*kr3/2 + 27*kr1*kr2*kr4/2 + sqrt((27*k1*k3*k4*m**2 + 27*k1*k3*kr
4*m**2 + 27*k1*k4*kr2*m + 27*k1*k4*kr3*m + 27*k1*kr2*kr3*m + 27*k1*kr2*kr4
*m + 27*k2*k3*k4*m + 27*k2*k3*kr1*m + 27*k2*k3*kr4*m + 27*k2*k4*kr3 + 27*k
2*kr1*kr3 + 27*k2*kr1*kr4 + 27*k3*kr1*kr4*m + 27*k4*kr2*kr3 + 27*kr1*kr2*k
r3 + 27*kr1*kr2*kr4 + 2*(k1*m + k2 + k3*m + k4 + kr1 + kr2 + kr3 + kr4)**3
- (9*k1*m + 9*k2 + 9*k3*m + 9*k4 + 9*kr1 + 9*kr2 + 9*kr3 + 9*kr4)*(k1*k3*m
**2 + k1*k4*m + k1*kr2*m + k1*kr3*m + k1*kr4*m + k2*k3*m + k2*k4 + k2*kr1
+ k2*kr3 + k2*kr4 + k3*k4*m + k3*kr1*m + k3*kr4*m + k4*kr2 + k4*kr3 + kr1*
kr2 + kr1*kr3 + kr1*kr4 + kr2*kr3 + kr2*kr4))**2 - 4*(-3*k1*k3*m**2 - 3*k1
*k4*m - 3*k1*kr2*m - 3*k1*kr3*m - 3*k1*kr4*m - 3*k2*k3*m - 3*k2*k4 - 3*k2*
kr1 - 3*k2*kr3 - 3*k2*kr4 - 3*k3*k4*m - 3*k3*kr1*m - 3*k3*kr4*m - 3*k4*kr2
- 3*k4*kr3 - 3*kr1*kr2 - 3*kr1*kr3 - 3*kr1*kr4 - 3*kr2*kr3 - 3*kr2*kr4 + (
k1*m + k2 + k3*m + k4 + kr1 + kr2 + kr3 + kr4)**2)**3)/2 + (k1*m + k2 + k3
*m + k4 + kr1 + kr2 + kr3 + kr4)**3 - (9*k1*m + 9*k2 + 9*k3*m + 9*k4 + 9*k
r1 + 9*kr2 + 9*kr3 + 9*kr4)*(k1*k3*m**2 + k1*k4*m + k1*kr2*m + k1*kr3*m +
k1*kr4*m + k2*k3*m + k2*k4 + k2*kr1 + k2*kr3 + k2*kr4 + k3*k4*m + k3*kr1*m
+ k3*kr4*m + k4*kr2 + k4*kr3 + kr1*kr2 + kr1*kr3 + kr1*kr4 + kr2*kr3 + kr2
*kr4)/2)**(1/3))
```

λ_3 = -k1*m/3 - k2/3 - k3*m/3 - k4/3 - kr1/3 - kr2/3 - kr3/3 - kr4/3 - (-1/2 - sqrt(3)*I/2)*(27*k1*k3*k4*m**2/2 + 27*k1*k3*kr4*m**2/2 + 27*k1*k4*kr2*m/2 + 27*k1*k4*kr3*m/2 + 27*k1*kr2*kr3*m/2 + 27*k1*kr2*kr4*m/2 + 27*k2*k3*k4*m/2 + 27*k2*k3*kr1*m/2 + 27*k2*k3*kr4*m/2 + 27*k2*k4*kr3/2 + 27*k2*kr1*kr3/2 + 27*k2*kr1*kr4/2 + 27*k3*kr1*kr4*m/2 + 27*k4*kr2*kr3/2 + 27*kr1*kr2*kr3/2 + 27*kr1*kr2*kr4/2 + sqrt((27*k1*k3*k4*m**2 + 27*k1*k3*kr4*m**2 + 27*k1*k4*kr2*m + 27*k1*k4*kr3*m + 27*k1*kr2*kr3*m + 27*k1*kr2*kr4*m + 27*k2*k3*k4*m + 27*k2*k3*kr1*m + 27*k2*k3*kr4*m + 27*k2*k4*kr3 + 27*k2*kr1*kr3 + 27*k2*kr1*kr4 + 27*k3*kr1*kr4*m + 27*k4*kr2*kr3 + 27*kr1*kr2*kr3 + 27*kr1*kr2*kr4 + 2*(k1*m + k2 + k3*m + k4 + kr1 + kr2 + kr3 + kr4)**3 - (9*k1*m + 9*k2 + 9*k3*m + 9*k4 + 9*kr1 + 9*kr2 + 9*kr3 + 9*kr4)*(k1*k3*m**2 + k1*k4*m + k1*kr2*m + k1*kr3*m + k1*kr4*m + k2*k3*m + k2*k4 + k2*kr1 + k2*kr3 + k2*kr4 + k3*k4*m + k3*kr1*m + k3*kr4*m + k4*kr2 + k4*kr3 + kr1*kr2 + kr1*kr3 + kr1*kr4 + kr2*kr3 + kr2*kr4))**2 - 4*(-3*k1*k3*m**2 - 3*k1*k4*m - 3*k1*kr2*m - 3*k1*kr3*m - 3*k1*kr4*m - 3*k2*k3*m - 3*k2*k4 - 3*k2*kr1 - 3*k2*kr3 - 3*k2*kr4 - 3*k3*k4*m - 3*k3*kr1*m - 3*k3*kr4*m - 3*k4*kr2 - 3*k4*kr3 - 3*kr1*kr2 - 3*kr1*kr3 - 3*kr1*kr4 - 3*kr2*kr3 - 3*kr2*kr4 + (k1*m + k2 + k3*m + k4 + kr1 + kr2 + kr3 + kr4)**2)**3)/2 + (k1*m + k2 + k3*m + k4 + kr1 + kr2 + kr3 + kr4)**3 - (9*k1*m + 9*k2 + 9*k3*m + 9*k4 + 9*kr1 + 9*kr2 + 9*kr3 + 9*kr4)*(k1*k3*m**2 + k1*k4*m + k1*kr2*m + k1*kr3*m + k1*kr4*m + k2*k3*m + k2*k4 + k2*kr1 + k2*kr3 + k2*kr4 + k3*k4*m + k3*kr1*m + k3*kr4*m + k4*kr2 + k4*kr3 + kr1*kr2 + kr1*kr3 + kr1*kr4 + kr2*kr3 + kr2*kr4)/2)**(1/3)/3 - (-3*k1*k3*m**2 - 3*k1*k4*m - 3*k1*kr2*m - 3*k1*kr3*m - 3*k1*kr4*m - 3*k2*k3*m - 3*k2*k4 - 3*k2*kr1 - 3*k2*kr3 - 3*k2*kr4 - 3*k3*k4*m - 3*k3*kr1*m - 3*k3*kr4*m - 3*k4*kr2 - 3*k4*kr3 - 3*kr1*kr2 - 3*kr1*kr3 - 3*kr1*kr4 - 3*kr2*kr3 - 3*kr2*kr4 + (k1*m + k2 + k3*m + k4 + kr1 + kr2 + kr3 + kr4)**2)/(3*(-1/2 - sqrt(3)*I/2)*(27*k1*k3*k4*m**2/2 + 27*k1*k3*kr4*m**2/2 + 27*k1*k4*kr2*m/2 + 27*k1*k4*kr3*m/2 + 27*k1*kr2*kr3*m/2 + 27*k1*kr2*kr4*m/2 + 27*k2*k3*k4*m/2 + 27*k2*k3*kr1*m/2 + 27*k2*k3*kr4*m/2 + 27*k2*k4*kr3/2 + 27*k2*kr1*kr3/2 + 27*k2*kr1*kr4/2 + 27*k3*kr1*kr4*m/2 + 27*k4*kr2*kr3/2 + 27*kr1*kr2*kr3/2 + 27*kr1*kr2*kr4/2 + sqrt((27*k1*k3*k4*m**2 + 27*k1*k3*kr4*m**2 + 27*k1*k4*kr2*m + 27*k1*k4*kr3*m + 27*k1*kr2*kr3*m + 27*k1*kr2*kr4*m + 27*k2*k3*k4*m + 27*k2*k3*kr1*m + 27*k2*k3*kr4*m + 27*k2*k4*kr3 + 27*k2*kr1*kr3 + 27*k2*kr1*kr4 + 27*k3*kr1*kr4*m + 27*k4*kr2*kr3 + 27*kr1*kr2*kr3 + 27*kr1*kr2*kr4 + 2*(k1*m + k2 + k3*m + k4 + kr1 + kr2 + kr3 + kr4)**3 - (9*k1*m + 9*k2 + 9*k3*m + 9*k4 + 9*kr1 + 9*kr2 + 9*kr3 + 9*kr4)*(k1*k3*m**2 + k1*k4*m + k1*kr2*m + k1*kr3*m + k1*kr4*m + k2*k3*m + k2*k4 + k2*kr1 + k2*kr3 + k2*kr4 + k3*k4*m + k3*kr1*m + k3*kr4*m + k4*kr2 + k4*kr3 + kr1*kr2 + kr1*kr3 + kr1*kr4 + kr2*kr3 + kr2*kr4))**2 - 4*(-3*k1*k3*m**2 - 3*k1*k4*m - 3*k1*kr2*m - 3*k1*kr3*m - 3*k1*kr4*m - 3*k2*k3*m - 3*k2*k4 - 3*k2*kr1 - 3*k2*kr3 - 3*k2*kr4 - 3*k3*k4*m - 3*k3*kr1*m - 3*k3*kr4*m - 3*k4*kr2 - 3*k4*kr3 - 3*kr1*kr2 - 3*kr1*kr3 - 3*kr1*kr4 - 3*kr2*kr3 - 3*kr2*kr4 + (k1*m + k2 + k3*m + k4 + kr1 + kr2 + kr3 + kr4)**2)**3)/2 + (k1*m + k2 + k3*m + k4 + kr1 + kr2 + kr3 + kr4)**3 - (9*k1*m + 9*k2 + 9*k3*m + 9*k4 + 9*kr1 + 9*kr2 + 9*kr3 + 9*kr4)*(k1*k3*m**2 + k1*k4*m + k1*kr2*m + k1*kr3*m + k1*kr4*m + k2*k3*m + k2*k4 + k2*kr1 + k2*kr3 + k2*kr4 + k3*k4*m + k3*kr1*m + k3*kr4*m + k4*kr2 + k4*kr3 + kr1*kr2 + kr1*kr3 + kr1*kr4 + kr2*kr3 + kr2*kr4)/2)**(1/3))

Chapter IV

Transient net flux analysis

Introduction

Theoretical work in this chapter was motivated by the analysis of the kinetic mechanism of activation of the monomeric *E. coli* UvrD helicase by *E. coli* MutL protein in Chapter III. Previously, we have shown that MutL can activate the UvrD monomer helicase [1]. Using single-molecule and ensemble fluorescence resonance energy transfer (FRET) experiments we demonstrated that MutL activates a UvrD monomer by shifting the UvrD 2B sub-domain conformation to a more closed state. In kinetic experiments monitoring rotation of the 2B sub-domain of UvrD upon binding of MutL to the UvrD monomer-DNA complex we observed three relaxation times. The simplest kinetic model that explained our data well is given in Figure 1A with the best-fit values of the rate constants given in Table 1. In this scheme, UvrD-DNA complexes exist in equilibrium between two states differing by an open (*A*) or closed (*B*) conformation of the 2B sub-domain ($A \leftrightarrow B$) and MutL (*L*) can bind to both conformations to form *AL* and *BL*, which are also in equilibrium ($AL \leftrightarrow BL$).

The scheme in Figure 1A is a cyclic four-state mechanism with three independent reaction steps, and therefore, three relaxation times (Figs. 1B,C,D). In general, the number of relaxation times is always equal to the number of independent reaction steps or the number of reactants minus one [2]. These three reciprocal relaxation times are complex functions of all rate constants. Usually the first two relaxation times are attributed to ligand binding steps and monotonically increase with the ligand concentration. The third reciprocal relaxation time can display a variety of behaviors as has been explored by Galburt et al [3-6]. It can hyperbolically increase, hyperbolically decrease, or have a nonmonotonic behavior with the initial decrease and the subsequent increase as a function of ligand concentration [3].

Kinetic studies of the rate of activation of UvrD by MutL showed that the closed state of the UvrD monomer in complex with MutL (*BL*) is the active form of the helicase. There are two pathways in the cycle that lead to formation of *BL*, the conformational selection pathway (steps 2 and 3) and induced fit pathway (steps 1 and 4). The relative contribution of each pathway can be measured as the fractional forward flux through a given pathway [7]. Our calculations based on the best-fit values of the rate constants (Chapter III, Table 1) indicate that in the range of experimentally used MutL concentrations, MutL activates UvrD predominantly through the conformational selection pathway (>90%) and to a much lesser degree through the induced fit pathway (<10%). Additionally, we estimated the relative contributions of CS and IF pathways using the fractional net fluxes and obtained similar results.

In this chapter, we elaborate more on the net flux analysis approach using the scheme in Figure 1A as an example. However, the net flux analysis approach is more general and can be applied to other kinetic mechanisms. We present methods for solving for the integrated net fluxes. We show a more detailed analysis of pathways leading to *BL* and show how to calculate the fractional net fluxes for each pathway. Furthermore, we analyze the normal reactions and relaxation times from the perspective of net fluxes. We explore the dependence of the reciprocal relaxation time on ligand concentration and find conditions for inflection points. Finally, we show another type of nonmonotonic behavior for the third reciprocal relaxation time as a function of ligand concentration where the initial increase is followed by the subsequent decrease.

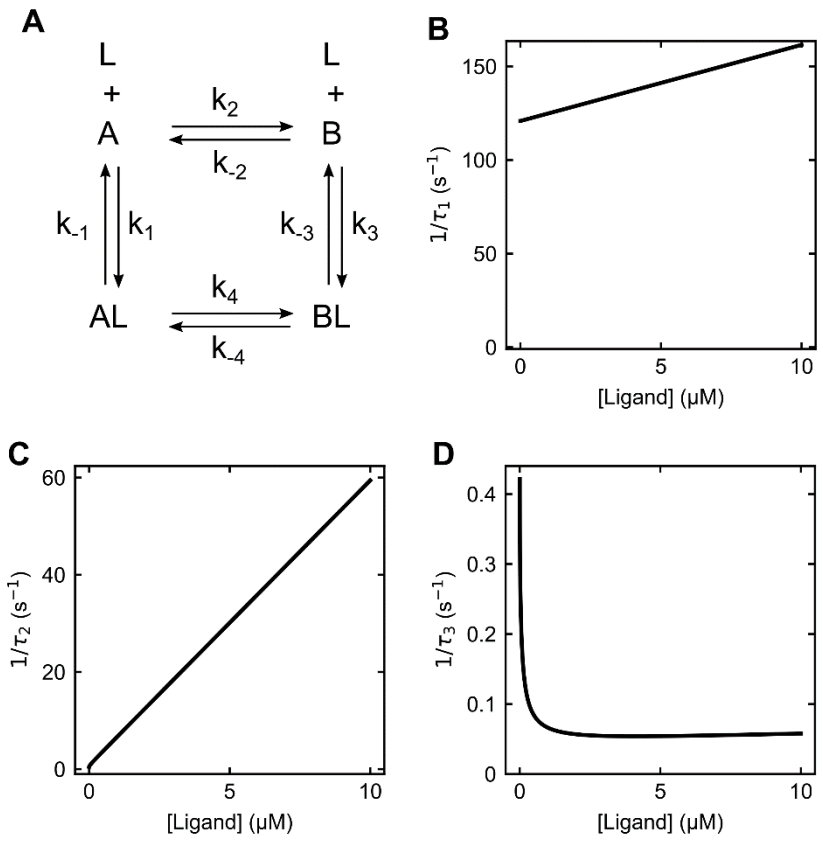

Figure 1. (**A**) The four-state cyclic kinetic model consisting of two isomerization steps (k_2/k_{-2} and k_4/k_{-4}) and two ligand binding steps (k_1/k_{-1} and k_3/k_{-3}). (**B-D**) The dependence of the reciprocal relaxation times on ligand concentration. Simulations were performed using the kinetic parameters in Table 1 (Chapter III).

Results

Definition of instantaneous and time-integrated net fluxes

The net reaction rate or the instantaneous net flux through a reaction step i, dJ_i/dt, is defined as the difference of forward and backward reaction rates given in Eq. (1). The sign of the net flux tells the direction in which the reaction is proceeding. The net flux is positive when the rate of forward reaction is greater than the rate of reverse reaction and negative if the reverse transformation is faster. Note that the sign of the net flux depends on the initial choice of direction of the net flux.

$$\begin{aligned}\frac{dJ_1}{dt} &= k_1[L][A] - k_{-1}[AL] \\ \frac{dJ_2}{dt} &= k_2[A] - k_{-2}[B] \\ \frac{dJ_3}{dt} &= k_3[L][B] - k_{-3}[BL] \\ \frac{dJ_4}{dt} &= k_4[AL] - k_{-4}[BL]\end{aligned} \tag{1}$$

The net flux defined in Eq. (1) describes instantaneous flow, but it lacks information about the net flux accumulated over time. Therefore, we calculate the time-integrated flux, $J_i(t)$, using Eq. (2) which considers the time course of the reaction from time zero to time *t*. Since we disregard any kind of flux before the start of the reaction, we define the integrated flux at time *t* = 0 as $J_i(0) = 0$ for $1 \leq i \leq 4$. When the reaction reaches equilibrium, the net flux through each reaction step vanishes, $dJ_i(\infty)/dt = 0$, while the time-integrated net flux reaches a constant value, $J_i(\infty) = const$. Analysis of the time-integrated net fluxes allows a more comprehensive view of the reactant transformation to intermediates and final products from the beginning of the reaction up to reaching the equilibrium state.

$$J_i(t) = \int_0^t \frac{dJ_i}{dt} dt \tag{2}$$

Relation to species concentrations

The rate of change of species concentrations and net fluxes are closely related to each other and the relationships are given in Eq. (3).

$$\begin{aligned}
\frac{d[A]}{dt} &= -k_2[A] - k_1[A][L] + k_{-2}[B] + k_{-1}[AL] = -\frac{dJ_1}{dt} - \frac{dJ_2}{dt} \\
\frac{d[B]}{dt} &= k_2[A] - k_{-2}[B] - k_3[B][L] + k_{-3}[BL] = \frac{dJ_2}{dt} - \frac{dJ_3}{dt} \\
\frac{d[AL]}{dt} &= k_1[A][L] - (k_{-1} + k_4)[AL] + k_{-4}[BL] = \frac{dJ_1}{dt} - \frac{dJ_4}{dt} \\
\frac{d[BL]}{dt} &= k_3[B][L] + k_4[AL] - (k_{-3} + k_{-4})[BL] = \frac{dJ_3}{dt} + \frac{dJ_4}{dt} \\
\frac{d[L]}{dt} &= -k_1[A][L] - k_3[B][L] + k_{-1}[AL] + k_{-3}[BL] = -\frac{dJ_1}{dt} - \frac{dJ_3}{dt}
\end{aligned} \tag{3}$$

Integrating Eq. (3) with the initial species concentrations of $[A]_0 = C_{\text{Tot}}k_{-1}/(k_1+k_{-1})$, $[B]_0 = C_{\text{Tot}}k_1/(k_1 + k_{-1})$, $[AL]_0 = 0$, $[BL]_0 = 0$, and $[L]_0 = L_{\text{Tot}}$, one obtains Eq. (4) describing the relationships between the concentrations of species and the time-integrated net fluxes.

$$\begin{aligned}
[A] &= [A]_0 - J_1 - J_2 \\
[B] &= [B]_0 + J_2 - J_3 \\
[AL] &= J_1 - J_4 \\
[BL] &= J_3 + J_4 \\
[L] &= [L]_0 - J_1 - J_3
\end{aligned} \tag{4}$$

Methods for obtaining solutions for the time dependence of the net fluxes

Introducing Eq. (4) into Eq. (3), one obtains the system of differential equations (5) describing the time courses of the net fluxes. This set of differential equations (5) given the initial values can be integrated numerically using Python `scipy.integrate.odeint` module.

$$\begin{aligned}
\frac{dJ_1}{dt} &= k_1[L]([A]_0 - J_1 - J_2) - k_{-1}(J_1 - J_4) \\
\frac{dJ_2}{dt} &= k_2([A]_0 - J_1 - J_2) - k_{-2}([B]_0 + J_2 - J_3) \\
\frac{dJ_3}{dt} &= k_3[L]([B]_0 + J_2 - J_3) - k_{-3}(J_3 + J_4) \\
\frac{dJ_4}{dt} &= k_4(J_1 - J_4) - k_{-4}(J_3 + J_4) \\
\frac{d[L]}{dt} &= -k_1[L]([A]_0 - J_1 - J_2) - k_3[L]([B]_0 + J_2 - J_3) + k_{-1}(J_1 - J_4) + k_{-3}(J_3 + J_4)
\end{aligned} \tag{5}$$

In order to examine the relaxation kinetics and to obtain closed-form expressions for the system (5) we used the matrix projection operator technique. The application of this approach to the analysis of stopped-flow kinetics has been described in detail [8]. In order to eliminate all higher-order terms in the differential equations (5) we consider pseudo-first order conditions with respect to the ligand concentration. The system of Eqs. (5) is given by Eqs. (6,7,8) in three different matrix notations that we use throughout this chapter: *expanded* matrix notation (6), *compact* matrix notation (7) where $\boldsymbol{M}$ is the coefficient matrix, and $\boldsymbol{J}$ is the vector of the integrated net fluxes, and *element-wise* notation (8). Element-wise expressions are helpful when coding these formulas in computer language.

$$\frac{d}{dt}\begin{pmatrix} J_1 \\ J_2 \\ J_3 \\ J_4 \\ C_{Tot} \end{pmatrix} = \begin{pmatrix} -k_1[L]-k_{-1} & -k_1[L] & 0 & k_{-1} & \frac{k_1[L]}{1+K_2} \\ -k_2 & -k_2-k_{-2} & k_{-2} & 0 & 0 \\ 0 & k_3[L] & -k_3[L]-k_{-3} & -k_{-3} & \frac{k_3[L]K_2}{1+K_2} \\ k_4 & 0 & -k_{-4} & -k_4-k_{-4} & 0 \\ 0 & 0 & 0 & 0 & 0 \end{pmatrix} \begin{pmatrix} J_1 \\ J_2 \\ J_3 \\ J_4 \\ C_{Tot} \end{pmatrix} \quad (6)$$

$$\frac{d\boldsymbol{J}}{dt} = \boldsymbol{M}\boldsymbol{J} \quad (7)$$

$$\frac{dJ_i}{dt} = \sum_{j=1}^{5} M_{ij}J_j \quad (8)$$

The solution of the differential equations (6-8) has the matrix exponential form given by Eq. (9) where $\boldsymbol{J_o}$ is the vector of the initial integrated net fluxes.

$$\boldsymbol{J} = e^{\boldsymbol{M}t}\boldsymbol{J_o} \quad (9)$$

The matrix exponential term, $e^{\boldsymbol{Mt}}$, can be expanded using its eigenvalues, λ_i, and associated projection operators, $\boldsymbol{Q}_i$. Eigenvalues of the coefficient matrix $\boldsymbol{M}$ at a given ligand concentration can be determined either numerically using the Python `numpy.linalg.eigvals` module or analytically (Chapter III, Appendix). The projection matrices, $\boldsymbol{Q}_i$, are given by Eq. (9), where $\boldsymbol{I}$ is the identity matrix of the same size as $\boldsymbol{M}$.

$$\boldsymbol{Q_i} = \prod_{\substack{j=0 \\ j \neq i}}^{3} \frac{\left(\boldsymbol{M} - \lambda_j \boldsymbol{I}\right)}{\lambda_i - \lambda_j} \tag{10}$$

The solution of the system of differential equations (6-8) in terms of matrix projection operators is given by Eq. (11-13), where $\boldsymbol{V}_{:j} = \boldsymbol{Q}_j \boldsymbol{J_o}$ is the column vector of the amplitudes corresponding to the *j*-th relaxation process and $e^{\boldsymbol{\lambda} t}$ is the column vector of the exponential terms. Note that in our notation, $\boldsymbol{V}_{:j}$ is the *j*-th column vector of the matrix $\boldsymbol{V}$ and $\boldsymbol{V}_{i:}$ is the *i*-th row vector of the matrix $\boldsymbol{V}$.

$$\boldsymbol{J} = \left(\sum_{j=0}^{3} \boldsymbol{Q_j} e^{\lambda_j t} \right) \boldsymbol{J_o} = \sum_{j=0}^{3} \boldsymbol{Q_j J_o} e^{\lambda_j t} = \sum_{j=0}^{3} \boldsymbol{V}_{:\boldsymbol{j}} e^{\lambda_j t} = \boldsymbol{V} e^{\boldsymbol{\lambda} t} \tag{11}$$

$$J_i = \sum_{j=0}^{3} V_{ij} e^{\lambda_j t} \tag{12}$$

$$\begin{pmatrix} J_1 \\ J_2 \\ J_3 \\ J_4 \\ C_{Tot} \end{pmatrix} = \begin{pmatrix} J_1(\infty) \\ J_2(\infty) \\ J_3(\infty) \\ J_4(\infty) \\ C_{Tot} \end{pmatrix} + \begin{pmatrix} V_{11} \\ V_{21} \\ V_{31} \\ V_{41} \\ 0 \end{pmatrix} e^{\lambda_1 t} + \begin{pmatrix} V_{12} \\ V_{22} \\ V_{32} \\ V_{42} \\ 0 \end{pmatrix} e^{\lambda_2 t} + \begin{pmatrix} V_{13} \\ V_{23} \\ V_{33} \\ V_{43} \\ 0 \end{pmatrix} e^{\lambda_3 t}$$
$$= \begin{pmatrix} J_1(\infty) & V_{11} & V_{12} & V_{13} \\ J_2(\infty) & V_{21} & V_{22} & V_{23} \\ J_3(\infty) & V_{31} & V_{32} & V_{33} \\ J_4(\infty) & V_{41} & V_{42} & V_{43} \\ C_{Tot} & 0 & 0 & 0 \end{pmatrix} \begin{pmatrix} 1 \\ e^{\lambda_1 t} \\ e^{\lambda_2 t} \\ e^{\lambda_3 t} \end{pmatrix} \quad (13)$$

Simulations of the time courses and amplitudes of the integrated net fluxes

The net flux analysis allows a determination of the net direction of the reaction. This can facilitate identification of intermediate species and final products in complex reaction mechanisms. Simulations of the time courses of the integrated net fluxes based on the rate constants given in Table 1 at 1 μM ligand concentration are shown in Figure 2B. There is a net positive flux in a direction from *A* to *BL* (Fig. 2A,B). The net transition from *A* to *BL* predominantly occurs through intermediate *B* (steps 2 and 3) and to a lesser degree through intermediate *AL* (steps 1 and 4) (Fig. 2B). Figure 2C shows the amplitudes of the integrated net fluxes at equilibrium as a function of ligand concentration. At higher ligand concentrations the net reaction proceeds through steps 1 and 4.

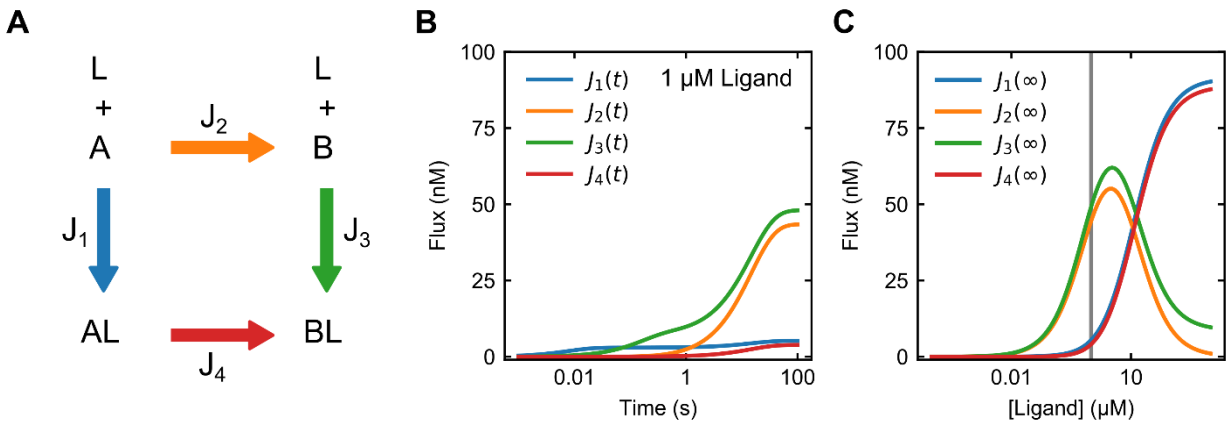

Figure 2. (**A**) The four-state kinetic model showing the directions of net fluxes. The net reaction proceeds from *A* to *BL* through the CS pathway (steps 2 and 3) and the IF pathway (steps 1 and 3). (**B**) Simulations of the time dependence of the integrated net fluxes at 1 μM ligand concentration. (**C**) The dependence of the amplitudes of the integrated net fluxes on ligand concentration. Simulations are based on the kinetic parameters in Table 1 (Chapter III).

Influx analysis

Depending on the sign of the value of the net flux in Eq. (3) and (4), the contribution of fluxes to each species can be interpreted as influx to represent its production rate and outflux to represent its consumption rate. The initial concentrations are interpreted as influxes. This enables one to trace the dynamic accumulation and consumption of species during the evolution of the system. The relationships between the concentrations of all species and the influx/outflux contributions through each step are given in Table 1. Figure 3A shows the time courses of *BL* concentration and influxes through steps 3 and 4, Figure 3B shows the final amplitudes as a function of ligand concentration, and Figure 3C shows the fractional influxes through step 3 and 4 as a function of ligand concentration. Since there is no outflux from *BL*, the sum of influxes through steps 3 and 4 equals the concentration of *BL*. The fractional influx through step 3 represents the total influx through the conformational selection (CS) pathway, while the fractional influx through step 4 reflects the total influx through the induced fit (IF) pathway.

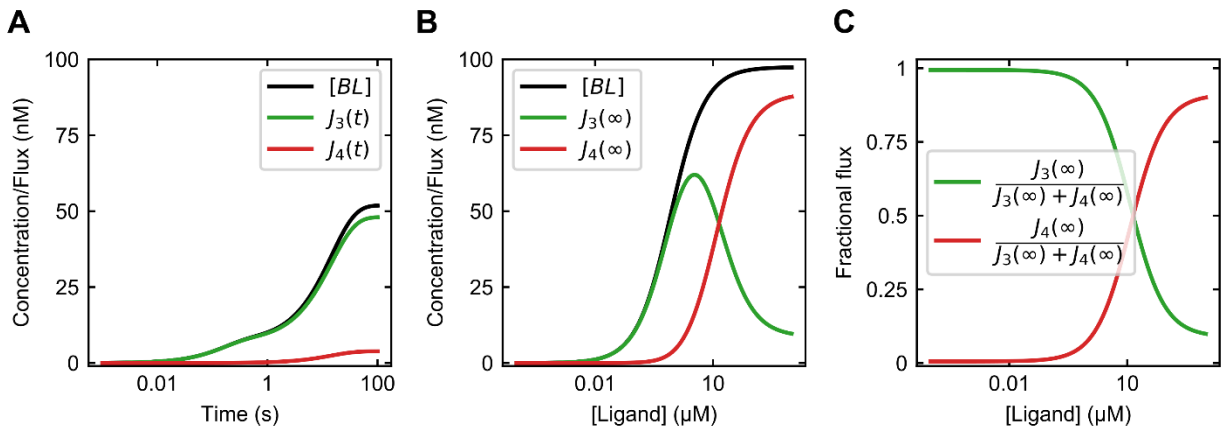

Figure 3. (**A**) The time dependence of the concentration of *BL* and the influxes J_3 and J_4 at 1 μM ligand concentration. The sum of J_3 and J_4 equals $[BL]$. (**B**) Simulations of $[BL]$ and the amplitudes of J_3 and J_4 at equilibrium as a function of ligand concentration. (**C**) The dependence of the fractional integrated net fluxes through J_3 and J_4 at equilibrium on ligand concentration. *BL* is formed predominantly through step 3 at low ligand concentrations and through step 4 at high ligand concentrations.

Table 1. Influxes, outfluxes, and concentrations of the species in a model in Figure 2A

Species	Influx	Outflux	Concentration
A	$[A]_0$	$J_1 + J_2$	$[A]_0 - J_1 - J_2$
B	$[B]_0 + J_2$	J_3	$[B]_0 + J_2 - J_3$
AL	J_1	J_4	$J_1 - J_4$
BL	$J_3 + J_4$	$-$	$J_3 + J_4$
L	$[L]_0$	$J_1 + J_3$	$[L]_0 - J_1 - J_3$

Pathway analysis

A more detailed understanding of the mechanism of production of *BL* requires not only calculating the net fluxes through individual steps 3 and 4, but analysis of the fractional net fluxes through each pathway starting from the initial components, A_0 and B_0, and leading to the final product, *BL*. We define the fractional net flux of the pathway as follows. For a given species of interest, production pathways are constructed as reaction steps starting from the initial

components of the system and ending at the final product. Next, for each step of the pathway the fractional *influx* to the product of this reaction step through a given step in a pathway is calculated. For example, *B* has two influxes through step 2 and from B_0. Therefore, the fractional influx to *B* through step 2 equals $J_2/(J_2 + [B]_0)$. Finally, the fractional net influx through a particular pathway to a given species is calculated as the product of fractional influxes for each species within the pathway (Eq. (13)).

$$Fractional\ pathway\ influx = \prod_i \frac{Influx_i(pathway)}{Influx_i(total)} \tag{14}$$

Table 2 shows the derived expressions for the fractional influxes for production of *BL* through four different pathways starting from concentrations of the initial components A_0 and B_0. Three pathways that have a non-zero value are displayed in Figure 4A. Computer simulations using these expressions based on the kinetic parameters in Table 1 are shown in Figure 4B. From these simulations we observe that at low ligand concentrations *BL* is formed primarily by direct binding of the ligand to *B* (direct binding pathway). At intermediate ligand concentrations *BL* is formed from *A* through steps 2 and 3 (CS pathway). At high ligand concentrations, *BL* is produced from *A* through steps 1 and 4 (IF pathway). Note that the first pathway involving the direct binding of the ligand to *B* does not vanish at high ligand concentrations.

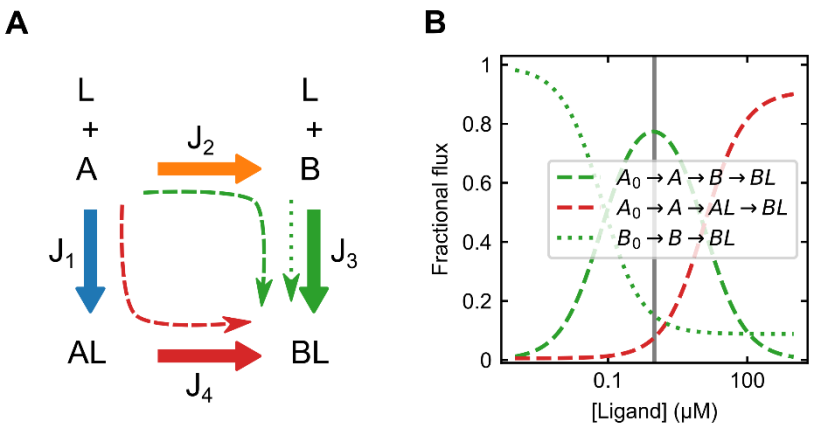

Figure 4. (**A**) Depiction of the fractional influxes to *BL* through $\{A_0\}\rightarrow A\rightarrow AL\rightarrow BL$ (dashed red line), $\{A_0\}\rightarrow A\rightarrow B\rightarrow BL$ (dashed green line), and $\{B_0\}\rightarrow B\rightarrow BL$ (dotted green line). (**B**) Simulations of the dependence of the fractional influxes on ligand concentration.

Table 2. Expressions for the fractional influxes to *BL* through given pathways.

Reaction pathway	**Fractional influx to *BL***
$\{A_0\}\rightarrow A\rightarrow B\rightarrow BL$	$\frac{[A]_0}{[A]_0}\cdot\frac{J_2}{J_2+[B]_0}\cdot\frac{J_3}{J_3+J_4}$
$\{A_0\}\rightarrow A\rightarrow AL\rightarrow BL$	$\frac{[A]_0}{[A]_0}\cdot\frac{J_1}{J_1}\cdot\frac{J_4}{J_3+J_4}$
$\{B_0\}\rightarrow B\rightarrow BL$	$\frac{[B]_0}{J_2+[B]_0}\cdot\frac{J_3}{J_3+J_4}$
$\{B_0\}\rightarrow B\rightarrow A\rightarrow AL\rightarrow BL$	$\frac{0}{[A]_0}\cdot\frac{J_1}{J_1}\cdot\frac{J_4}{J_3+J_4}=0$

Normal reaction analysis

In complex reaction systems individual reaction steps are coupled to each other. Therefore, the relaxation times, in general, are functions of all the microscopic rate constants. Bernasconi *et al*. [2] introduced the concept of "normal mode of reactions" or "normal reactions". Normal reactions are defined as uncoupled reactions of the system and can be obtained as linear combinations of the individual reaction steps. The linear combination coefficients are given by the inverse matrix $\boldsymbol{V}^{-1}$ if $\boldsymbol{V}$ is a square matrix or, in general, by the pseudoinverse $\boldsymbol{V}^{+}$ of the matrix $\boldsymbol{V}$. Since the matrix $\boldsymbol{V}$ has linearly independent columns (Eq. (15-

17)) it follows that $\boldsymbol{V}^{+}$ is a left inverse of $\boldsymbol{V}$ and $\boldsymbol{V}^{+}\boldsymbol{V} = \boldsymbol{I}$. From our definition it follows that the amplitudes of normal reactions are normalized to one, $\sum_{j=1}^{5} V_{ij}^{+} V_{ji} = 1$. Therefore, quantities, $V_{ij}^{+} V_{ji}$, can be interpreted as the degree of coupling (relative contribution) of the *j*-th step to the *i*-th normal reaction. If the value of $V_{ij}^{+} V_{ji}$ is close to zero, that means that there is a very weak coupling from *j*-th reaction step to the *i*-th normal reaction. Conversely, if the value of $V_{ij}^{+} V_{ji}$ is close to one that means that the *i*-th normal reaction is dominated by the *j*-th reaction step.

$$\boldsymbol{S} = \boldsymbol{V}^{+}\boldsymbol{J} = \boldsymbol{V}^{+}\boldsymbol{V}e^{\boldsymbol{\lambda} t} = \boldsymbol{I}e^{\boldsymbol{\lambda} t} = e^{\boldsymbol{\lambda} t} \tag{15}$$

$$S_i = \sum_{j=1}^{5} V_{ij}^{+} J_j = \sum_{k=0}^{3} \sum_{j=1}^{5} V_{ij}^{+} V_{jk}\, e^{\lambda_k t} = \sum_{j=1}^{5} V_{ij}^{+} V_{ji} e^{\lambda_i t} = e^{\lambda_i t} \tag{16}$$

$$\begin{pmatrix} S_1 \\ S_2 \\ S_3 \\ S_4 \end{pmatrix} = \begin{pmatrix} V_{10} & V_{11} & V_{12} & V_{13} \\ V_{20} & V_{21} & V_{22} & V_{23} \\ V_{30} & V_{31} & V_{32} & V_{33} \\ V_{40} & V_{41} & V_{42} & V_{43} \\ C_{Tot} & 0 & 0 & 0 \end{pmatrix}^{+} \begin{pmatrix} J_1 \\ J_2 \\ J_3 \\ J_4 \\ C_{Tot} \end{pmatrix}$$

$$= \begin{pmatrix} V_{10} & V_{11} & V_{12} & V_{13} \\ V_{20} & V_{21} & V_{22} & V_{23} \\ V_{30} & V_{31} & V_{32} & V_{33} \\ V_{40} & V_{41} & V_{42} & V_{43} \\ C_{Tot} & 0 & 0 & 0 \end{pmatrix}^{+} \begin{pmatrix} V_{10} & V_{11} & V_{12} & V_{13} \\ V_{20} & V_{21} & V_{22} & V_{23} \\ V_{30} & V_{31} & V_{32} & V_{33} \\ V_{40} & V_{41} & V_{42} & V_{43} \\ C_{Tot} & 0 & 0 & 0 \end{pmatrix} \begin{pmatrix} 1 \\ e^{\lambda_1 t} \\ e^{\lambda_2 t} \\ e^{\lambda_3 t} \end{pmatrix} \tag{17}$$

$$= \begin{pmatrix} 1 & 0 & 0 & 0 \\ 0 & 1 & 0 & 0 \\ 0 & 0 & 1 & 0 \\ 0 & 0 & 0 & 1 \end{pmatrix} \begin{pmatrix} 1 \\ e^{\lambda_1 t} \\ e^{\lambda_2 t} \\ e^{\lambda_3 t} \end{pmatrix} = \begin{pmatrix} 1 \\ e^{\lambda_1 t} \\ e^{\lambda_2 t} \\ e^{\lambda_3 t} \end{pmatrix}$$

In a similar way, we can obtain expanded expressions for the eigenvalues. By taking the derivate of the normal reactions one obtains Eq. (18-20).

$$\frac{d\boldsymbol{S}}{dt} = \frac{d(\boldsymbol{V}^{+}\boldsymbol{J})}{dt} = \boldsymbol{V}^{+}\boldsymbol{M}\boldsymbol{J} = \boldsymbol{V}^{+}\boldsymbol{M}\boldsymbol{V}e^{\boldsymbol{\lambda} t} \tag{18}$$

$$\frac{dS_i}{dt} = \sum_{j=1}^{5} V_{ij}^{+} \frac{dJ_j}{dt} = \sum_{j=1}^{5} V_{ij}^{+} \sum_{k=1}^{5} M_{jk} V_{ki}\, e^{\lambda_i t} = \lambda_i e^{\lambda_i t} \tag{19}$$

From Eq. (19) it follows that $\lambda_i = \sum_{j=1}^{5} V_{ij}^{+} \sum_{k=1}^{5} M_{jk} V_{ki}$, where the *i*-th eigenvalues is expressed in terms of the linear combination coefficients of the reaction steps, the rate constants, and the amplitudes of the reaction steps. Using the known form of the coefficient matrix $\boldsymbol{M}$ we obtain Eq. (20). Notice that the values in square brackets on the right side of the rate constants are the amplitudes of reactants for the *i*-th eigenvalue which we rewrite in Eq. (21). The values in round brackets in Eq. (21) are the rates of the *j*-th reaction step for the *i*-th normal reaction. Therefore, quantities, $V_{ij}^{+} \sum_{k=1}^{5} M_{jk} V_{ki}$, can be interpreted as the relative rate contribution (eigenrate) of the *j*-th step to the *i*-th normal reaction.

$$\begin{gathered}\lambda_i = V_{i1}^{+}(k_1[L][-V_{1i} - V_{2i}] - k_{-1}[V_{1i} - V_{4i}]) + V_{i2}^{+}(k_2[-V_{1i} - V_{2i}] - k_{-2}[V_{2i} - V_{3i}]) \\ + V_{i3}^{+}(k_3[L][V_{2i} - V_{3i}] - k_{-3}[V_{3i} + V_{4i}]) + V_{i4}^{+}(k_4[V_{1i} - V_{4i}] - k_{-4}[V_{3i} + V_{4i}])\end{gathered} \tag{20}$$

$$\begin{gathered}\lambda_i = V_{i1}^{+}(k_1[L][A]_i - k_{-1}[AL]_i) + V_{i2}^{+}(k_2[A]_i - k_{-2}[B]_i) \\ + V_{i3}^{+}(k_3[L][B]_i - k_{-3}[B]_i) + V_{i4}^{+}(k_4[AL]_i - k_{-4}[BL]_i)\end{gathered} \tag{21}$$

Ligand concentration dependence of the reciprocal relaxation times

One important aspect of kinetic studies is the analysis of the dependence of the reciprocal relaxation times on ligand concentration. We perform a function analysis of λ_i by taking a first derivative with respect to $[L]$ (Eq. (21)).

$$\frac{d\lambda_i}{d[L]} = \sum_{j,k} \frac{dV_{ij}^{+}}{d[L]} M_{jk} V_{ki} + \sum_{j,k} V_{ij}^{+} \frac{dM_{jk}}{d[L]} V_{ki} + \sum_{j,k} V_{ij}^{+} M_{jk} \frac{dV_{ki}}{d[L]} \tag{22}$$

The first and the third terms on the right side of the equation are equal to zero. Using the known form of the matrix $\boldsymbol{M}$, one obtains Eq. (23).

$$\frac{d\lambda_i}{d[L]} = V_{i1}^{+} k_1 [A]_i + V_{i3}^{+} k_3 [B]_i \qquad (23)$$

The sign of the derivative in Eq. (23) determines the increase or decrease in the reciprocal relaxation time as a function of ligand concentration. Inflection points can be found at ligand concentrations where the derivative vanishes.

Analysis of normal reaction

In Figure 5, we plot the computer simulated eigenvalues, coupling coefficients, eigenrates, and derivatives of the reciprocal relaxation times with respect to $[L]$ for each normal reaction for the mechanism in Figure 1A using the parameter values in Table 1 (Chapter III). Within the range of ligand concentrations that we consider, the first normal reaction is completely dominated by step 1 (Fig. 5D) and, therefore, the first reciprocal relaxation time has an intercept of k_{-1} and a slope of k_1 (Fig. 5A) and a constant positive derivative (Fig. 5G) The second normal reaction at low ligand concentration starts as a coupled reaction of steps 2 and 3 but then is dominated by step 3 at higher ligand concentrations (Fig. 5E). Correspondingly, the second reciprocal relaxation time is nonlinear at the beginning and then becomes linear with the slope of k_3 at higher ligand concentrations (Figs. 5B,H). Finally, the third normal reaction represents binding step 3 at low ligand concentration with the spike of the conformational change step 2 and eventual rise of the conformational change step 4 at higher ligand concentrations (Fig. 5F). At zero ligand concentration the third reciprocal relaxation time equals k_{-3} and at infinite ligand concentration it asymptotically reaches to k_4 (Fig. 5C). The derivative changes its sign from negative to positive pointing to the inflection point at vanishing derivative (Fig. 5I).

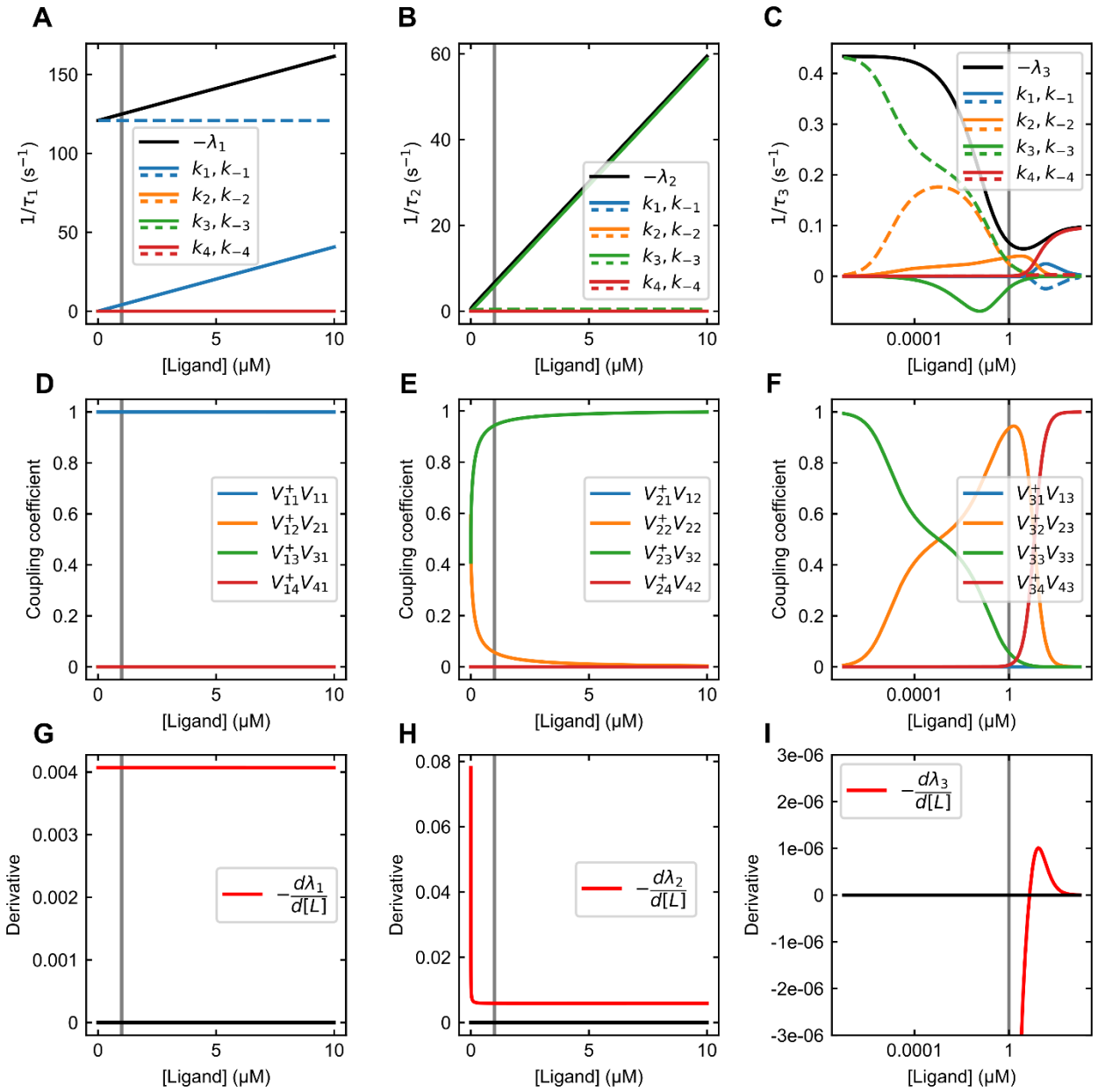

Figure 5. (**A-C**) The reciprocal relaxation times and eigenrates of the three normal reactions were simulated as a function of ligand concentration. (**D-F**) Relative contributions of each step in the reaction model to each normal reaction. Step 1 is blue, step 2 is orange, step 3 is green, and step 4 is red. (**G-I**) The derivatives of eigenvalues of normal reactions with respect to ligand concentration (red lines) calculated using Eq. (23).

Non-monotonic behavior of the third reciprocal relaxation time

Galbrut *et al*. [3] have demonstrated that the third reciprocal relaxation time can have a non-monotonic behavior as a function of ligand concentration where the initial decrease is followed by the subsequent increase (Fig. 6, blue curve). We discovered another type non-monotonic behavior where the initial increase is followed by the decrease in the reciprocal relaxation time (Fig. 6, orange curve). This type of behavior is observed when the sum of the isomerization rate constants of step 2 is higher than the dissociation rate constant of step 3 (k_2+k_{-2} > k_{-3}).

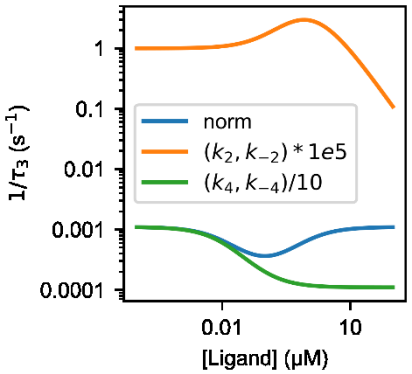

Figure 6. The dependence of the third reciprocal relaxation time on ligand concentration. The blue curve was simulated using k_1 = 0.1 M^{-1} s^{-1}, k_{-1} = 100 s^{-1}, k_2 = 10^{-4} s^{-1}, k_{-2} = 10^{-3} s^{-1}, k_3 = 0.1 M^{-1} s^{-1}, k_{-3} = 1 s^{-1}, k_4 = 10^{-3} s^{-1}, k_{-4} = 10^{-4} s^{-1} and values at extremities $1/\tau_3(L = 0) = k_2 + k_{-2}$ and $1/\tau_3(L = \infty) = k_4 + k_{-4}$. Increasing the rates of the isomerization step 2 to k_2 = 1 s^{-1} and k_{-2} = 10 s^{-1} produces the orange curve with opposite non-monotonic behavior. The reciprocal relaxation time initially increases and then decreases at higher ligand concentrations. Values at extremities are $1/\tau_3(L = 0) = k_{-3}$ and $1/\tau_3(L = \infty) = k_4 + k_{-4}$. Decreasing the rates of the isomerization step 4 to k_4 = 10^{-4} s^{-1} and k_{-4} = 10^{-5} s^{-1} produces the green curve where the reciprocal relaxation time monotonically decreases. Values at extremities are $1/\tau_3(L = 0) = k_2 + k_{-2}$ and $1/\tau_3(L = \infty) = k_4 + k_{-4}$.

References

1. Ordabayev, Y.A., et al., *Regulation of UvrD Helicase Activity by MutL.* J Mol Biol, 2018. **430**(21): p. 4260-4274.
2. Bernasconi, C.F., *Relaxation Kinetics*. 1976, New York: Academic Press.
3. Galburt, E.A. and J. Rammohan, *A Kinetic Signature for Parallel Pathways: Conformational Selection and Induced Fit. Links and Disconnects between Observed Relaxation Rates and Fractional Equilibrium Flux under Pseudo-First-Order Conditions.* Biochemistry, 2016. **55**(50): p. 7014-7022.
4. Rammohan, J., et al., *CarD stabilizes mycobacterial open complexes via a two-tiered kinetic mechanism.* Nucleic Acids Res, 2015. **43**(6): p. 3272-85.
5. Galletto, R., M.J. Jezewska, and W. Bujalowski, *Kinetics of allosteric conformational transition of a macromolecule prior to ligand binding: analysis of stopped-flow kinetic experiments.* Cell Biochem Biophys, 2005. **42**(2): p. 121-44.
6. Vogt, A.D. and E. Di Cera, *Conformational selection or induced fit? A critical appraisal of the kinetic mechanism.* Biochemistry, 2012. **51**(30): p. 5894-902.
7. Hammes, G.G., Y.C. Chang, and T.G. Oas, *Conformational selection or induced fit: a flux description of reaction mechanism.* Proc Natl Acad Sci U S A, 2009. **106**(33): p. 13737-41.
8. Bujalowski, W. and M.J. Jezewska, *Kinetic Mechanism of the Single-stranded DNA Recognition by Escherichia coli Replicative Helicase DnaB Protein. Application of the Matrix Projection Operator Technique to Analyze Stopped-flow Kinetics.* J. Mol. Biol., 2000. **295**: p. 831-852.

Chapter V

Summary

Summary

Goal of the research project

The goal of my thesis work is to elucidate the molecular mechanism of activation and regulation of the UvrD helicase activity by an accessory protein MutL. Helicases are essential components of most DNA metabolic processes *in vivo*. *E. coli* UvrD and UvrD-like helicases possess both ssDNA translocase and DNA helicase activities (Timothy M. Lohman, Tomko, and Wu 2008). These activities require regulation *in vivo* since not all DNA metabolic processes require the DNA helicase activity, with some functions necessitating ssDNA translocase activity alone. Furthermore, an unregulated helicase can be harmful to the cell by destabilizing duplex DNA. It has been shown that the helicase and translocase activities of UvrD are regulated by its self-assembly state *in vitro* in the absence of other protein factors (Maluf, Fischer, and Lohman 2003; Fischer, Maluf, and Lohman 2004; Ali, Maluf, and Lohman 1999). However, in bacteria, UvrD-like helicases often function as parts of multiprotein assemblies. Therefore, it is of interest to understand how an interaction with cellular partners regulate the helicase activity versus ssDNA translocase activity of these motor proteins.

UvrD and MutL are components of *E. coli* methyl-directed mismatch repair (MMR) machinery. UvrD and MutL is an excellent system to study the interaction between the regulatory and helicase proteins since it was shown that MutL alone is sufficient to stimulate UvrD helicase activity *in vitro* (Yamaguchi, Dao, and Modrich 1998; Mechanic, Frankel, and Matson 2000). Furthermore, the biochemical activities of individual UvrD and MutL proteins have been well characterized which enables one to formulate and develop a strong/detailed hypothesis about the mechanism of activation/regulation of UvrD helicase by MutL. The results and conclusions of the studies performed during the course my thesis work provide insight about

the molecular and kinetic mechanism of activation of UvrD helicase by MutL, which in turn furthers our understanding of how helicases function and are regulated.

Hypotheses

The premise of my hypotheses are based on extensive amount of studies characterizing biochemical and biophysical properties of UvrD and MutL. *E. coli* UvrD can self-associate both free in solution and on the DNA substrate (Maluf and Lohman 2003). The self-assembly state of UvrD plays a regulatory role for its translocase and helicase activities. A UvrD monomer can translocate processively in 3' to 5' direction along ssDNA (Fischer, Maluf, and Lohman 2004; Tomko et al. 2007, 2010; Tomko, Fischer, and Lohman 2012; K. S. Lee et al. 2013; Tomko and Lohman 2017), however, processive DNA unwinding activity requires formation of at least a UvrD dimer or higher order oligomer in the absence of protein factors (Maluf, Fischer, and Lohman 2003; Maluf, Ali, and Lohman 2003; K. S. Lee et al. 2013; Comstock et al. 2015; Nguyen et al. 2017). UvrD dimerization on the DNA substrate is accompanied by a swiveling of the 2B sub-domain of the lead UvrD monomer to a more closed state resulting in helicase activation (Nguyen et al. 2017). Furthermore, it was shown that the monomeric forms of *E. coli* UvrD and its close relatives, *E. coli* Rep and *B. stearothermophilus* PcrA, possess latent helicase activity that can be stimulated by the assistance of the pulling force onto the DNA substrate (Comstock et al. 2015), relieving the auto-inhibitory effect of the 2B sub-domain (Brendza et al. 2005; Arslan et al. 2015), or in the presence of an accessory protein (Chisty et al. 2013).

Previous studies have shown that MutL alone is sufficient to stimulate the UvrD-catalyzed DNA unwinding (Mechanic, Frankel, and Matson 2000; Yamaguchi, Dao, and Modrich 1998). However, the details of the mechanism of stimulation of UvrD by MutL remain

unclear. Mechanic *et al.* (Mechanic, Frankel, and Matson 2000) concluded from their studies that MutL functions solely as a UvrD loading factor and does not affect the DNA unwinding processivity of UvrD. However, in this study, single round DNA unwinding experiments show increase in unwinding activity in the presence of MutL, consistent with MutL functioning as a processivity factor, and the results of multiple turnover DNA unwinding experiments are inconclusive and do not exclude the possibility of MutL functioning as a processivity factor (Mechanic, Frankel, and Matson 2000). *Therefore, it is possible that MutL forms a stable complex with UvrD on DNA and this complex results in increased processivity of DNA unwinding.* Furthermore, the model proposed by Mechanic *et al*. does not consider the oligomeric state of UvrD and its effect on DNA unwinding activity. *My hypothesis is that MutL either activates the latent UvrD monomer helicase activity or, alternatively, stabilizes UvrD dimerization on the DNA.* Finally, since the conformational state of the 2B sub-domain has been shown to regulate unwinding activity, *it might be that MutL activates helicase activity of UvrD by modulating the rotational conformational state of the 2B sub-domain.*

Research Methodology

All of the questions above seek to elucidate the mechanism of stimulation of UvrD by MutL on a molecular level. Therefore, experiments in this research project were designed to correlate the assembly state, conformational state, and activity of the functional UvrD in complex with MutL. Based on a quantitative correlation between *activity* and *state*, one can gain significant insight into the molecular mechanism of a system under study. Single molecule experiments allow to examine the activities of individual UvrD monomer molecules. In ensemble experiments, the equilibrium distribution of UvrD oligomeric states bound to the duplex DNA substrate can be investigated using analytical ultracentrifugation methods. Then, by

using single round DNA unwinding experiments under identical solution conditions one can measure the helicase activity of the UvrD species bound to the DNA substrate at equilibrium at the start of the reaction. Importantly, by using suitable DNA substrates single round DNA unwinding experiments allow to directly measure the processivity of UvrD-catalyzed DNA unwinding. It is difficult to extract this information from multiple turnover unwinding experiments since DNA unwinding reaction becomes coupled with the initiation step. Information about the kinetic pathways leading to helicase activation can be obtained from pre-steady state stopped-flow experiments by using a sequential-mixing mode to separate steps involving the formation of the active helicase species from the single round DNA unwinding reaction.

Results discussion

The specific activity of UvrD helicase *in vitro* is subject to inhibition when the DNA concentration exceeds the UvrD concentration due to formation of singly ligated UvrD-DNA complexes (Maluf, Fischer, and Lohman 2003). Using single round DNA unwinding experiments at constant total UvrD concentration I showed that the DNA substrate inhibition of UvrD is relieved in the presence of MutL. It is possible that MutL activates the UvrD monomer helicase by substituting the stimulatory role of the second UvrD monomer. Alternatively, it could be argued that the stability of the UvrD dimer on the DNA is increased in the presence of MutL. Experimental challenge in testing these two competing hypotheses lies in correctly assigning the observed helicase activity to the monomeric UvrD. I provided three independent lines of evidence that show that MutL can activate the monomeric UvrD helicase. First, single molecule FRET experiments allowed to observe unwinding of 18-bp duplex DNA by individual UvrD monomers in the presence of MutL. Second, performing analytical ultracentrifugation and single

round DNA unwinding experiments under identical solution conditions demonstrated that a single MutL dimer-UvrD monomer complex on a 3'-$(dT)_{10}$ tailed DNA substrate is capable of unwinding 18-bp duplex DNA. Third, by performing a series of single round DNA unwinding experiments as a function of UvrD concentration in the presence of excess MutL, at high enough DNA substrate concentrations to ensure stoichiometric binding conditions, I determined that the DNA-unwinding amplitudes increase linearly with $[UvrD]_t/[DNA]_t$ and level off at one UvrD per DNA for DNA substrates with the 3' tail length of 10, 12, and 14 nt indicating activation of the monomeric UvrD by MutL. Also note that the 3' ssDNA tail length of 10 nt is too short to form a stable UvrD dimer-DNA complex. Interestingly, I also found that for DNA substrates possessing longer 3′-$(dT)_N$ tails of $N \geq 20$ nt, MutL can stimulate the helicase activity of a UvrD dimer beyond that observed for UvrD dimers on their own.

I also studied the 3'-ssDNA tail-length requirements for MutL stimulated DNA unwinding by UvrD monomer under conditions of excess DNA over UvrD. These experiments showed no detectable unwinding for DNA substrates with 3' ssDNA tail length ≤ 8 nt, whereas a sharp increase in DNA-unwinding amplitude is observed for 3' ssDNA tail lengths from 10 to 14 nt, with no further increase in amplitude for longer tail lengths. Given that a single UvrD monomer can bind with specificity to the 3' ssDNA/dsDNA junction with the 3' ssDNA tail lengths as short as 4-5 nucleotides (Maluf, Fischer, and Lohman 2003; J. Y. Lee and Yang 2006), these results indicate that activation of a UvrD monomer at the ssDNA/dsDNA junction requires interaction of MutL with the 3' ssDNA tail. MutL is known to bind DNA with a preference for ssDNA (Mechanic, Frankel, and Matson 2000; Niedziela-Majka et al. 2011; Ban, Junop, and Yang 1999; Guarné et al. 2004; Robertson, Pattishall, and Matson 2006). The dimerization of the N-terminal ATPase domain of MutL upon ATP binding leads to formation of

a positively charged DNA binding groove (Ban, Junop, and Yang 1999). Additionally, a point mutation in these groove, MutL-R266E, abolishes both DNA binding and stimulation of UvrD by MutL (Robertson, Pattishall, and Matson 2006). Based on these results one can hypothesize that interaction of MutL with DNA is required to stabilize MutL-UvrD complex on the DNA substrate.

Mechanic et al. (Mechanic, Frankel, and Matson 2000) concluded from their studies that MutL functions to continually load multiple UvrD molecules onto a DNA substrate rather than to increase the DNA-unwinding processivity of UvrD. This predicts no increase in DNA unwinding activity in single round unwinding experiments under stoichiometric binding conditions and saturating UvrD concentrations. However, using single round unwinding studies with a series of DNA substrates of varying duplex length we experimentally observed that MutL increases the DNA-unwinding processivity of UvrD by 2- to 3-fold compared to UvrD dimers alone which supports the model where MutL functions as a processivity factor. DNA unwinding processivity depends on the ratio of the rate of unwinding, mk_{obs}, and the rate of dissociation of UvrD from DNA, k_d. The reason for the increase in the processivity is likely due to the reduced rate of dissociation since the rate of unwinding by UvrD in the presence of MutL is similar to the rate of unwinding by UvrD dimers alone. The decreases in the dissociation rate of UvrD from DNA is presumably achieved through interactions of the DNA binding groove in the N-terminal domain of MutL with the ssDNA, and/or maybe even physically encircling the DNA by a MutL clamp. Another prediction of the processivity factor model for MutL that can be tested experimentally is that MutL has to move in a complex with UvrD along the DNA during unwinding.

Apparent contradictions with the results obtained by Mechanic et al. (Mechanic, Frankel, and Matson 2000) can be explained by carefully examining the kinetics of multiple turnover

DNA unwinding reactions. A key experiment in their study involves unwinding of a 148-bp blunt duplex DNA under multiple turnover unwinding conditions. The overall rate of DNA unwinding under this condition is slow and proceeds on a timescale of several minutes. It should be noted that the rate-limiting step in such multiple turnover unwinding reaction of a fully duplex DNA is the rate of initiation of unwinding. The rate of actual unwinding of a 148-bp duplex DNA is relatively fast and is completed in less than ~3 s. Therefore, the authors argument that if MutL increased processivity then DNA unwinding would continue upon addition of a protein trap due to any UvrD that was already bound to the DNA is misleading since this argument does not consider the fact the fraction of actively unwinding UvrD molecules at any time is small and that addition of a protein trap inhibits the re-initiation step. Therefore, the aforementioned experiment cannot be used as a processivity test and its results do not exclude a model where MutL functions as a processivity factor.

My experiments with *E. coli* Rep showed that MutL does not activate a Rep monomer, consistent with a prior report (Yamaguchi, Dao, and Modrich 1998). This suggests that stimulation of UvrD by MutL is due to specific interaction. Based on yeast two-hybrid system experiments, it was suggested that the C-terminal domain of MutL and both the N- and C-termini of UvrD are important for the interaction (Hall, Jordan, and Matson 1998). The C-terminal domain of MutL is poorly conserved among MutL homologs which makes it a primary candidate as a region responsible for specific interactions with UvrD, however, this requires further testing. The disordered C-terminal tail of UvrD is one of the least conserved regions among SF1 helicases and was suggested to be responsible for specific protein-protein interactions (Manelyte et al. 2009; Gwynn et al. 2013). However, a truncated UvrDΔ73 variant lacking its C-terminal tail is activated by MutL as observed in single round DNA unwinding experiments, indicating

that the unstructured C-terminal tail of UvrD is dispensable for this activity. Interestingly, in a similar way, it was reported that the C-terminal tail of UvrD interacts with UvrB, but the truncated UvrDΔ73 version is still functional in nucleotide excision repair (Manelyte et al. 2009).

Structural and functional studies of UvrD, Rep, and PcrA suggested that the rotationally flexible 2B sub-domain is involved in regulation of helicase activity (Brendza et al. 2005; Timothy M. Lohman, Tomko, and Wu 2008; Cheng et al. 2002; J. Y. Lee and Yang 2006; Jia et al. 2011; Arslan et al. 2015). Since the 2B sub-domain has a variable sequence among SF1A helicases, regulation potentially might occur through specific protein-protein interactions. To test the possibility that the 2B sub-domain of UvrD might be involved in specific UvrD-MutL interactions, I used a UvrD(Rep2B) chimera, in which the UvrD 2B sub-domain was replaced with the Rep 2B subdomain. The UvrD(Rep2B) chimera preserves both ssDNA translocase and helicase activities that is comparable to wtUvrD. However, no stimulation of monomeric UvrD(Rep2B) by MutL in single round DNA unwinding experiments is observed under conditions of excess DNA over UvrD(Rep2B). This result shows that the 2B sub-domain of UvrD is essential for activation of UvrD by MutL.

How does MutL activate the monomeric UvrD helicase activity? As discussed above, the conformational state of the 2B sub-domain is implicated in regulation of the helicase activity, specifically, the closed form of the 2B sub-domain has been shown to correlate with the unwinding activity for SF1A helicases (Arslan et al. 2015; Nguyen et al. 2017; Comstock et al. 2015). Using single molecule FRET experiments I studied the effect of MutL binding on the rotational conformational state of the 2B sub-domain of FRET labeled UvrD. UvrD monomer binds to 3'-ssDNA/dsDNA predominantly in an open state (Jia et al. 2011; Nguyen et al. 2017)

which I observed as a dynamic equilibrium between an open and closed states, favoring an open state. Upon binding of MutL I observed three FRET populations with a new intermediate, partially closed state.

However, just based on these results it is not possible to determine if the the closing of the 2B subdomain is required for helicase activity. To find the correlation between the helicase activity and the conformational state of the 2B sub-domain in the presence of MutL I designed and performed two sets of pre-steady state kinetic experiments under the same solution conditions. In the first set of stopped-flow experiments I monitored conformational changes in the 2B sub-domain upon binding of MutL to the pre-formed UvrD monomer-DNA complex. In another set of sequential-mixing stopped-flow experiments I monitored the formation of the active helicase, by isolating experimentally the unwinding reaction from the kinetics of binding of MutL to the UvrD monomer-DNA complex. These parallel studies demonstrated that upon binding of MutL, the 2B sub-domain of UvrD assumes a partially closed conformation and formation of this more closed state is on the pathway to forming the active helicase. The kinetic analysis of these two sets of experiments revealed that the active MutL-UvrD species are formed via two pathways. In the conformational selection (CS) pathway, UvrD undergoes slow conformational change step into a closed conformation, followed by MutL binding step immediately forming the functional MutL-UvrD complex. In the induced fit (IF) pathway, MutL binding to the open state UvrD is followed by a slow isomerization step which leads to the functional MutL-UvrD (closed state) complex. Using the four-state mixed kinetic model which combines both CS and IF pathways showed that under the MutL concentrations used in the experiments, formation of the active MutL-UvrD helicase occurs predominantly through the CS pathway (>90%), and to a smaller extent via the IF pathway (<10%).

Future directions

My thesis studies of the *E. coli* UvrD helicase and the regulatory protein MutL have revealed aspects of helicase regulation, which can be common among SF1 helicases. I showed that a single MutL dimer specifically activates the latent UvrD monomer helicase activity and also stimulates UvrD dimer helicase activity. However, the interaction interface in the MutL-UvrD complex and its orientation on the DNA substrate is still largely unknown and requires mutational/structural studies. Furthermore, it is speculated that ATP binding/hydrolysis by MutL and associated clamp formation/dissociation processes play a role in stimulating UvrD helicase activity by tethering UvrD to the DNA, however, this also needs further investigations.

I showed that MutL functions as a processivity factor and increases the processivity of UvrD-catalyzed DNA unwinding by 2–3-fold under single round conditions. One may expect that increase in the unwinding processivity would be more pronounced in the presence of MutL since in mismatch repair the distance between the nick, an initiation site for UvrD, and the mismatch site can be as far removed as 1–2 kb in length (Dao and Modrich 1998). It is possible that MutL apart from being a processivity factor also functions as a loading factor since the experiments presented in this work are conducted under single round conditions and do not exclude such possibility. I should note that the processivity factor model for MutL assumes that MutL is moving along in a complex with UvrD during DNA unwinding, however, the experiments presented in my thesis work do not provide direct evidence for this. Additionally, the further enhancement in the processivity maybe related to interactions with other cofactors involved in MMR, such as MutS protein. It was shown that MutS and MutL enhance unwinding of a nicked DNA by UvrD in the presence of a mismatch (Yamaguchi, Dao, and Modrich 1998). Furthermore, it was shown that MutS, MutL, and mismatch-dependent unwinding by UvrD starts

at the nick and unwinding is biased toward the shorter path between the nick and the mismatch (Dao and Modrich 1998), suggesting that MutS-MutL complex is also responsible for orienting the UvrD helicase toward the mismatch. Therefore, it is of great interest to study how MutS-MutL complex transmits the mismatch recognition signal to UvrD and facilitates initiation of unwinding from the nick.

References

Abdel-Monem, Mahmoud, Marie-Christine Chanal, and Hartmut Hoffmann-Berling. 1977. "DNA Unwinding Enzyme II of Escherichia Coli: 1. Purification and Characterization of the ATPase Activity." *European Journal of Biochemistry / FEBS* 79 (1): 33–38.

Abdel-Monem, Mahmoud, Hildegard Dürwald, and Hartmut Hoffmann-Berling. 1977. "DNA Unwinding Enzyme II of Escherichia Coli: 2. Characterization of the DNA Unwinding Activity." *European Journal of Biochemistry / FEBS* 79 (1): 39–45.

Acharya, Samir, Patricia L. Foster, Peter Brooks, and Richard Fishel. 2003. "The Coordinated Functions of the E. Coli MutS and MutL Proteins in Mismatch Repair." *Molecular Cell* 12 (1): 233–46.

Ali, J. A., and T. M. Lohman. 1997. "Kinetic Measurement of the Step Size of DNA Unwinding by Escherichia Coli UvrD Helicase." *Science* 275 (5298): 377–80.

Ali, J. A., N. K. Maluf, and T. M. Lohman. 1999. "An Oligomeric Form of E. Coli UvrD Is Required for Optimal Helicase Activity." *Journal of Molecular Biology* 293 (4): 815–34.

Allen, D. J., A. Makhov, M. Grilley, J. Taylor, R. Thresher, P. Modrich, and J. D. Griffith. 1997. "MutS Mediates Heteroduplex Loop Formation by a Translocation Mechanism." *The EMBO Journal* 16 (14): 4467–76.

Arslan, Sinan, Rustem Khafizov, Christopher D. Thomas, Yann R. Chemla, and Taekjip Ha. 2015. "Protein Structure. Engineering of a Superhelicase through Conformational Control." *Science* 348 (6232): 344–47.

Arthur, H. M., and R. G. Lloyd. 1980. "Hyper-Recombination in uvrD Mutants of Escherichia Coli K-12." *Molecular & General Genetics: MGG* 180 (1): 185–91.

Atkinson, John, Colin P. Guy, Chris J. Cadman, Geri F. Moolenaar, Nora Goosen, and Peter McGlynn. 2009. "Stimulation of UvrD Helicase by UvrAB." *The Journal of Biological Chemistry* 284 (14): 9612–23.

Atkinson, John, and Peter McGlynn. 2009. "Replication Fork Reversal and the Maintenance of Genome Stability." *Nucleic Acids Research* 37 (11): 3475–92.

Au, K. G., K. Welsh, and P. Modrich. 1992. "Initiation of Methyl-Directed Mismatch Repair." *The Journal of Biological Chemistry* 267 (17): 12142–48.

Ban, C., M. Junop, and W. Yang. 1999. "Transformation of MutL by ATP Binding and Hydrolysis: A Switch in DNA Mismatch Repair." *Cell* 97 (1): 85–97.

Ban, C., and W. Yang. 1998. "Crystal Structure and ATPase Activity of MutL: Implications for DNA Repair and Mutagenesis." *Cell* 95 (4): 541–52.

Brendza, Katherine M., Wei Cheng, Christopher J. Fischer, Marla A. Chesnik, Anita Niedziela-Majka, and Timothy M. Lohman. 2005. "Autoinhibition of Escherichia Coli Rep Monomer Helicase Activity by Its 2B Subdomain." *Proceedings of the National Academy of Sciences of the United States of America* 102 (29): 10076–81.

Bruand, C., and S. D. Ehrlich. 2000. "UvrD-dependent Replication of Rolling-circle Plasmids in Escherichia Coli." *Molecular Microbiology*. https://onlinelibrary.wiley.com/doi/abs/10.1046/j.1365-2958.2000.01700.x.

Burdett, V., C. Baitinger, M. Viswanathan, S. T. Lovett, and P. Modrich. 2001. "In Vivo Requirement for RecJ, ExoVII, ExoI, and ExoX in Methyl-Directed Mismatch Repair." *Proceedings of the National Academy of Sciences of the United States of America* 98 (12): 6765–70.

Cheng, Wei, Katherine M. Brendza, George H. Gauss, Sergey Korolev, Gabriel Waksman, and Timothy M. Lohman. 2002. “The 2B Domain of the Escherichia Coli Rep Protein Is Not Required for DNA Helicase Activity.” *Proceedings of the National Academy of Sciences of the United States of America* 99 (25): 16006–11.

Cheng, Wei, John Hsieh, Katherine M. Brendza, and Timothy M. Lohman. 2001. “E. Coli Rep Oligomers Are Required to Initiate DNA Unwinding in vitro1.” *Journal of Molecular Biology* 310 (2): 327–50.

Chi, N. W., and R. D. Kolodner. 1994. “Purification and Characterization of MSH1, a Yeast Mitochondrial Protein That Binds to DNA Mismatches.” *The Journal of Biological Chemistry* 269 (47): 29984–92.

Chisty, Liisa T., Christopher P. Toseland, Natalia Fili, Gregory I. Mashanov, Mark S. Dillingham, Justin E. Molloy, and Martin R. Webb. 2013. “Monomeric PcrA Helicase Processively Unwinds Plasmid Lengths of DNA in the Presence of the Initiator Protein RepD.” *Nucleic Acids Research* 41 (9): 5010–23.

Cho, Won-Ki, Cherlhyun Jeong, Daehyung Kim, Minhyeok Chang, Kyung-Mi Song, Jeungphill Hanne, Changill Ban, Richard Fishel, and Jong-Bong Lee. 2012. “ATP Alters the Diffusion Mechanics of MutS on Mismatched DNA.” *Structure* 20 (7): 1264–74.

Comstock, Matthew J., Kevin D. Whitley, Haifeng Jia, Joshua Sokoloski, Timothy M. Lohman, Taekjip Ha, and Yann R. Chemla. 2015. “Protein Structure. Direct Observation of Structure-Function Relationship in a Nucleic Acid-Processing Enzyme.” *Science* 348 (6232): 352–54.

Cooper, D. L., R. S. Lahue, and P. Modrich. 1993. “Methyl-Directed Mismatch Repair Is Bidirectional.” *The Journal of Biological Chemistry* 268 (16): 11823–29.

Dao, V., and P. Modrich. 1998. “Mismatch-, MutS-, MutL-, and Helicase II-Dependent Unwinding from the Single-Strand Break of an Incised Heteroduplex.” *The Journal of Biological Chemistry* 273 (15): 9202–7.

Dessinges, Marie-Noëlle, Timothée Lionnet, Xu Guang Xi, David Bensimon, and Vincent Croquette. 2004. “Single-Molecule Assay Reveals Strand Switching and Enhanced Processivity of UvrD.” *Proceedings of the National Academy of Sciences of the United States of America* 101 (17): 6439–44.

Dillingham, Mark S. 2011. “Superfamily I Helicases as Modular Components of DNA-Processing Machines.” *Biochemical Society Transactions* 39 (2): 413–23.

Dillingham, Mark S., Dale B. Wigley, and Martin R. Webb. 2002. “Direct Measurement of Single-Stranded DNA Translocation by PcrA Helicase Using the Fluorescent Base Analogue 2-Aminopurine.” *Biochemistry* 41 (2): 643–51.

Dillingham, M. S., D. B. Wigley, and M. R. Webb. 2000. “Demonstration of Unidirectional Single-Stranded DNA Translocation by PcrA Helicase: Measurement of Step Size and Translocation Speed.” *Biochemistry* 39 (1): 205–12.

Drotschmann, K., A. Aronshtam, H. J. Fritz, and M. G. Marinus. 1998. “The Escherichia Coli MutL Protein Stimulates Binding of Vsr and MutS to Heteroduplex DNA.” *Nucleic Acids Research* 26 (4): 948–53.

Dutta, R., and M. Inouye. 2000. “GHKL, an Emergent ATPase/kinase Superfamily.” *Trends in Biochemical Sciences* 25 (1): 24–28.

Fischer, Christopher J., and Timothy M. Lohman. 2004. “ATP-Dependent Translocation of Proteins along Single-Stranded DNA: Models and Methods of Analysis of Pre-Steady State Kinetics.” *Journal of Molecular Biology* 344 (5): 1265–86.

Fischer, Christopher J., Nasib K. Maluf, and Timothy M. Lohman. 2004. “Mechanism of ATP-

Dependent Translocation of E.coli UvrD Monomers along Single-Stranded DNA." *Journal of Molecular Biology* 344 (5): 1287–1309.
Galio, L., C. Bouquet, and P. Brooks. 1999. "ATP Hydrolysis-Dependent Formation of a Dynamic Ternary Nucleoprotein Complex with MutS and MutL." *Nucleic Acids Research* 27 (11): 2325–31.
Geider, K., and H. Hoffmann-Berling. 1981. "Proteins Controlling the Helical Structure of DNA." *Annual Review of Biochemistry* 50: 233–60.
Gorbalenya, Alexander E., and Eugene V. Koonin. 1993. "Helicases: Amino Acid Sequence Comparisons and Structure-Function Relationships." *Current Opinion in Structural Biology* 3 (3): 419–29.
Gorman, Jason, Arindam Chowdhury, Jennifer A. Surtees, Jun Shimada, David R. Reichman, Eric Alani, and Eric C. Greene. 2007. "Dynamic Basis for One-Dimensional DNA Scanning by the Mismatch Repair Complex Msh2-Msh6." *Molecular Cell* 28 (3): 359–70.
Gorman, Jason, Feng Wang, Sy Redding, Aaron J. Plys, Teresa Fazio, Shalom Wind, Eric E. Alani, and Eric C. Greene. 2012. "Single-Molecule Imaging Reveals Target-Search Mechanisms during DNA Mismatch Repair." *Proceedings of the National Academy of Sciences of the United States of America* 109 (45): E3074–83.
Gradia, S., S. Acharya, and R. Fishel. 1997. "The Human Mismatch Recognition Complex hMSH2-hMSH6 Functions as a Novel Molecular Switch." *Cell* 91 (7): 995–1005.
———. 2000. "The Role of Mismatched Nucleotides in Activating the hMSH2-hMSH6 Molecular Switch." *The Journal of Biological Chemistry* 275 (6): 3922–30.
Gradia, Scott, Deepa Subramanian, Teresa Wilson, Samir Acharya, Alexander Makhov, Jack Griffith, and Richard Fishel. 1999. "hMSH2–hMSH6 Forms a Hydrolysis-Independent Sliding Clamp on Mismatched DNA." *Molecular Cell* 3 (2): 255–61.
Grilley, M., J. Griffith, and P. Modrich. 1993. "Bidirectional Excision in Methyl-Directed Mismatch Repair." *The Journal of Biological Chemistry* 268 (16): 11830–37.
Grilley, M., K. M. Welsh, S. S. Su, and P. Modrich. 1989. "Isolation and Characterization of the Escherichia Coli mutL Gene Product." *The Journal of Biological Chemistry* 264 (2): 1000–1004.
Grossman, L., P. R. Caron, S. J. Mazur, and E. Y. Oh. 1988. "Repair of DNA-Containing Pyrimidine Dimers." *FASEB Journal: Official Publication of the Federation of American Societies for Experimental Biology* 2 (11): 2696–2701.
Guarné, Alba, Santiago Ramon-Maiques, Erika M. Wolff, Rodolfo Ghirlando, Xiaojian Hu, Jeffrey H. Miller, and Wei Yang. 2004. "Structure of the MutL C-Terminal Domain: A Model of Intact MutL and Its Roles in Mismatch Repair." *The EMBO Journal* 23 (21): 4134–45.
Gwynn, Emma J., Abigail J. Smith, Colin P. Guy, Nigel J. Savery, Peter McGlynn, and Mark S. Dillingham. 2013. "The Conserved C-Terminus of the PcrA/UvrD Helicase Interacts Directly with RNA Polymerase." *PloS One* 8 (10): e78141.
Haber, L. T., and G. C. Walker. 1991. "Altering the Conserved Nucleotide Binding Motif in the Salmonella Typhimurium MutS Mismatch Repair Protein Affects Both Its ATPase and Mismatch Binding Activities." *The EMBO Journal* 10 (9): 2707–15.
Hall, M. C., J. R. Jordan, and S. W. Matson. 1998. "Evidence for a Physical Interaction between the Escherichia Coli Methyl-Directed Mismatch Repair Proteins MutL and UvrD." *The EMBO Journal* 17 (5): 1535–41.
Hall, M. C., and S. W. Matson. 1999a. "The Escherichia Coli MutL Protein Physically Interacts

with MutH and Stimulates the MutH-Associated Endonuclease Activity." *The Journal of Biological Chemistry* 274 (3): 1306–12.
———. 1999b. "Helicase Motifs: The Engine That Powers DNA Unwinding." *Molecular Microbiology* 34 (5): 867–77.
Ha, Taekjip, Ivan Rasnik, Wei Cheng, Hazen P. Babcock, George H. Gauss, Timothy M. Lohman, and Steven Chu. 2002. "Initiation and Re-Initiation of DNA Unwinding by the Escherichia Coli Rep Helicase." *Nature* 419 (6907): 638–41.
Heller, Ryan C., and Kenneth J. Marians. 2007. "Non-Replicative Helicases at the Replication Fork." *DNA Repair* 6 (7): 945–52.
Iyer, Ravi R., Anna Pluciennik, Vickers Burdett, and Paul L. Modrich. 2006. "DNA Mismatch Repair: Functions and Mechanisms." *Chemical Reviews* 106 (2): 302–23.
Jeong, Cherlhyun, Won-Ki Cho, Kyung-Mi Song, Christopher Cook, Tae-Young Yoon, Changill Ban, Richard Fishel, and Jong-Bong Lee. 2011. "MutS Switches between Two Fundamentally Distinct Clamps during Mismatch Repair." *Nature Structural & Molecular Biology* 18 (3): 379–85.
Jia, Haifeng, Sergey Korolev, Anita Niedziela-Majka, Nasib K. Maluf, George H. Gauss, Sua Myong, Taekjip Ha, Gabriel Waksman, and Timothy M. Lohman. 2011. "Rotations of the 2B Sub-Domain of E. Coli UvrD Helicase/translocase Coupled to Nucleotide and DNA Binding." *Journal of Molecular Biology* 411 (3): 633–48.
Jiricny, J., S. S. Su, S. G. Wood, and P. Modrich. 1988. "Mismatch-Containing Oligonucleotide Duplexes Bound by the E. Coli mutS-Encoded Protein." *Nucleic Acids Research* 16 (16): 7843–53.
Junop, M. S., G. Obmolova, K. Rausch, P. Hsieh, and W. Yang. 2001. "Composite Active Site of an ABC ATPase: MutS Uses ATP to Verify Mismatch Recognition and Authorize DNA Repair." *Molecular Cell* 7 (1): 1–12.
Kolodner, R. D. 1995. "Mismatch Repair: Mechanisms and Relationship to Cancer Susceptibility." *Trends in Biochemical Sciences* 20 (10): 397–401.
Korolev, S., J. Hsieh, G. H. Gauss, T. M. Lohman, and G. Waksman. 1997. "Major Domain Swiveling Revealed by the Crystal Structures of Complexes of E. Coli Rep Helicase Bound to Single-Stranded DNA and ADP." *Cell* 90 (4): 635–47.
Lahue, R. S., K. G. Au, and P. Modrich. 1989. "DNA Mismatch Correction in a Defined System." *Science* 245 (4914): 160–64.
Lahue, R. S., S. S. Su, and P. Modrich. 1987. "Requirement for d(GATC) Sequences in Escherichia Coli mutHLS Mismatch Correction." *Proceedings of the National Academy of Sciences of the United States of America* 84 (6): 1482–86.
Lamers, M. H., A. Perrakis, J. H. Enzlin, H. H. Winterwerp, N. de Wind, and T. K. Sixma. 2000. "The Crystal Structure of DNA Mismatch Repair Protein MutS Binding to a G X T Mismatch." *Nature* 407 (6805): 711–17.
Längle-Rouault, F., G. Maenhaut-Michel, and M. Radman. 1987. "GATC Sequences, DNA Nicks and the MutH Function in Escherichia Coli Mismatch Repair." *The EMBO Journal* 6 (4): 1121–27.
Lee, Jae Young, and Wei Yang. 2006. "UvrD Helicase Unwinds DNA One Base Pair at a Time by a Two-Part Power Stroke." *Cell* 127 (7): 1349–60.
Lee, Kyung Suk, Hamza Balci, Haifeng Jia, Timothy M. Lohman, and Taekjip Ha. 2013. "Direct Imaging of Single UvrD Helicase Dynamics on Long Single-Stranded DNA." *Nature Communications* 4: 1878.

Liu, Jiaquan, Jeungphill Hanne, Brooke M. Britton, Jared Bennett, Daehyung Kim, Jong-Bong Lee, and Richard Fishel. 2016. “Cascading MutS and MutL Sliding Clamps Control DNA Diffusion to Activate Mismatch Repair.” *Nature* 539 (7630): 583–87.
Lohman, Timothy M., Eric J. Tomko, and Colin G. Wu. 2008. “Non-Hexameric DNA Helicases and Translocases: Mechanisms and Regulation.” *Nature Reviews. Molecular Cell Biology* 9 (5): 391–401.
Lohman, T. M. 1992. “Escherichia Coli DNA Helicases: Mechanisms of DNA Unwinding.” *Molecular Microbiology* 6 (1): 5–14.
Lohman, T. M., and K. P. Bjornson. 1996. “Mechanisms of Helicase-Catalyzed DNA Unwinding.” *Annual Review of Biochemistry* 65: 169–214.
Lucius, Aaron L., Nasib K. Maluf, Christopher J. Fischer, and Timothy M. Lohman. 2003. “General Methods for Analysis of Sequential ‘n-Step’ Kinetic Mechanisms: Application to Single Turnover Kinetics of Helicase-Catalyzed DNA Unwinding.” *Biophysical Journal* 85 (4): 2224–39.
Lynch, H. T., and A. de la Chapelle. 1999. “Genetic Susceptibility to Non-Polyposis Colorectal Cancer.” *Journal of Medical Genetics* 36 (11): 801–18.
Makurath, Monika A., Kevin D. Whitley, Binh Nguyen, Timothy M. Lohman, and Yann R. Chemla. 2019. “Regulation of Rep Helicase Unwinding by an Auto-Inhibitory Subdomain.” *Nucleic Acids Research* 47 (5): 2523–32.
Maluf, Nasib K., Janid A. Ali, and Timothy M. Lohman. 2003. “Kinetic Mechanism for Formation of the Active, Dimeric UvrD Helicase-DNA Complex.” *The Journal of Biological Chemistry* 278 (34): 31930–40.
Maluf, Nasib K., Christopher J. Fischer, and Timothy M. Lohman. 2003. “A Dimer of Escherichia Coli UvrD Is the Active Form of the Helicase in Vitro.” *Journal of Molecular Biology* 325 (5): 913–35.
Maluf, Nasib K., and Timothy M. Lohman. 2003. “Self-Association Equilibria of Escherichia Coli UvrD Helicase Studied by Analytical Ultracentrifugation.” *Journal of Molecular Biology* 325 (5): 889–912.
Manelyte, Laura, Colin P. Guy, Rachel M. Smith, Mark S. Dillingham, Peter McGlynn, and Nigel J. Savery. 2009. “The Unstructured C-Terminal Extension of UvrD Interacts with UvrB, but Is Dispensable for Nucleotide Excision Repair.” *DNA Repair* 8 (11): 1300–1310.
Matson, Steven W. 1986. “Escherichia Coli Helicase II (urvD Gene Product) Translocates Unidirectionally in a 3’to 5'direction.” *The Journal of Biological Chemistry* 261 (22): 10169–75.
Matson, Steven W., and Adam B. Robertson. 2006. “The UvrD Helicase and Its Modulation by the Mismatch Repair Protein MutL.” *Nucleic Acids Research* 34 (15): 4089–97.
Matson, S. W., and J. W. George. 1987. “DNA Helicase II of Escherichia Coli. Characterization of the Single-Stranded DNA-Dependent NTPase and Helicase Activities.” *The Journal of Biological Chemistry* 262 (5): 2066–76.
Matson, S. W., and B. S. Morton. 1991. “Escherichia Coli DNA Helicase I Catalyzes a Site- and Strand-Specific Nicking Reaction at the F Plasmid oriT.” *The Journal of Biological Chemistry* 266 (24): 16232–37.
Mechanic, L. E., B. A. Frankel, and S. W. Matson. 2000. “Escherichia Coli MutL Loads DNA Helicase II onto DNA.” *The Journal of Biological Chemistry* 275 (49): 38337–46.
Mechanic, L. E., M. C. Hall, and S. W. Matson. 1999. “Escherichia Coli DNA Helicase II Is Active as a Monomer.” *The Journal of Biological Chemistry* 274 (18): 12488–98.

Modrich, P., and R. Lahue. 1996. “Mismatch Repair in Replication Fidelity, Genetic Recombination, and Cancer Biology.” *Annual Review of Biochemistry* 65: 101–33.
Myong, Sua, Ivan Rasnik, Chirlmin Joo, Timothy M. Lohman, and Taekjip Ha. 2005. “Repetitive Shuttling of a Motor Protein on DNA.” *Nature* 437 (7063): 1321–25.
Nguyen, Binh, Yerdos Ordabayev, Joshua E. Sokoloski, Elizabeth Weiland, and Timothy M. Lohman. 2017. “Large Domain Movements upon UvrD Dimerization and Helicase Activation.” *Proceedings of the National Academy of Sciences of the United States of America* 114 (46): 12178–83.
Niedziela-Majka, Anita, Nasib K. Maluf, Edwin Antony, and Timothy M. Lohman. 2011. “Self-Assembly of Escherichia Coli MutL and Its Complexes with DNA.” *Biochemistry* 50 (37): 7868–80.
Obmolova, G., C. Ban, P. Hsieh, and W. Yang. 2000. “Crystal Structures of Mismatch Repair Protein MutS and Its Complex with a Substrate DNA.” *Nature* 407 (6805): 703–10.
Parker, B. O., and M. G. Marinus. 1992. “Repair of DNA Heteroduplexes Containing Small Heterologous Sequences in Escherichia Coli.” *Proceedings of the National Academy of Sciences of the United States of America* 89 (5): 1730–34.
Petrova, Vessela, Stefanie H. Chen, Eileen T. Molzberger, Eric Tomko, Sindhu Chitteni-Pattu, Haifeng Jia, Yerdos Ordabayev, Timothy M. Lohman, and Michael M. Cox. 2015. “Active Displacement of RecA Filaments by UvrD Translocase Activity.” *Nucleic Acids Research* 43 (8): 4133–49.
Qiu, Ruoyi, Vanessa C. DeRocco, Credle Harris, Anushi Sharma, Manju M. Hingorani, Dorothy A. Erie, and Keith R. Weninger. 2012. “Large Conformational Changes in MutS during DNA Scanning, Mismatch Recognition and Repair Signalling.” *The EMBO Journal* 31 (11): 2528–40.
Robertson, Adam, Steven R. Pattishall, and Steven W. Matson. 2006. “The DNA Binding Activity of MutL Is Required for Methyl-Directed Mismatch Repair in Escherichia Coli.” *The Journal of Biological Chemistry* 281 (13): 8399–8408.
Runyon, G. T., D. G. Bear, and T. M. Lohman. 1990. “Escherichia Coli Helicase II (UvrD) Protein Initiates DNA Unwinding at Nicks and Blunt Ends.” *Proceedings of the National Academy of Sciences of the United States of America* 87 (16): 6383–87.
Runyon, G. T., I. Wong, and T. M. Lohman. 1993. “Overexpression, Purification, DNA Binding, and Dimerization of the Escherichia Coli uvrD Gene Product (helicase II).” *Biochemistry* 32 (2): 602–12.
Runyon S, Gregory T., and Timothy M. Lohman SBfl. 1989. “Escherichia Coli Helicase I1 (UvrD) Protein Can Completely Unwind Fully Duplex Linear and Nicked Circular DNA.” *S, Pp.* 17502: 17512.
Sancar, A. 1994. “Mechanisms of DNA Excision Repair.” *Science* 266 (5193): 1954–56.
———. 1996. “DNA Excision Repair.” *Annual Review of Biochemistry* 65 (1): 43–81.
Sanders, Kelly, Chia-Liang Lin, Abigail J. Smith, Nora Cronin, Gemma Fisher, Vasileios Eftychidis, Peter McGlynn, Nigel J. Savery, Dale B. Wigley, and Mark S. Dillingham. 2017. “The Structure and Function of an RNA Polymerase Interaction Domain in the PcrA/UvrD Helicase.” *Nucleic Acids Research* 45 (7): 3875–87.
Schofield, M. J., S. Nayak, T. H. Scott, C. Du, and P. Hsieh. 2001. “Interaction of Escherichia Coli MutS and MutL at a DNA Mismatch.” *The Journal of Biological Chemistry* 276 (30): 28291–99.
Selmane, Tassadite, Mark J. Schofield, Sunil Nayak, Chunwei Du, and Peggy Hsieh. 2003.

"Formation of a DNA Mismatch Repair Complex Mediated by ATP." *Journal of Molecular Biology* 334 (5): 949–65.
Singleton, Martin R., Mark S. Dillingham, and Dale B. Wigley. 2007. "Structure and Mechanism of Helicases and Nucleic Acid Translocases." *Annual Review of Biochemistry* 76: 23–50.
Sokoloski, Joshua E., Alexander G. Kozlov, Roberto Galletto, and Timothy M. Lohman. 2016. "Chemo-Mechanical Pushing of Proteins along Single-Stranded DNA." *Proceedings of the National Academy of Sciences of the United States of America* 113 (22): 6194–99.
Spampinato, C., and P. Modrich. 2000. "The MutL ATPase Is Required for Mismatch Repair." *The Journal of Biological Chemistry* 275 (13): 9863–69.
Subramanya, H. S., L. E. Bird, J. A. Brannigan, and D. B. Wigley. 1996. "Crystal Structure of a DExx Box DNA Helicase." *Nature* 384 (6607): 379–83.
Su, S. S., R. S. Lahue, K. G. Au, and P. Modrich. 1988. "Mispair Specificity of Methyl-Directed DNA Mismatch Correction in Vitro." *The Journal of Biological Chemistry* 263 (14): 6829–35.
Su, S. S., and P. Modrich. 1986. "Escherichia Coli mutS-Encoded Protein Binds to Mismatched DNA Base Pairs." *Proceedings of the National Academy of Sciences of the United States of America* 83 (14): 5057–61.
Tanner, N. Kyle, Olivier Cordin, Josette Banroques, Monique Doère, and Patrick Linder. 2003. "The Q Motif: A Newly Identified Motif in DEAD Box Helicases May Regulate ATP Binding and Hydrolysis." *Molecular Cell* 11 (1): 127–38.
Tomko, Eric J., Christopher J. Fischer, and Timothy M. Lohman. 2010. "Ensemble Methods for Monitoring Enzyme Translocation along Single Stranded Nucleic Acids." *Methods* 51 (3): 269–76.
———. 2012. "Single-Stranded DNA Translocation of E. Coli UvrD Monomer Is Tightly Coupled to ATP Hydrolysis." *Journal of Molecular Biology* 418 (1-2): 32–46.
Tomko, Eric J., Christopher J. Fischer, Anita Niedziela-Majka, and Timothy M. Lohman. 2007. "A Nonuniform Stepping Mechanism for E. Coli UvrD Monomer Translocation along Single-Stranded DNA." *Molecular Cell* 26 (3): 335–47.
Tomko, Eric J., Haifeng Jia, Jeehae Park, Nasib K. Maluf, Taekjip Ha, and Timothy M. Lohman. 2010. "5'-Single-Stranded/duplex DNA Junctions Are Loading Sites for E. Coli UvrD Translocase." *The EMBO Journal* 29 (22): 3826–39.
Tomko, Eric J., and Timothy M. Lohman. 2017. "Modulation of Escherichia Coli UvrD Single-Stranded DNA Translocation by DNA Base Composition." *Biophysical Journal* 113 (7): 1405–15.
Tuteja, Narendra, and Renu Tuteja. 2004. "Unraveling DNA Helicases. Motif, Structure, Mechanism and Function." *European Journal of Biochemistry / FEBS* 271 (10): 1849–63.
Veaute, Xavier, Stéphane Delmas, Marjorie Selva, Josette Jeusset, Eric Le Cam, Ivan Matic, Francis Fabre, and Marie-Agnès Petit. 2005. "UvrD Helicase, Unlike Rep Helicase, Dismantles RecA Nucleoprotein Filaments in Escherichia Coli." *The EMBO Journal* 24 (1): 180–89.
Velankar, S. S., P. Soultanas, M. S. Dillingham, H. S. Subramanya, and D. B. Wigley. 1999. "Crystal Structures of Complexes of PcrA DNA Helicase with a DNA Substrate Indicate an Inchworm Mechanism." *Cell* 97 (1): 75–84.
Viswanathan, M., V. Burdett, C. Baitinger, P. Modrich, and S. T. Lovett. 2001. "Redundant Exonuclease Involvement in Escherichia Coli Methyl-Directed Mismatch Repair." *The Journal of Biological Chemistry* 276 (33): 31053–58.

Watson, J. D., and F. H. Crick. 1953. “Molecular Structure of Nucleic Acids; a Structure for Deoxyribose Nucleic Acid.” *Nature* 171 (4356): 737–38.
Welsh, K. M., A. L. Lu, S. Clark, and P. Modrich. 1987. “Isolation and Characterization of the Escherichia Coli mutH Gene Product.” *The Journal of Biological Chemistry* 262 (32): 15624–29.
Yamaguchi, M., V. Dao, and P. Modrich. 1998. “MutS and MutL Activate DNA Helicase II in a Mismatch-Dependent Manner.” *The Journal of Biological Chemistry* 273 (15): 9197–9201.

Appendix

Globalfit User Guide

User Guide

The Globalfit program (https://github.com/ordabayev/global-fit) has been written with the purpose of simultaneously fitting multiple datasets to a global kinetic model. Globalfit script is a wrapper around lmfit (https://lmfit.github.io/lmfit-py)

File types

(here "my_model" is the name of the model defined by the user)

- "data.csv" – stores experimental data in four columns "x, y, noise, flag". x is the independent variable, y is the dependent variable, noise is the noise in the data, and flag is a unique integer number for each dataset.
- "params_my_model.csv" – contains model parameters. This file will be created at the first run of the model. Parameters that are floated individually for each dataset will have "_flag" attached at the end.
- "simulation_my_model.csv" – contains simulated data based on the parameter values and the residual ("x, simulation, residual, flag"). This file is created upon calling ".save()" method.
- "model.py" – stores all model functions defined by the user. See below how to add a new model function.
- "globalfit.py" – this file contains the GlobalModel class which performs all the necessary operations to load/plot/fit/save/etc the data. See below for details.

Adding a new model

The models used for fitting are saved in the 'model.py' file. Add a new model as follows. Define a new function which has an independent variable as its first argument, followed by model parameters. The function must be able to accept an (numpy) array of independent variables and return an (numpy) array of function values. Decorate the function with "@model" (this will add it to "models" dictionary which later will be accessed by "GlobalModel" class).

The code snippet below shows an example of "nstep_kckend" (sequential n-step translocation with two-step dissociation) model defined using Talbot's method for the numerical inversion of the Laplace transform (imported from "laplace.py").

```
"""
model.py
This file contains fitting models
"""
# import any library that is needed for your model
import numpy as np
from laplace import Talbot

# this dictionary will containt all models decorated with '@model'
models = {}

def model(model_func):
    '''''Add functions decorated with @model to the models list'''
    models[model_func.__name__] = model_func
    return model_func

@model
def nstep_kckend(t, A, n, kt, kd, kc, kend, r, C):
    """Sequential n-step translocation with two-step dissociation
    A/(1+n*r) * (1/(s+kc) * (1+kt*r/(s+kd)*(1-
(kt/(s+kt+kd))**n))*(1+C*kc/(s+kend)))"""
    F = lambda s: A/(1+n*r) * (1/(s+kc) * (1+kt*r/(s+kd)*(1-
(kt/(s+kt+kd))**n))*(1+C*kc/(s+kend)))
    y = Talbot(F,t,N=24)
    return y
```

Generating and saving the data

To generate new data, do experiments. Here, for illustration purposes, I will generate simulated data using the "n-step translocation with two-step dissociation" model. Model parameters used for simulations: k_t = 40 steps/s^{-1}, k_d = 0.5 s^{-1}, k_c = 11 s^{-1}, k_{end} = 2 s^{-1}, r = 1.35, C = 0.05, n = 5, 8, 11, 14 steps, and random noise = 0.01.

```
import numpy as np
import matplotlib.pyplot as plt
from globalfit import models

# parameters used for simulations
# kt, kd, kc, kend, r, C are global parameters
kt = 40.0; kd = 0.5; kc = 11.; kend = 2.; r = 1.35; C = 0.05
# A and n
A = np.array([-1., -1., -1., -1.])
n = np.array([5., 8., 11., 14.])
```

```
# step-size
m = 4
# DNA lengths (nt)
L = m * n
noise = 0.01
# 1.5 sec 150 points
t = np.linspace(0.004, 1.5, 150)

# simulate toy data
data = np.zeros((600,4))
np.random.seed(42)
for i in range(4):
    data[i*150:(i+1)*150,0] = t
    data[i*150:(i+1)*150,3] = n[i]
    data[i*150:(i+1)*150,1] = models['nstep_kckend'](t, A[i], n[i], kt, kd, kc, kend, r
, C) + noise * np.random.randn(len(t))

# save the data
np.savetxt('example2/data.csv', data, delimiter=',')

# plot the data
plt.figure(figsize=(5,4))
for i in range(4):
    plt.plot(t, data[i*150:(i+1)*150,1], 'o')
plt.title('Simulated data')
plt.ylabel('Signal (a.u.)')
plt.xlabel('Time (s)')
plt.show()
```

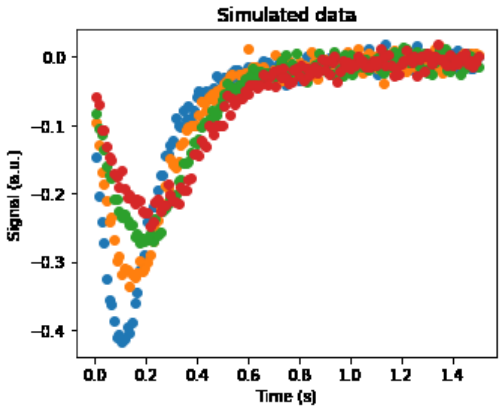

The data must be saved in “data.csv” file which contains four comma-separated columns “time, y, noise, flag”. Use unique-valued integer number for each data set as a flag. The data simulated above is stored in the “example2” folder.

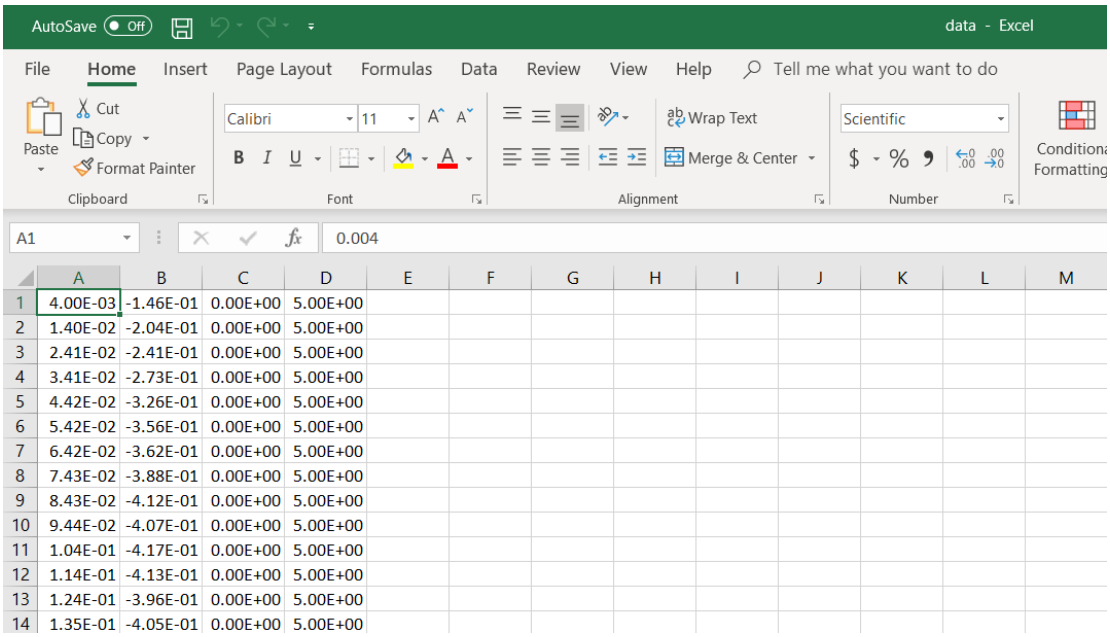

	A	B	C	D	E	F	G	H	I	J	K	L	M
1	4.00E-03	-1.46E-01	0.00E+00	5.00E+00									
2	1.40E-02	-2.04E-01	0.00E+00	5.00E+00									
3	2.41E-02	-2.41E-01	0.00E+00	5.00E+00									
4	3.41E-02	-2.73E-01	0.00E+00	5.00E+00									
5	4.42E-02	-3.26E-01	0.00E+00	5.00E+00									
6	5.42E-02	-3.56E-01	0.00E+00	5.00E+00									
7	6.42E-02	-3.62E-01	0.00E+00	5.00E+00									
8	7.43E-02	-3.88E-01	0.00E+00	5.00E+00									
9	8.43E-02	-4.12E-01	0.00E+00	5.00E+00									
10	9.44E-02	-4.07E-01	0.00E+00	5.00E+00									
11	1.04E-01	-4.17E-01	0.00E+00	5.00E+00									
12	1.14E-01	-4.13E-01	0.00E+00	5.00E+00									
13	1.24E-01	-3.96E-01	0.00E+00	5.00E+00									
14	1.35E-01	-4.05E-01	0.00E+00	5.00E+00									

Load the data and the model

The class GlobalModel contains all the functions required for loading & fitting the data using the user-defined model. Import GlobalModel from “globalfit.py”. Then instantiate your model using the GlobalModel class. At the prompt type the model name and the folder name containing the “data.csv” file.

```
# import GlobalModel class
from globalfit import GlobalModel

# create a new instance (my_model) of the GlobalModel class
my_model = GlobalModel()
```

Model name: nstep_kckend Data folder name: example2

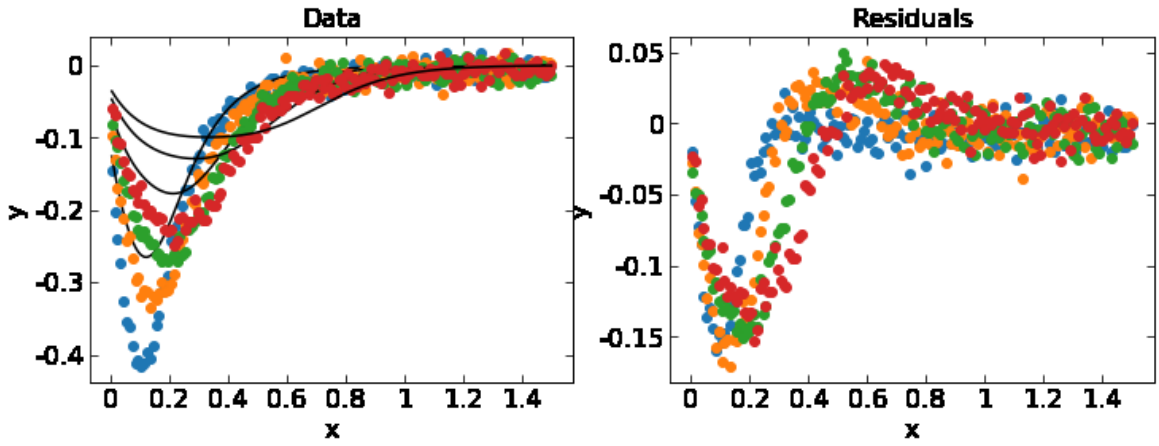

Fit the data using ".fit()"

Fitting is performed by calling ".fit()" method. Fitting options are given below.

- constrain= True – allows to fix and float parameters before the fit, False – constrains from the parameter file are used.
- method= 'leastsq' is the default fitting method. Other fitting methods are described at https://lmfit.github.io/lmfit-py/fitting.html
- weighted= False – data points are not adjusted for the noise, True – data will be weighted using the third column from the "data.csv" file.
- alarm= False – no alarm, True – alarm sound will beep at the end of the fit.
- logscale= False – data is plotted on the linear scale by default, True – data will be plotted on the log scale
- report= False – short report printed by default, True – long report is printed including the correlation coefficients.

Below is the code snippet and results of fitting with all parameters floated.

```
1.  # float all parameters
2.  my_model.fit(constrain=True, method='leastsq', weighted=False, alarm=False, logscale=Fa
    lse, report=False)
```

```
MODEL parameters: ['A', 'n', 'kt', 'kd', 'kc', 'kend', 'r', 'C']
FIXED parameters (comma separated):
Fitting .....
```

```
Fit report:
Name      Value      Min      Max   Stderr     Vary     Expr Brute_Step
A_11     -1.017     -inf      inf  0.04194     True     None     None
A_14     -1.047     -inf      inf  0.04542     True     None     None
A_5     -0.9922     -inf      inf  0.04802     True     None     None
A_8     -0.9897     -inf      inf  0.04353     True     None     None
C        0.0463     -inf      inf  0.00856     True     None     None
kc        10.27     -inf      inf     0.89     True     None     None
kd         1.03     -inf      inf   0.3728     True     None     None
kend      1.834     -inf      inf   0.2941     True     None     None
kt        45.81     -inf      inf    6.761     True     None     None
n_11      13.05     -inf      inf    1.964     True     None     None
n_14      16.61     -inf      inf    2.626     True     None     None
n_5       5.848     -inf      inf   0.7848     True     None     None
n_8        9.22     -inf      inf    1.307     True     None     None
r         1.176     -inf      inf   0.2207     True     None     None
RSS 5.52624429e-02
```

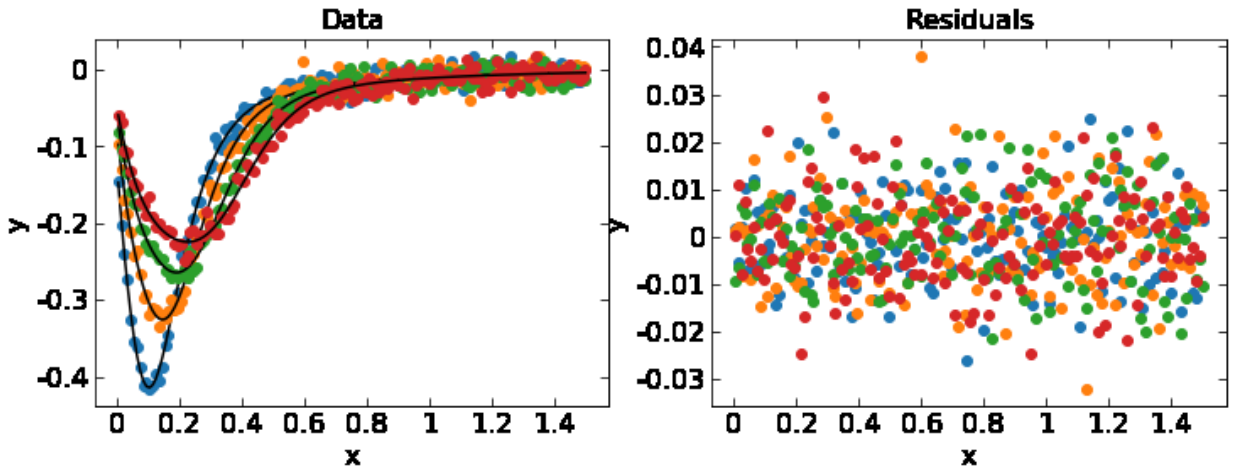

Alternatively, if we had determined $k_d = 0.5\ s^{-1}$ independently and we could fix it in our fit as shown below. The best-fit parameter values have improved significantly (this happens due to high correlation between k_d and other parameters).

```
1. # fix kd
2. my_model.fit(constrain=True, method='leastsq', weighted=False, alarm=False, logscale=Fa
   lse, report=False)
```

```
MODEL parameters: ['A', 'n', 'kt', 'kd', 'kc', 'kend', 'r', 'C']
FIXED parameters (comma separated): kd
Fitting .....
Fit report:
Name      Value      Min      Max   Stderr     Vary     Expr Brute_Step
A_11     -1.026     -inf      inf  0.04753     True     None     None
A_14     -1.036     -inf      inf  0.04832     True     None     None
```

```
A_5     -1.041      -inf       inf   0.04513     True      None      None
A_8     -1.021      -inf       inf   0.04626     True      None      None
C       0.04992     -inf       inf 0.007582     True      None      None
kc        11.38     -inf       inf    0.6726     True      None      None
kd          0.5     -inf       inf         0    False      None      None
kend      2.007     -inf       inf    0.2458     True      None      None
kt        39.16     -inf       inf     3.113     True      None      None
n_11      11.05     -inf       inf    0.8405     True      None      None
n_14      13.87     -inf       inf     1.049     True      None      None
n_5        5.13     -inf       inf    0.4189     True      None      None
n_8       7.938     -inf       inf    0.6166     True      None      None
r         1.411     -inf       inf    0.1821     True      None      None
RSS 5.54139955e-02
```

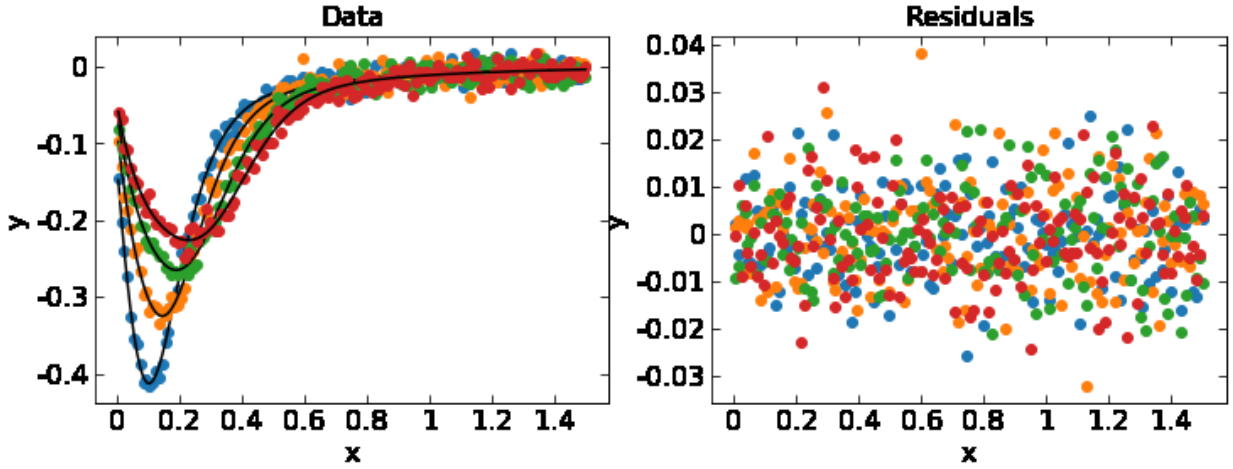

If the current fit values are satisfying, these parameter values must be written (accepted) first before performing the next round of fitting.

```
# write and fit again
my_model.write()
my_model.fit()
```

Plotting and saving the fit results

To save the best-fit parameter values and simulations use the ".save()" method.

```
# save the fit result
my_model.save()

# plot the data
my_model.plot()
```

“globalfit.py” code

```
"""
GLOBAL NON-LINEAR LEAST-SQUARES MINIMIZATION PROGRAM

Globalfit is a wrapper around lmfit (https://lmfit.github.io/lmfit-
py) providing an interface
for simultaneous multi-curve fitting with global parameters.

version: 1.2
last-update: 2019-April-26
author: Yerdos Ordabayev
        Dept. of Biochemistry and Molecular Biophysics
        Washington University School of Medicine
        Saint Louis, MO 63110
"""

import numpy as np
import matplotlib.pyplot as plt
from matplotlib.ticker import FormatStrFormatter
import lmfit
import inspect
import itertools
import sys
import corner
from multiprocessing import Pool
import os
import json
import pandas as pd
import winsound
duration = 2000  # milliseconds
freq = 840  # Hz

from models import models

class GlobalModel:
    def __init__(self, func=None, data=None):
        # choose a model function
        self._select_func()

        # load data
        self.data = self._load_data()

        self.N = np.unique(self.data[:,3])

        self._make_params()

        # initiate program
        self._eval()
        self.plot()
        self._menu()

    def __repr__(self):
        '''''Return representation of GlobalModel.'''
        return '{}.{}(func={})'.format(self.__module__, self.__class__.__name__, self._
name)

    def _menu(self):
        print('------------------------------------------------------------------------
----')
```

```
        print('| .fit() | .write() | .read() | .plot() | | .report() | .save() | .emcee() |')
        print('-------------------------------------------------------------------------')

    def _select_func(self):
        '''Select a function from the models list.'''
        print('List of models from model.py:')
        for i, m in enumerate(models):
            print('{}. {}'.format(i+1, m))
        func_input = input('Model name: ')
        if func_input in models:
            self.func = models[func_input]
            self._name = self.func.__name__
            '''Build parameters from function argumets.'''
            self._param_names = list(inspect.signature(self.func).parameters)
            self.independent_vars = self._param_names[0]
            self._param_names.remove(self.independent_vars)
        else:
            raise KeyError('{!r} is not found in the list of models'.format(func_input))

    def _load_data(self):
        data_input = input('Data folder name: ').strip()
        if data_input:
            self.path = data_input
            data = np.loadtxt(os.path.join(self.path, 'data.csv'), dtype='float', delimiter=',')
            if data.shape[1] != 4:
                raise ValueError('Data file must have 4 columns (x y error flag)')
            else:

                return data
        else:
            raise ValueError('Folder name cannot empty!')

    def _make_params(self):
        if os.path.isfile(os.path.join(self.path, 'params_{}.csv'.format(self._name))):

            self.params = self.read()
            return

        '''Set global parameters for the Model.'''
        print('MODEL parameters: {}'.format(self._param_names))
        params_input = input('GLOBAL parameters (comma separated): ')
        self.global_params = [p.strip() for p in params_input.split(',') if p.strip() in self._param_names]

        '''Create a Parameters object for a Model.'''
        params = lmfit.Parameters()
               for name in self._param_names:
                    if name in self.global_params:
                        param = 0
                        param_input = input('{} [default={}]: '.format(name, param))
                        if param_input: param = float(param_input)
                        params.add(name, value=param)
                    else:
                        for i in self.N:
                            param = 0
```

```
                            param_input = input('{}_{} [default={}]: '.format(name, int(i), param))
                            if param_input: param = float(param_input)
                            params.add('{}_{}'.format(name, int(i)), value=param)

                self.save(params=params)
                self.params = params

            def fit(self, constrain=True, method='leastsq', weighted=False, alarm=False, logscale=False, report=False):
                '''''Fit the model to the data.'''
                if constrain: self._set_fixed()
                self.thinking = itertools.cycle(['.', '..', '...', '....', '.....'])
                if weighted:
                    self.result = lmfit.minimize(self._residual_w, self.params, method=method, nan_policy='omit', iter_cb=self._iteration)
                else:
                    self.result = lmfit.minimize(self._residual, self.params, method=method, nan_policy='omit', iter_cb=self._iteration)
                print('\nFit report:')
                if report: print(lmfit.fit_report(self.result.params))
                else: self.result.params.pretty_print()
                print('RSS {:.8e}'.format(self.result.chisqr))
                self._eval(params=self.result.params)
                self.plot(logscale=logscale)
                if alarm: winsound.Beep(freq, duration)

            def _eval(self, params=None):
                '''''Evaluate the model with supplied parameters.'''
                if params is None:
                    params = self.params
                self.y_sim = np.zeros_like(self.data[:,0])
                for i in self.N:
                    kwargs = {name.split('_')[0]: par.value for name, par in params.items() if name.endswith('_{}'.format(int(i)))}
                    for name in self.global_params:
                        kwargs[name] = params[name].value
                    # select data with the flag = i
                    idx = self.data[:,3] == int(i)
                    kwargs[self.independent_vars] = self.data[idx,0]
                    self.y_sim[idx] = self.func(**kwargs)
                #return self.y_sim

            def _set_fixed(self):
                '''''Set fixed parameters for the fitting.'''
                print('MODEL parameters: {}'.format(self._param_names))
                params_input = input('FIXED parameters (comma separated): ')
                self.fixed_params = [p.strip() for p in params_input.split(',') if p.strip() in self._param_names]
                for name in self._param_names:
                    if name in self.fixed_params:
                        if name in self.global_params:
                            self.params[name].set(vary=False)
                        else:
                            for i in self.N:
                                self.params['{}_{}'.format(name,int(i))].set(vary=False)

                    else:
                        if name in self.global_params:
                            self.params[name].set(vary=True)
```

```
                    else:
                        for i in self.N:
                            self.params['{}_{}'.format(name,int(i))].set(vary=True)

    def _residual(self, params):
        '''''Return the residual.'''
        self._eval(params=params)
        return self.y_sim - self.data[:,1]

    def _residual_w(self, params):
        '''''Return the residual.'''
        self._eval(params=params)
        return (self.y_sim - self.data[:,1]) / self.data[:,2]

    def _iteration(self, params, it, resid):
        '''''have some fun while fitting'''
        char = next(self.thinking)
        sys.stdout.write('\rFitting ' + char)
        #sys.stdout.write('\rRSS: ' + str(rss))

    '''''Bayesian credible region estimation using MCMC'''
    def emcee(self, burn=300, steps=1000, thin=10, ntemps=20):
        self.params.add('noise', value=np.sqrt(self.result.chisqr / self.result.ndata), min=0)
        mini = lmfit.Minimizer(self._log_posterior, self.params)
        with Pool() as pool:
            self.posterior = mini.emcee(burn=burn, steps=steps, thin=thin, ntemps=ntemps, workers=pool)
        self.mini = mini
        corner.corner(self.posterior.flatchain, quantiles=[0.05, 0.5, 0.95], labels=self.posterior.var_names, truths=list(self.posterior.params.valuesdict().values()), show_titles=True)
        plt.savefig(os.path.join(self.path, 'posterior.png'), dpi=300)
        print("median of posterior probability distribution")
        print('------------------------------------------')
        lmfit.report_fit(self.posterior.params)
        self._menu()

    def _log_likelihood(self, params):
        noise = params['noise']
        return -
0.5 * np.sum((self._residual(params) / noise)**2 + np.log(2 * np.pi * noise**2))

    def write(self):
        '''''Update parameters and simulations.'''
        self.params = self.result.params
        self._eval()

    def plot(self, logscale=False):
        plt.figure(figsize=(12,4))
        plt.subplot(1,2,1)
        for i in self.N:
            idx = self.data[:,3] == int(i)
            plt.plot(self.data[idx,0], self.data[idx,1], 'o')
            plt.plot(self.data[idx,0], self.y_sim[idx], 'k-', lw=1.5)
        if logscale: plt.xscale('log')
        plt.title('Data', size=16)
        plt.ylabel('y', size=16)
        plt.xlabel('x', size=16)
```

```
216.                 plt.tick_params(axis='both', direction='in', top=True, right=True, lengt
    h=5)
217.                 plt.yticks(size=16)
218.                 plt.xticks(size=16)
219.                 plt.gca().xaxis.set_major_formatter(FormatStrFormatter('%g'))
220.                 plt.gca().yaxis.set_major_formatter(FormatStrFormatter('%g'))
221.
222.                 plt.subplot(1,2,2)
223.                 for i in self.N:
224.                     idx = self.data[:,3] == int(i)
225.                     plt.plot(self.data[idx,0], self.data[idx,1]-self.y_sim[idx], 'o')
226.                 if logscale: plt.xscale('log')
227.                 plt.title('Residuals', size=16)
228.                 plt.ylabel('y', size=16)
229.                 plt.xlabel('x', size=16)
230.                 plt.tick_params(axis='both', direction='in', top=True, right=True, lengt
    h=5)
231.                 plt.yticks(size=16)
232.                 plt.xticks(size=16)
233.                 plt.gca().xaxis.set_major_formatter(FormatStrFormatter('%g'))
234.                 plt.gca().yaxis.set_major_formatter(FormatStrFormatter('%g'))
235.
236.                 plt.show()
237.
238.             def report(self):
239.                 print(lmfit.fit_report(self.params))
240.
241.             def read(self):
242.                 '''''Read parameter values from the file'''
243.                 params = lmfit.Parameters()
244.                 params_df = pd.read_csv(os.path.join(self.path, 'params_{}.csv'.format(s
    elf._name)), index_col='Name')
245.                 #print(params_df)
246.                 self.global_params = [p for p in params_df.index if '_' not in p]
247.                 for p in params_df.index:
248.                     params.add(p, value=float(params_df.loc[p, 'Value']), min=float(para
    ms_df.loc[p, 'Min']), max=float(params_df.loc[p, 'Max']))
249.                 return params
250.
251.             def save(self, params=None):
252.                 if params is None: params = self.result.params
253.                 params_list = json.loads(params.dumps())
254.                 params_df = pd.DataFrame.from_records(params_list['params'], columns=['N
    ame', 'Value', 'Vary', 'Expr', 'Min', 'Max', 'None', 'Stderr', 'Correl', 'Guess', 'None
    2'])
255.                 params_df['Min']=' '+params_df['Min'].astype('str')
256.                 params_df.to_csv(os.path.join(self.path, 'params_{}.csv'.format(self._na
    me)), index=False, columns=['Name', 'Value', 'Vary', 'Expr', 'Min', 'Max', 'Stderr'])
257.                 self._eval(params=params)
258.                 y_sim = np.copy(self.data)
259.                 y_sim[:,1] = self.y_sim
260.                 y_sim[:,2] = self.data[:,1] - self.y_sim
261.                 np.savetxt(os.path.join(self.path, 'simulation_{}.csv'.format(self._name
    )), y_sim, fmt='%.8e', delimiter=',')
262.                 print('Saved parameters into file: params_{}.csv'.format(self._name))
263.                 print('Saved simulation into file: simulation_{}.csv'.format(self._name)
    )
264.
265.             def help(self):
266.                 self._menu()
```